Research & Technology Transfer

Durability of the Grouted Shear Stud Connection at Low Temperatures

FINAL REPORT

Prepared by:
Arjun Jayaprakash, Ph.D. Candidate
James M. Nau, Professor, Ph.D.
Mohammad Pour-Ghaz, Associate Professor, Ph.D.
Mervyn J. Kowalsky, Professor, Ph.D.

May 2019

Prepared for:
Alaska Department of Transportation & Public Facilities
Statewide Research Office
3132 Channel Drive
Juneau, AK 99801-7898

REPORT DOCUMENTATION PAGE		Form approved OMB No.

Public reporting for this collection of information is estimated to average 1 hour per response, including the time for reviewing instructions, searching existing data sources, gathering and maintaining the data needed, and completing and reviewing the collection of information. Send comments regarding this burden estimate or any other aspect of this collection of information, including suggestion for reducing this burden to Washington Headquarters Services, Directorate for Information Operations and Reports, 1215 Jefferson Davis Highway, Suite 1204, Arlington, VA 22202-4302, and to the Office of Management and Budget, Paperwork Reduction Project (0704-1833), Washington, DC 20503

1. AGENCY USE ONLY (LEAVE BLANK) 4000(162)	2. REPORT DATE May 15, 2019	3. REPORT TYPE AND DATES COVERED Final Report, May 2016 through May 2019

4. TITLE AND SUBTITLE Durability of the Grouted Shear Stud Connection at Low Temperatures	5. FUNDING NUMBERS State project numbers Federal project numbers HFHWY00039 4000(162)
6. AUTHOR(S) Arjun Jayaprakash, James Nau, Mohammad Pour-Ghaz, and Mervyn Kowalsky	

7. PERFORMING ORGANIZATION NAME(S) AND ADDRESS(ES) Department of Civil, Construction, and Environmental Engineering North Carolina State University Raleigh, NC 27606	8. PERFORMING ORGANIZATION REPORT NUMBER 4000(162)

9. SPONSORING/MONITORING AGENCY NAME(S) AND ADDRESS(ES) State of Alaska, Alaska Dept. of Transportation and Public Facilities Research and Technology Transfer 3132 Channel Drive Juneau, AK 99801-7898	10. SPONSORING/MONITORING AGENCY REPORT NUMBER Federal project numbers 4000(162)

11. SUPPLEMENTARY NOTES

12a. DISTRIBUTION / AVAILABILITY STATEMENT No restrictions	12b. DISTRIBUTION CODE

13. ABSTRACT (Maximum 200 words)

The grouted shear stud (GSS) connection for steel bridge substructures was developed as a ductile alternative to directly welded column to cap-beam connections. The GSS connection utilizes plastic hinge relocation to eliminate brittle cracking at the weld region and provides full strength and ductility capacity for steel bridge columns. However, the grout material used as part of the GSS connection is susceptible to damage through years of exposure, especially in extremely cold climates. This report presents the study conducted to evaluate the durability of the GSS connection in cold climates. First, a series of experiments was performed to ascertain the durability of commonly available high-strength cementitious grouts. While there were grouts that exhibited good durability, inconsistencies in results within the same grout were observed. Next, four large scale tests were performed on two-column steel bridge bents to determine the consequences of grout deterioration in the GSS connection. Results indicate that grout deterioration is unlikely to compromise the structural integrity of the connection. The large scale experimental data was then used to determine the predominant force transfer mechanism in the GSS connection. The socket depth of the connection was found to be a crucial factor for successful plastic hinge relocation.

14- KEYWORDS : Steel bridge substructures, Grouted shear stud connection, Socket connection, Plastic hinge relocation, Grout durability, Physical damage simulation	15. NUMBER OF PAGES 191
	16. PRICE CODE N/A

17. SECURITY CLASSIFICATION OF REPORT Unclassified	18. SECURITY CLASSIFICATION OF THIS PAGE Unclassified	19. SECURITY CLASSIFICATION OF ABSTRACT Unclassified	20. LIMITATION OF ABSTRACT N/A

METRIC (SI*) CONVERSION FACTORS

APPROXIMATE CONVERSIONS TO SI UNITS

Symbol	When You Know	Multiply By	To Find	Symbol
		LENGTH		
in	inches	25.4	millimeters	mm
ft	feet	0.3048	meters	m
yd	yards	0.914	meters	m
mi	Miles (statute)	1.61	kilometers	km
		AREA		
in^2	square inches	645.2	millimeters squared	cm^2
ft^2	square feet	0.0929	meters squared	m^2
yd^2	square yards	0.836	meters squared	m^2
mi^2	square miles	2.59	kilometers squared	km^2
ac	acres	0.4046	hectares	ha
		MASS (weight)		
oz	Ounces (avdp)	28.35	grams	g
lb	Pounds (avdp)	0.454	kilograms	kg
T	Short tons (2000 lb)	0.907	megagrams	mg
		VOLUME		
fl oz	fluid ounces (US)	29.57	milliliters	mL
gal	Gallons (liq)	3.785	liters	liters
ft^3	cubic feet	0.0283	meters cubed	m^3
yd^3	cubic yards	0.765	meters cubed	m^3

Note: Volumes greater than 1000 L shall be shown in m^3

Symbol	When You Know	Multiply By	To Find	Symbol
		TEMPERATURE (exact)		
ºF	Fahrenheit temperature	5/9 (ºF-32)	Celsius temperature	ºC
		ILLUMINATION		
fc	Foot-candles	10.76	lux	lx
fl	foot-lamberts	3.426	candela/m^2	cd/cm^2
		FORCE and PRESSURE or STRESS		
lbf	pound-force	4.45	newtons	N
psi	pound-force per square inch	6.89	kilopascals	kPa

These factors conform to the requirement of FHWA Order 5190.1A *SI is the symbol for the International System of Measurements

APPROXIMATE CONVERSIONS FROM SI UNITS

Symbol	When You Know	Multiply By	To Find	Symbol
		LENGTH		
mm	millimeters	0.039	inches	in
m	meters	3.28	feet	ft
m	meters	1.09	yards	yd
km	kilometers	0.621	Miles (statute)	mi
		AREA		
mm^2	millimeters squared	0.0016	square inches	in^2
m^2	meters squared	10.764	square feet	ft^2
km^2	kilometers squared	0.39	square miles	mi^2
ha	hectares (10,000 m^2)	2.471	acres	ac
		MASS (weight)		
g	grams	0.0353	Ounces (avdp)	oz
kg	kilograms	2.205	Pounds (avdp)	lb
mg	megagrams (1000 kg)	1.103	short tons	T
		VOLUME		
mL	milliliters	0.034	fluid ounces (US)	fl oz
liters	liters	0.264	Gallons (liq)	gal
m^3	meters cubed	35.315	cubic feet	ft^3
m^3	meters cubed	1.308	cubic yards	yd^3

Symbol	When You Know	Multiply By	To Find	Symbol
		TEMPERATURE (exact)		
ºC	Celsius temperature	9/5 ºC+32	Fahrenheit temperature	ºF
		ILLUMINATION		
lx	lux	0.0929	foot-candles	fc
cd/cm^2	candela/m^2	0.2919	foot-lamberts	fl
		FORCE and PRESSURE or STRESS		
N	newtons	0.225	pound-force	lbf
kPa	kilopascals	0.145	pound-force per square inch	psi

Contents

List of Figures

List of Tables

Executive Summary

The grouted shear stud (GSS) connection was developed as a ductile alternative to conventional directly welded connections in steel bridge substructures. The connection is a socket type in which the socket is formed by a pipe stub which is shop welded to the cap-beam. The steel columns can then be inserted into the socket, and the annular region thus formed can be filled with high-strength cementitious grout to complete the connection. In addition to superior ductility capacity, the GSS connection provides other advantages such as potential use in accelerated bridge construction (ABC), and as a retrofitting option for seismically deficient bridges.

Although the GSS connection has been shown to exhibit exceptional structural performance under laboratory conditions, other issues required consideration before widespread deployment of the connection in practice. Since the Alaska Department of Transportation and Public Facilities (AKDOT) is interested in using this connection in their bridges, there was a need to investigate its long term durability in extreme cold climates. This project began with the motivation of investigating the durability of the GSS connection in cold climates. The GSS connection can be said to be durable if either the grout material is durable in cold climates, or if grout deterioration does not compromise the structural integrity of the connection.

First, four commonly available commercial grouts were chosen to determine their vulnerability to freeze and thaw damage and their propensity to cracking under restrained shrinkage. Experiments suggested that some grouts are indeed vulnerable to freeze and thaw

degradation while others show exceptional performance. However, material inconsistency was pervasive even among the grouts that performed well.

Since material durability tests were not conclusive in determining the connection durability, the next step was to determine if grout deterioration significantly impairs the structural capabilities of the GSS connection. Four Large scale steel bridge bent specimens (tests 1 through 4) incorporating the GSS connection were structurally tested. To determine the structural consequences of grout deterioration, the performance of specimens with deteriorated GSS connections (test 2 and test 3) was compared to that of a control specimen (test 1). The control specimen had standard high strength grout in its GSS connections, while the remainder of the specimens had grout mixed with expanded polystyrene (EPS) aggregates. The addition of EPS aggregates reduced the structural properties of the grout, such as its compressive strength and elastic modulus, simulating a GSS connection exposed to multiple years of service in cold climates.

Direct comparison between the global structural behavior of the bents with deteriorated connections and the control specimen suggested that grout deterioration does not have a significant impact on the capability of the GSS connection to successfully relocate the plastic hinge. Therefore, it can be concluded that the GSS connection is durable in cold climates.

For designing an optimum GSS connection, there was a need to better understand the force transfer mechanism within the connection. Large scale experimental data was subsequently used to investigate the force transfer mechanism. It was found that the number of shear studs in the connection does not significantly impact its structural performance. The socket depth of the GSS connection was found to be the most important parameter for successful relocation of plastic hinge into the steel columns.

Chapter 1

Introduction

1.1   Background

The grouted shear stud (GSS) connection for steel bridge substructures was developed by Fulmer et al. [16] as a ductile alternative to directly welded column to cap-beam connections. The use of structural systems consisting of hollow circular steel piles directly welded to HP or W-shape cap beams has been widespread. Fulmer et al. [17, 18] investigated multiple weld configurations to connect the pipe columns to cap-beams, including fillet weld, complete joint penetration (CJP) weld, CJP weld with a reinforcing fillet outside the pipe, and CJP weld with reinforcing fillets both inside and outside the pipe. They tested large scale two-column steel bents fabricated using the aforementioned weld details (Figure 1.1). The specimens were tested under cyclic quasi-static lateral loading until failure. Irrespective of the weld configuration, they observed undesirable brittle cracking at the weld or heat affected zones in the pile (Figure 1.2). They concluded that while welding steel pipe columns to cap-beams may be acceptable for non-seismic regions, designing such a connection in seismic regions without explicit consideration for protection of welded regions results in undesirable brittle cracking.

The GSS connection shifts the failure mode to the desirable plastic hinge formation in

Figure 1.1: Test set up from Fulmer et al. [17, 18] to test directly welded connections.

the column section thereby preventing premature damage at the weld or the heat affected zone.

The GSS connection is an external socket type connection and consists of a prefabricated cap beam (double wide HP was used by Fulmer et al. [16]) to which a stub pipe section is welded, as shown in Figure 1.3a. The stub pipe, larger in diameter than the column, acts as a socket into which the column can be inserted. In Figure 1.3a, the cap beam is shown on the left, resting on its top surface. The inner wall of the stub pipe contained 12 vertical lines of $\frac{3}{4}$ inch diameter shear studs. Similarly, the top of each pile section had 12 lines of studs, as shown in Figure 1.3a.

In the field, shear studs are welded to the pile after driving and cutting it at the proper elevation. No field welding (other than installation of the shear studs) is required in the construction of the GSS connection. After inserting the pile in the stub (Figure 1.3b), the moment resisting connection is completed by pumping a high-strength, non-shrink flowable grout into the annular region (Figure 1.3c). Fulmer et al. [16] tested two-column steel bents that use the GSS connection detail by subjecting them to cyclic quasi-static lateral loading. These tests showed the proof of concept that the GSS connection can successfully protect

<div align="center">(a)   (b)</div>

Figure 1.2: Brittle failure observed in [17, 18] on directly welded connections(a) Fillet weld (b) Complete Joint Penetration weld.

the welded region by relocating the plastic hinge formation to the steel column (Figure 1.3d) below the larger diameter pipe stub. The GSS connection also provided increased system displacement capacity when compared to the directly welded connections.

1.2 Advantages of the GSS connection

Seismic resistance

The primary motivation that led to the development of the GSS connection was enhanced performance under seismic conditions. The GSS connection enables a designer to make efficient use of the column moment and ductility capacity. By using capacity design principles, the connection and the cap-beam can be protected resulting in the column being the weakest link. As a consequence, the GSS connection eliminates premature brittle failure modes such as cracking at the weld or heat affected zones.

Accelerated bridge construction

Accelerated bridge construction (ABC) has received increasing attention over the last several years. The goal of ABC is to improve quality and reduce the duration of bridge construction. Rapid, high quality construction is especially important in regions that have short

(a)

(b)

(c)

(d)

Figure 1.3: Stages of the GSS connection: (a) Constituent components, (b) Connection before grouting, (c) Connection after grouting, (d) Failure by plastic hinge relocation.

construction seasons, such as cold climate regions. The interest in ABC has led to studies in socket and pocket style details of column connections. The majority of the previous studies have focused on pre-cast concrete. There have also been a few studies on steel bridge sub-structures for seismic applications. The GSS connection can be employed as part of ABC for steel bridge substructures. The cap-beam with pipe stub sockets can be pre-fabricated and brought to the site where it can be lowered onto driven piles until the bottom of the cap-beam bears on the pile top. The connection can then be formed and pumped with commercially available grout in little time to complete the construction process. The time required for field welding and welding inspection under conventional construction processes is mostly eliminated with the GSS connection.

Retrofitting option

Although the GSS connection was developed for new construction, it can be readily adapted for retrofit of steel bridges in which the pipe column to cap-beam connections are deficient. To accomplish this retrofit, the stub pipe is cut longitudinally to produce two semicircular stub pipe sections. Shear studs are welded to these stub pipe sections and to the top section of the existing pipe column. The stub pipe sections are then welded to the existing cap beam, and finally the two halves of the stub are welded together prior to grouting. While there is field welding to be performed, these welds are capacity protected, ensuring their satisfactory performance.

Redundant load paths

The results of large scale experiments discussed in this report indicate that multiple load transfer mechanisms are mobilized within the GSS connection to resist the axial force, shear force, and bending moment demands on the connection. This redundancy of load paths is desirable in structures. Conventional directly welded connections only provide a single load path, i.e. through the weld, for the same demand. A full qualitative description of the

components that contribute to the capacity of the connections is provided in Chapter 4.

Low sensitivity to construction tolerance

A high degree of quality control is necessary during the construction of directly welded connections as these welds are critical to the structural integrity of the system. This leads to high costs of welding. The structural performance of systems incorporating the GSS connection has a higher tolerance to construction errors. Fulmer et al. [16] compared the performance of two systems with the GSS connection where the first system had concentric columns and stubs, while the second system had the columns offset with respect to the stub. Both systems performed comparably under cyclic quasi-static lateral loading protocols. In one of the large scale experiments performed by us, the specimen had an out of plane inclination because one of the columns was inclined due to a fabrication error. The structural performance of this test was also comparable to the performance of the control test. These results indicate a higher allowable tolerance in the construction of the GSS connection.

Suitability for any system

The underlying mechanism of the GSS connection is plastic hinge relocation. The column to cap-beam interface is capacity protected to ensure plastic hinging in the column section. This mechanism is independent of the structural system. The GSS connection can hence be employed in steel, reinforced concrete, or reinforced concrete filled steel tube columns.

1.3 Motivation for this study

1.3.1 Understanding the implications of using the GSS connection

The GSS connection is relatively in its infancy compared to conventional approaches of connecting steel bridge columns to cap-beams. An understanding of the full set of implications of its use in practice requires further study. However, with reasonable and conservative as-

sumptions, Alaska Department of Transportation (AKDOT) can deploy these connections in practice sooner rather than later. A few areas that require attention to fully understand the implications of the GSS connection are:

1. Durability of the GSS connection in cold climates

2. Force transfer mechanism within the GSS connection

3. Sensitivity of the structural performance of the GSS connection to scaling in size

The scope of this project was to tackle the first item on the list, i.e., the durability of the GSS connection in cold climates. This report primarily focuses on the question of durability, the approach devised to address this question, the results, and the conclusion. A detailed discussion of the problem is provided in the next subsection.

The second and third items on the list are important aspects too but are beyond the scope of this project. However, an inquiry into understanding the force transfer mechanism within the GSS connection is discussed qualitatively in Chapter 4. This could be used as a starting point for further studies.

1.3.2   Application in Cold Climates

A geographical area of interest for practical application of the GSS connection for steel bridges is the state of Alaska, United States. It is widely known that Alaska is in a seismically active zone. Hence, the GSS connection is a good option to be used as it forces plastic hinge formation into the pile/column section as well as to provide satisfactory ductility capacity. However, the climate of Alaska is dominated by sub-zero temperatures for major portions of the year. It is therefore essential to characterize the durability of the GSS connection in cold climates.

To assess the durability of the GSS connection, it is necessary to investigate the durability of the constituent materials (structural steel and high-strength grout). One possible concern regarding low temperature performance of the columns is the undesirable brittle fracture of

steel. AKDOT prefers to use high quality steel, grade API 5L X52 PSL2, for pipe columns in new construction of bridge substructures. The mill certificates for the pipes that were ordered show that all of them have Charpy V-notch (CVN) toughness values exceeding 200 ft-lb at 32° F, which is typical of all API 5L PSL2 pipes. This high value of CVN toughness will be sufficient for satisfactory performance of the steel in the low temperature climate in Alaska [12]. A good summary of realistic performance requirements for structural steel is provided by Bjorhovde [12].

The use of grout makes the construction of the GSS connection rapid, which is desirable because of the short construction seasons in Alaska. However, during the service life of a bridge, these connections are exposed to a large number of freeze-thaw (FT) cycles, low temperature events, and large thermal gradients. These environmental conditions may adversely affect the performance of the connection due to mechanical degradation, i.e., cracking of the grout. In addition, the geometry of the connection and the presence of the shear studs might contribute to degradation of the grout as they provide restraint against shrinkage. The thermal strain mismatch between the grout and shear studs, and between the grout and the steel pipe pile may also cause cracking. Properly designed grouts can withstand a large number of FT cycles without degradation. This study aims to investigate whether the factors listed above pose significant concerns to the durability of the GSS connection.

To summarize, the questions that motivate this study are the following:

1. *Can the GSS connection be used in cold climates?*
   This will depend mostly on the grout filler used in the connection.

2. *How durable are commercial cementitious grouts in cold climates?*
   AKDOT prefers the use of commercial grouts over specifically designed grout mixes for ease of construction and to reduce construction errors. Hence, it is worth characterizing the durability of some commercially available grouts.

3. *Does the durability of the grout filler matter?*

The contribution of the grout properties to the overall structural integrity of the system is not fully understood. It could be that the grout filler may not have a significant contribution. Perhaps a deteriorated grout may not necessarily lead to a significant drop in structural performance. Experiments were necessary to answer this question.

1.4   Research Approach

To answer the questions posed earlier, this study approaches the problem from two different perspectives and is divided into two phases:

1. Grout Durability Tests, to assess the durability of the grout material, and

2. Large Scale Steel Bent Tests, to assess the consequences of deteriorated connections on the overall structural behavior.

Phase 1: Grout Durability Tests

In a journal article in 1980 [25], Litvan commented:

> "A statement concerning durability is meaningful only in the context of specified geographical areas and particular applications."

To evaluate grout durability, it was therefore essential to identify the specific geographical area and the practical application. Results and conclusions from the experiments discussed here are concerned with application of the grout material in the GSS connection in cold climate regions. From this perspective, the physical processes that cause concern are

1. Freeze and Thaw (FT) cracking

2. Early age shrinkage cracking

These concerns are discussed in detail in Chapter 2. Chapter 2 provides a full discussion of damage inducing mechanisms, standardized tests for evaluation, test results, and conclusions.

Investigation to determine the durability of cementitious grouts is referred to as Phase 1 in this report. The objective of Phase 1 was to identify behavior of some readily available commercial grouts with respect to aforementioned durability concerns. During Phase 1, typical characteristics of common cementitious grouts under short- and long-term exposure to cold climates were also observed and are reported in Chapter 2.

Although it would have been ideal to be able to specify and control the durability of the grout used in the GSS connection, Phase 1 results suggested that this may not be possible. In Phase 1, there were cases where specimens of a specific batch of a certain commercial grout performed well under freeze and thaw, while a different batch of the same grout showed poor results. There were also grouts from different manufacturers with similar bag labelled properties that showed highly variable results, ranging from excellent to poor, under freeze and thaw. All of the above led us to conclude that specifying an "ideal" grout for the GSS connection was unlikely.

Before delving deeper into the material level properties of cementitious grout, we moved to Phase 2 of the project to investigate whether grout durability significantly impacts the overall structural performance of the system in use.

Phase 2: Large Scale Tests

To determine the consequences of grout durability damage on their overall structural performance, three large scale two-column steel bridge bent specimens employing the GSS connection were tested. These were representative of typical steel bridge bents above the point of contraflexure under in-plane bending. The first test used standard unaltered high-strength grout to fill the annular space in the GSS connections. The second and third tests used the same high-strength grout, but with its compressive strength and elastic modulus artificially reduced to 40% and 70% of initial by adding a low density admixture. This reduction simulated an effective state of damage equivalent to when the grout is exposed to multiple years of service in extreme cold climates. If grout durability significantly impairs adequate struc-

tural performance of the GSS connection, the tests employing connections with simulated damage should have resulted in poorer performance compared to the control test. However, this was not the case. All three tests showed similar structural behavior which led us to conclude that grout durability is of little concern for the long-term performance of the GSS connection.

After completion of the first two tests, a meeting with Alaska Department of Transportation and Public Facilities (AKDOT) introduced a minor change of scope in the project. The remaining two large scale tests were subsequently used to better understand the force transfer mechanism within the GSS connection. We found that the dominant force transfer mechanism that resists the bending moment demand on the connection is the action of two equal and opposite normal forces developed within the connection. These forces act as a moment couple to resist the moment demand on the connection. We also found that a long stub length, as described later in this report, is necessary to achieve successful relocation of the plastic hinge into the columns. Moreover, the role of the number of shear present in a connection was found to be less impactful than was previously assumed.

The method of artificial damage simulation, through which a grout damage state was achieved representative of years of service life, is discussed in Chapter 3. The large scale tests performed to determine the consequences of grout damage on the structural performance of the GSS connection is discussed in detail in Chapter 4. The investigation conducted to better understand the force transfer mechanism in the GSS connection is discussed in Chapter 5.

1.5   Chapter Summary

This chapter introduced the grouted shear stud connection, also referred to as the GSS connection. The GSS connection was developed as a ductile alternative to directly welded connections in steel bridge substructures. In addition to its superior seismic performance, the GSS connection scores highly in its potential to be used within the framework of ac-

celerated bridge construction. It is suitable for use as a connection detail for structural steel, reinforced concrete, or reinforced concrete filled steel tube bridge bent systems. Unlike directly welded connections, the GSS connection provides redundant load paths for force transfer. Construction of systems with the GSS connection offer higher tolerances compared to directly welded connections. With minor modification in the construction process, the GSS connection can also be deployed as a retrofitting option for deficient bridge systems.

The primary motivation for this study can be summarized in a single question: *Can the GSS connection be used in cold climates?*. To answer this question, the project was divided into two phases. Phase 1 investigated the durability at the material level, i.e., durability of cementitious grouts that could potentially be used in the GSS connection. Phase 2 investigated at the system level, whether grout durability matters from the perspective of long-term structural performance. The project was able to successfully show that although some grouts are durable and some are not, durability does not affect the overall structural performance. This report discusses these results in detail.

Durability of cementitious grouts (Phase 1) is discussed in Chapter 2 while the structural consequences of durability damage on the GSS connection (Phase 2) is discussed in Chapter 4. A qualitative assessment of the force transfer mechanism within the GSS connection is provided in Chapter 5. Finally, Chapter 6 provides overall conclusions and recommendations regarding the GSS connection for engineering practice.

Chapter 2

Durability of Cementitious Grouts in Cold Climates

2.1   Introduction

The GSS connection is a composite connection composed of a hollow steel socket, an inner steel pipe, steel shear studs, and a high-strength cementitious grout. The force transfer between the column pipe and cap-beam takes place through the grout ring and hence it is important to characterize the properties of cementitious grout. Tests performed on GSS connections by Fulmer et al. [16] have shown that a high-strength grout can successfully transfer the forces and relocate the plastic hinge to the column section. However, these tests were performed in laboratory conditions on specimens with standard grout. In reality, bridges are exposed to a variety of extreme environments for many years. If engineers were to use the GSS connection in practice, they must expect some amount of grout deterioration. The amount of deterioration that could be expected is currently unknown, as few studies have investigated the durability of cementitious grouts, let alone in the specific setting of the GSS connection. Our objective for Phase 1 of this project was to obtain information in this regard through various experimental means.

In porous materials, water is generally involved in every form of deterioration, and with cementitious materials, the ease of penetration of water into the solid usually determines the rate of deterioration. Durability under one set of conditions does not equate to durability under another, and therefore it is important to specify a target environmental condition before proceeding with durability determination. Phase 1 of this project evaluated the durability of commercially available cementitious grouts in extreme cold climates.

Durability of concrete has been widely studied, and there exist standard test procedures to evaluate the durability of different concrete mixtures. The assumption in this study is that grouts are different from concrete only with respect to the absence of coarse aggregates. Both are porous materials, and therefore the standard test methods to evaluate degradation of one can be applied to the other. In the specific application of the GSS connection, two major issues that can potentially cause degradation and in turn cracking of the grout material in Alaskan cold climates are freeze and thaw cracking, and restrained shrinkage cracking. Cementitious materials are prone to damage under repeated freezing and thawing when they contain water at or above a critical degree of saturation. The major focuses of this chapter are to 1) explain the mechanisms of frost damage, (2) describe different test methods that are prevalent to assess freeze-thaw (FT) resistance of cementitious materials, (3) describe tests performed as part of this study, and (4) provide conclusions.

Due to the complex geometry and the presence of embedded steel shear studs, the GSS connection may cause considerable early age restrained shrinkage cracking. Early age cracking is important since it can result in the reduction of service life of the grout, and in turn of the connection by allowing water and contaminants to enter the cracks causing corrosion to occur furthering grout cracking and deterioration.

In this chapter, a study carried out to determine the compressive strengths of some commonly available high-strength cementitious grouts is discussed. After introducing the different grouts used in this study, mechanisms of FT damage are discussed followed by a review of some of the most used test methods to assess FT resistance of porous materials.

Following this discussion, the results of the tests performed as part of this study are provided.

The materials that performed well under FT testing were chosen to perform restrained shrinkage tests (ring tests) to investigate their early age cracking potential. To assess the impact of the presence of shear studs in the GSS connection on the shrinkage cracking behavior, the ring tests were then performed on specimens with shear studs embedded in them. These specimens simulated actual geometrical conditions within a real GSS connection. Before discussing the results of all the restrained ring tests, a review of the latest literature on the ring test is presented. This chapter is then concluded with a section summarizing the inquiry into assessing the durability of commercial grouts. A set of qualitative recommendations are provided regarding good practices for choosing, mixing, and placing of the grout.

2.2 High-Strength Cementitious Grouts

Cementitious grouts are proportioned Portland cement based mixtures prepared by combining Portland cement, fine aggregate, and some combination of mineral and chemical admixtures, that are sold commercially in bags for instant use. Normally, these bags are mixed, in situ, with a manufacturer specified amount of water. These grouts are proportioned so that they exhibit good flowability and workability. Over the years, high-strength cementitious grouts have been used in a multitude of applications such as crack injection, anchorage sealing, and post-tensioning applications [22, 37]. Lately, high-performance grouts are also being used for structural repair and retrofit of bridges [36]. The GSS connection is yet another example of cementitious grouts making their way into large scale applications.

Before moving to the durability aspects of commercial grouts, a small study was undertaken to ascertain the strength characteristics of cementitious grouts to gauge the current state-of-practice. As part of testing the compressive strengths of the grout filler being used in the large scale tests, the scope was again expanded to include a series of compressive strength tests performed on four different high strength cementitious grout materials. Tests were per-

formed on both 2" × 2" cubic samples and 4" × 8" cylindrical samples. The objectives of the tests were to investigate the following:

1. Variability of compressive strength values for cubic samples.

2. Differences between cylinder strength and cube strength of cementitious grouts.

3. Compare compressive strengths of typical high strength grouts.

All the different grout materials that were tested are given in Table 2.1. These were labelled CG1 to CG4. The size and testing protocol for testing cylindrical samples followed ASTM C39 [4]. ASTM C109 [1] specifies the cubes to be cured in lime water after 24 hours whereas the specimens tested here were sealed cured. The standard does not specify the use of polymer pad caps over the loading faces. However, such caps were used to test these samples. Samples were tested on their 3rd, 7th, 28th and 90th day after casting.

Table 2.1: Material used, bag weights, and the amount of water added in each mixture

Material	Bag Weight (lbs.)	Water added per bag (lbs.)	Consistency label[*]
CG1	55	8.5	-
CG2	50	8.4	Flowable
CG3	50	6.6	Flowable
CG4	50	9.3	Flowable

[*] Label specified by manufacturer corresponding to the amount of water

The average strengths of cube and cylinder samples at different ages are provided in Table 2.2 . The coefficients of variation of each value in Table 2.2 are provided in Table 2.3 .

Overall, cylinder strength values showed less variation compared to cube strength values. This was expected as cylinders, being large samples, are more homogeneous along the length-scale as compared to the smaller cubes. The average coefficients of variation for cubes and cylinders were 0.06 and 0.03, respectively. Figure 2.1 provides a graphical representation of the data. Note that the cubes for CG3 show almost equal strength at all ages, a result which is not consistent with the cylinders from the same batch. A likely reason for this is

Table 2.2: Summary of the results - average compressive strengths

Average Strengths (ksi)

Grout	3-day		7-day		28-day		90-day	
	Cube	Cylinder	Cube	Cylinder	Cube	Cylinder	Cube	Cylinder
CG1	8.44	7.84	10.20	8.80	11.47	10.60	12.27	11.04
CG2	7.19	7.16	8.93	8.04	9.91	9.05	10.44	9.60
CG3	10.21	8.10	10.41	8.91	10.41	9.86	-	-
CG4	6.47	5.60	7.15	7.42	8.60	8.43	10.76	9.44

Table 2.3: Summary of the results - coefficients of variation for average compressive strengths

Coefficients of Variation

Grout	3-day		7-day		28-day		90-day	
	Cube	Cylinder	Cube	Cylinder	Cube	Cylinder	Cube	Cylinder
CG1	0.05	0.03	0.03	0.00	0.07	0.07	0.04	0.07
CG2	0.02	0.04	0.04	0.04	0.05	0.02	0.10	0.05
CG3	0.05	0.01	0.03	0.03	0.08	0.03	-	-
CG4	0.11	0.02	0.12	0.02	0.09	0.05	0.08	0.04

improper curing. Cubes of CG3 grout were not sealed after demolding due to misplacement. Drying ensued preventing further hydration. This halted strength gain. The authors would like to emphasize the importance of curing for strength test samples, especially for cubic specimens since they can lose significant amount of moisture rapidly. Data from other grouts, which were cured without moisture loss, show an increase in strength with age. The error bars indicate one standard deviation above and below the mean of the sample data. Compressive strengths of cubes are higher than those of cylinders, on average. This conforms to expectations as specimens with higher aspect ratios show lower strengths due to localization [27]. Cube and cylinder samples had an aspect ratio of 1 and 2 respectively. Both classifications of strength show the same pattern of increase with age, which indicates that measuring strength of grout cubes can be a valid alternative to measuring strength of grout cylinders, if all steps of testing are performed properly. CG1 and CG3 showed high strengths very early and kept increasing up to 90 and 28 days respectively. CG2 and CG4 had comparatively lower early age strength and a lower 90-day strength compared to
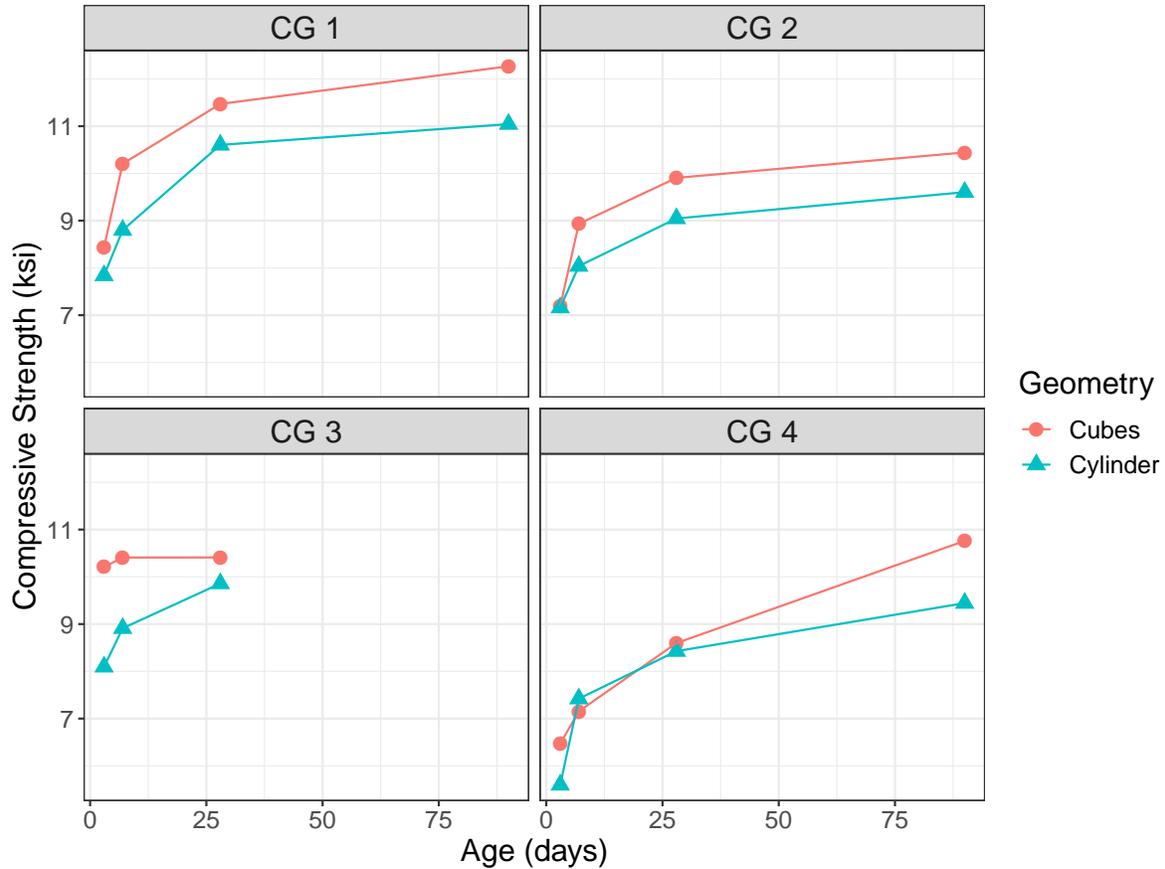
Figure 2.1: Comparison of cube strength and cylinder strength for all the tested grouts.

CG1 and CG3. A comparison between the measured and manufacturer specified values of compressive strength are provided in Table 2.4. Note that the measured strengths equal or exceed the manufacturer specified strength.

All the average cylinder strengths are compared to their corresponding average cube strengths in Figure 2.2. Any point on the red line are points of equal strength. Cube strengths are almost always greater than cylinder strengths as can be observed from the fact that almost all points lie above the red line. The data is also suggestive of a linear correlation between cube and cylinder strengths. A linear fit to the data is shown in Figure 2.2.

To summarize, high-strength cementitious grouts are Portland cement based mixtures that can be readily used by mixing with water. They have high flowability and workability to be able to fill structural cracks, post-tensioned cable sleeves, anchor holes etc. They

Table 2.4: Comparison between the measured and manufacturer specified compressive strength values for cementitious grouts.

Material	Water added per bag (lbs.) [1]	Specified Strength (ksi)[2]	Measured Strength (ksi) [3]
CG1	8.5	8.0	10.6
CG2	8.4	8.0	9.1
CG3	6.6	10.0	9.9
CG4	9.3	8.0	8.4

[1] Amount of water corresponds to flowable consistency.
[2] Specified by the manufacturer for corresponding consistency.
[3] 4"×8" cylindrical samples.

generally develop high early age strength which can be measured using either cylindrical or cubical samples. For sufficient strength development, good curing practices are crucial.

2.3 Freeze and Thaw Cracking

2.3.1 Mechanisms of Freeze-Thaw Damage

Concrete is made up of four main components: cement, water, fine aggregates, and coarse aggregates. Cement in combination with water (also called as cement paste) binds the aggregates together to form structural concrete. Cyclic freezing and thawing can result in damage and degradation of concrete in the presence of a sufficient amount of moisture in its pore structure. The component of concrete largely vulnerable to freeze and thaw damage is the cement paste. The main mechanism by which formation of ice damages cement paste is the repeated expansion and accumulation of water during FT cycles. A large body of literature exists regarding frost damage mechanisms in porous materials. The two most accepted mechanisms for FT damage in concrete are:

1. The hydraulic pressure mechanism due to ice formation, and

2. The microscopic ice body growth

The hydraulic pressure mechanism is caused by the 9% volume increase when water
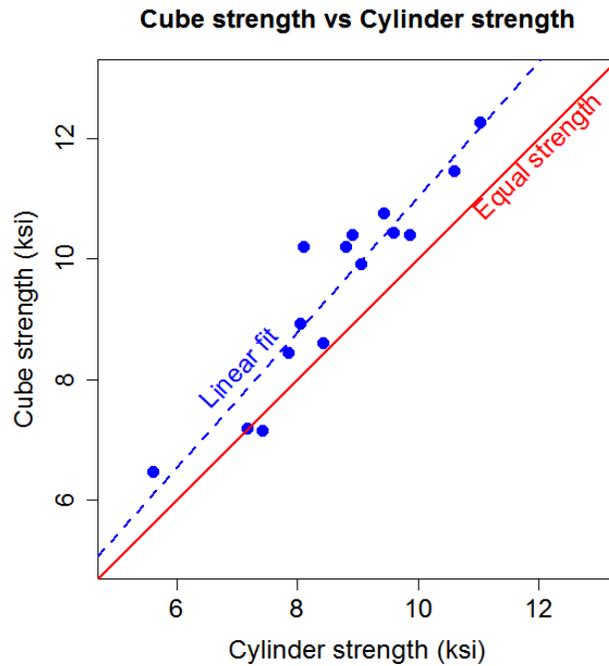
Figure 2.2: All average cube strengths versus average cylinder strengths.

transforms to ice [10]. In a saturated pore system, this leads to an increase in the water pressure which, if greater than the tensile strength of the surrounding cement paste matrix, results in crack formation. According to the microscopic ice body formation theory, ice forms as micro lenses in the pores. Such micro lenses in porous materials act in two opposing ways [34]:

1. The free pore water moves towards the micro ice lenses which will therefore grow and exert pressure on the surrounding pore walls, leading to an increase in volume of the paste.

2. On the other hand, the driving forces that cause the water to move towards these ice lenses also may draw water from the gel pores resulting in shrinkage of the paste.

The resulting damage is believed to be a cumulative effect of the two processes which may depend upon a number of other factors such as the critical degree of saturation (discussed later), availability of external water, rigidity of the microstructure gel [34] etc. Any volume

dilation due to ice formation in the freeze cycle can propagate cracks which can then be filled with more water in the subsequent thaw cycle. With each successive FT cycle, damage accumulates [34].

It has also been found over the years that there are common factors that influence frost damage in any porous cementitious material [25] such as:

1. Flow Distance (D)

2. Degree of Saturation (S)

3. Cooling Rate

Flow distance is an approximate measure of the greatest distance that water must travel to the nearest air-filled space (or the surface) without causing damage. Damage occurs when the flow distance is greater than the critical flow distance (D_{cr}). In theory, if water could leave the capillary pores of the material during the cooling period, ice forms outside the capillary pores or within large empty air voids, causing no damage. Due to a high cooling rate, high degree of saturation, or a long diffusion path, if water cannot escape and solidifies inside the capillary pores, mechanical damage ensues. Any porous material can be destroyed by enough freezing and thawing by saturating it above the critical degree of saturation. This means that for frost resistance testing, there is a need to assess the FT resistance of the material under representative exposure conditions.

Degree of saturation (S) is the ratio of the total volume of water/moisture to the total volume of voids present in the porous material. A fully saturated system will experience significant damage even in a single FT cycle [26]. In general, FT damage occurs when the degree of saturation is greater than the critical degree of saturation (S_{cr}). The critical degree of saturation (S_{cr}) is considered as the point (or a region) along the saturation axis beyond which considerable damage occurs, measured usually by the decline in the elastic modulus. Figure 2.3 shows an example plot from several experiments collected by Fagerlund [15]. The decline in elastic modulus can be clearly seen for tests done on different specimens in

21
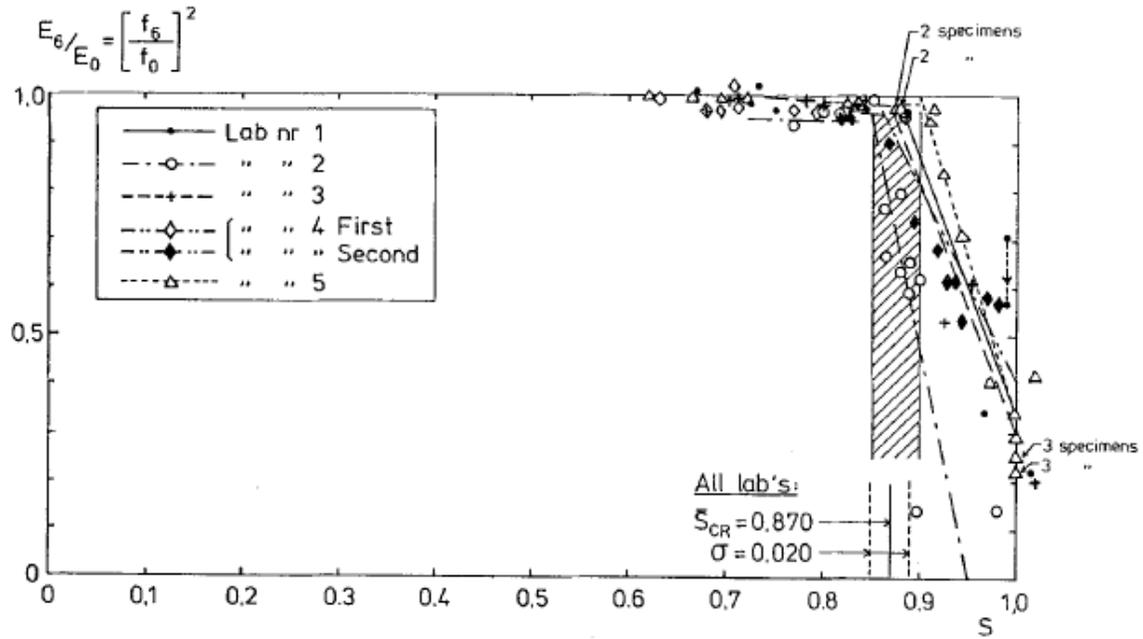
Figure 2.3: A sample plot showing dynamic elastic modulus vs degree of saturation for concrete specimens tested in five different laboratories [15].

different labs. It is also worthwhile to note that most S_{cr} values lie within a common region (the striped region in Figure 2.3). This was found to be approximately within 0.86-0.88 degree of saturation. A simplistic way to understand this is by using the idea of volume expansion of water when frozen. Water expands by about 9% when frozen. After allowing for this expansion, the critical degree of saturation should become 0.91. This is close to the measured values between 0.86 to 0.88. The water expansion model is a simplified model and the deviation from the measured values can be attributed to more complex mechanisms.

Li et al. [24] studied the effect of water ingress and the role of air content in FT damage of pavement joints. It was found that water ingress had deleterious effects on the concrete, corroborating earlier observations of Litvan [25]. It was also found that air entrainment, which is a widely accepted method of preventing frost damage, provides resistance by delaying the attainment of the critical degree of saturation (S_{cr}). This means that the value of S_{cr} is more or less fixed for cementitious materials. This value also helps in many ways to determine the potential of frost damage and also, to an extent, predict the service life of the
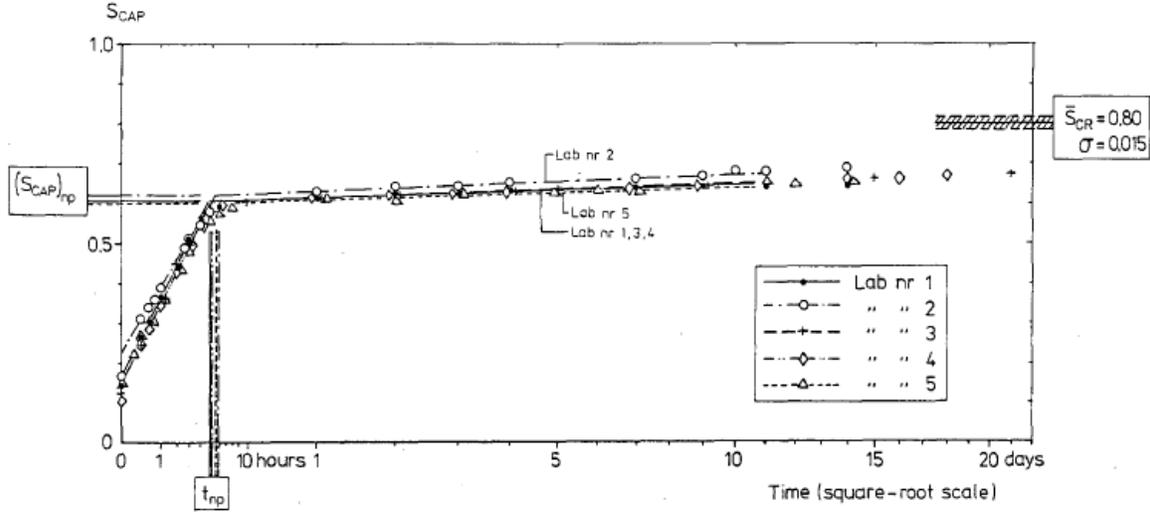
Figure 2.4: A sample plot showing mean values of capillary degree of saturation vs time of water uptake [15].

material.

Water uptake is another measure that can be related to frost damage. It is normally measured by having a thin slice of the material in contact with the surface of water. Weight measurements can be made at regular intervals to determine water uptake. Water uptake or absorption potential depends on the capillary system formed within the material. There are two different aspects of water uptake that have interested researchers. One is the absorption without undergoing FT cycling and the second is the absorption under FT cycling. Fagerlund [15] introduced a term called capillary degree of saturation (S_{cap}) which proved to be a convenient parameter to estimate the frost resistance of concrete. If a concrete specimen is subjected to a test in which its ability to absorb water is measured, its absorption rate can be monitored, and a point in time is reached when this rate declines drastically, as shown in Figure 2.4. The degree of saturation of the specimen at this point is called the capillary degree of saturation (S_{cap}). For each type of concrete, each environment can be translated to a certain water uptake time or S_{cap} value. The difference between S_{cr} and S_{cap} for a material can be used as a good indicator of potential FT resistance of the material.

Generally, FT resistance for cementitious materials is achieved by

1. Reducing the water-to-cement (w/c) ratio of the mixture,

2. Increasing the air content, and/or

3. Decreasing the paste content (increasing the aggregate content).

Reducing the w/c ratio

The w/c ratio is the ratio of the amount of water by weight, to the amount of cement in a mixture. Water in the cement mixture is mostly consumed in the chemical reaction of cement hydration which forms the hardened microstructure. However, the excess water that is not consumed ends up as capillary pores within the material microstructure. The larger the amount of excess water, the larger the pore volume inside the material. The water inside these pores expands when freezing which in turn causes cracking inside the material. Hence, reducing the w/c ratio of the mixture is one way to reduce FT vulnerability.

Increasing the air content

Air entrainment is an alternate way of increasing the FT resistance of cementitious materials. Air voids when introduced into the microstructure allow space for water to expand into, thus reducing the tensile stress on the rest of the microstructure. However, air entrainment only delays FT damage. When all the air voids are filled by the cumulative effect of FT cycling, subsequent cycles can damage induce damage.

Decreasing paste content

This method is only effective in concrete, not grout, as it has the additional component of coarse aggregates in its microstructure. The water in concrete is held as part of the hardened cement paste. This cement paste is the most vulnerable component to FT damage. An indirect way of increasing FT resistance of concrete is by reducing the cement paste content. This can be achieved by increasing the volume fraction of the coarse aggregate in the design

mix.

2.3.2 A Review of Freeze-Thaw Testing Methods

A large number of FT test methods exist in the literature. Albeit different in other aspects, they all follow the same core principle. Concrete specimens are subjected to a predetermined freezing and thawing cycle for a specified number of cycles. Based on the requirement of the application, different variations have emerged over time. The most widely used FT test is the ASTM C666 [5].

ASTM C666 provides an accelerated test method in which specimens are subjected to a maximum of 300 FT cycles. The damage in the specimens is monitored by measuring the dynamic elastic modulus after a predetermined number of cycles. This test may be terminated before 300 cycles if the reduction in elastic modulus is greater than 40%. The 40% value is derived from empirical observations correlated to the point where visible cracking is observed in FT specimens. In this test, specimens are subjected to FT cycles between 40°F (4°C) and 0°F (-18°C). The specimens are prismatic (12" × 3" × 3") and are cured for 14 days in saturated lime water after demolding. The outcome of a single test is a dimensionless Durability Factor (DF) which is based on the terminal relative dynamic modulus of elasticity and the total number of FT cycles. Further details of ASTM C666 test method is provided later in this report.

According to Janssen [21], a good assessment of FT resistance should be based on three factors:

1. Internal cracking of the paste,

2. Internal cracking of aggregates, and

3. Surface scaling.

Among these factors, only the internal cracking of the paste is relevant to the durability of the GSS connection because sound fine aggregates, i.e., aggregates resistant to degradation,

as defined by ASTM C88 [6], are used in the mixture. Due to the small exposed surface of the GSS connection grout, surface scaling is also not of concern. Janssen [21] also added that it is vital to have a good simulation of the exposure conditions that include temperature exposure, moisture availability, and drying conditions. Specifically, to closely simulate the microstructural damage of the cementitious material that corresponds to damage in field exposure conditions, "some" method of specimen conditioning that includes cycles of drying and rewetting, is required.

According to Auberg [7], estimation of service life can only be accomplished by knowing the expected environmental loading on the material. The duration and temperature range of the test should therefore be representative of the actual exposure conditions. The actual degree of saturation at the beginning of frost attack and the additional water absorption in the thawing phases are the main parameters that should be considered in investigating FT durability.

Over the years, ASTM C666 has been criticized for specifying a severe exposure that does not represent normal field exposure. Furthermore, the specimens are tested immediately after the curing period and hence no specimen conditioning is carried out. Since the outcome of ASTM C666 is only a Durability Factor (DF), a complete picture of the frost resistance and service life of the material cannot be obtained. Quantities such as the critical degree of saturation (S_{cr}) and water uptake potential, not obtained from the ASTM C666 testing protocol, are more meaningful in assessing material durability. Nevertheless, ASTM C666 is a simple and straightforward test to compare the FT performance of different materials. The scope of this study is limited to investigating the current state of high-strength cementitious grouts with respect to applicability in the GSS connection under cold environmental conditions. Hence, it was established as the standardized test of choice for this study.

Among other alternatives, two test methods are discussed next for completeness in presenting past literature. These test methods are: the Critical Degree of Saturation method [14] and the Capillary suction, Internal damage, and freeze-thaw (CIF) test [35]. Although

26

these test methods provide more information regarding FT resistance of a material, they require more complicated test setups compared to ASTM C666, and both require significantly more time. Furthermore, application of these test methods to the GSS connection is impractical due to the required measurements of degree of saturation as a function of time, critical degree of saturation, and water sorption characteristics of the material as further described below. Both of these tests have been part of RILEM (International Union of Laboratories and Experts in Construction Materials, Systems, and Structures) recommendations in the years 1977 and 2004, respectively, and their relevance is discussed in some detail here.

Critical Degree of Saturation method

This method, proposed by Fagerlund [14, 15], is based on the existence of critical moisture contents or degrees of saturation beyond which materials experience damage during freezing. The test is carried out in two parts, first the critical degree of saturation (S_{cr}) is determined and second, the determination of the capillary degree of saturation (S_{cap}). S_{cr} is determined by a test in which sealed specimens containing different amounts of water are subjected to a few FT cycles. Other specimens of the same material type are subjected to a test in which their ability to absorb water is measured. The FT resistance, F, is then defined by:

$$F = S_{cr} - S_{cap} \tag{2.1}$$

S_{cr} is essentially independent of outer climatic conditions. Theoretically, for each type of concrete, each environment can be translated to a certain S_{cap}. Therefore, F expresses the potential FT resistance of a certain concrete type used in different environments. The fundamental difference between this method and other traditional methods is that traditional methods investigate specimens of only a single degree of saturation and indicate whether the concrete is damaged at that particular water content. In other words, traditional methods such as ASTM C666 evaluate the material at the most severe degree of saturation which may not represent true exposure conditions, and a material that may fail the test may still

perform well under actual conditions.

In the S_{cr} method, the initial degree of saturation of specimens is varied and the corresponding damage after equal numbers of cycles is plotted. This means that one can consult these plots to estimate the expected damage for any initial degree of saturation. While the initial degree of saturation may be important to estimate the expected damage, it is unknown and difficult to determine. Therefore, the initial degree of saturation is not a consideration in this study of the durability of the GSS connection. The risk for an increase of water content can also be judged from the experimentally determined water absorption curves such as those provided by Fagerlund [14, 15]. Hence, all materials can be tested and evaluated in exactly the same way, irrespective of where and how they are used. However, this method of testing is elaborate and requires a significant amount of work to perform.

Capillary suction, Internal damage, and Freeze-thaw (CIF) Test

The CIF test was proposed to obtain a large amount of information regarding durability of a concrete material from a single test. This test incorporates conditions representative of the realistic exposure conditions. The aim is to conduct a test from which it would be possible for designers to predict FT durability and service life of a material. The test method is combined with the measurement of surface scaling. Although the duration of the test is shorter compared to ASTM C666, it requires more complicated instrumentation.

Adding to the methods that have been listed here, there exist numerous other techniques developed for FT testing. A comparison of different test methods is difficult because each of them has been designed for specific purposes. Moreover, the criteria for durability is greatly dependent on environmental loading, specific application in practice, and the test methods used. Standardized test methods have been developed principally for the purpose of quality control. For research applications, the best understanding of concrete behavior may be obtained using multiple methods simultaneously.

2.4 Freeze and Thaw Resistance of Commercial Grouts

2.4.1 ASTM C666 Test Procedure

Four commonly available commercial grouts were tested according to ASTM C666. The specimens were 3"×3"×12" prismatic beams prepared in steel molds, as shown in Figures 2.5a and 2.5b. The specimens were cured under saturated lime water for 14 days after de-molding. Identical specimens were required as controls to monitor the temperature inside the material during the testing because ASTM C666 specifies the control of the core temperature of the samples rather than the ambient temperature. Thermocouples were embedded within the control specimens (Figure 2.5c) for continuous acquisition of temperature data. A cycle period of 6 hours was used which enabled 4 cycles per day. The specimens were submerged in water throughout the testing and were kept in steel trays that were fabricated in-house meeting ASTM requirements. The specimens were subjected to FT cycles between 40 ± 3 °F (4 ± 2 °C) and 0 ± 3 °F (-18 ± 2 °C) in an environmental chamber (Figure 2.5d and Figure 2.5e) that was capable of being programmed with a pre-defined temperature cycle. A typical temperature cycle for the control specimens and the chamber air is shown in Fig 2.6.

ASTM C666 specifies to assess material damage by monitoring the reduction in its relative dynamic elastic modulus. This was done in the following manner. The fundamental frequency of all specimens was measured at 40°F prior to subjecting them to testing. During testing, the specimens were removed from the chamber at intervals of no greater than 36 cycles to measure their fundamental frequency at that point. Since the dynamic elastic modulus of the material is directly proportional to the square of its fundamental frequency (Equation 2.2), the ratio of the squares of the frequencies is equal to the relative dynamic elastic modulus (RDME) as shown in Equation 2.3. The results are plotted in a graph with the number of cycles on the x-axis and RDME (E_N/E_0) on the y-axis. Specimen damage is represented by a decrease in RDME as the number of cycles increase. Note that the term
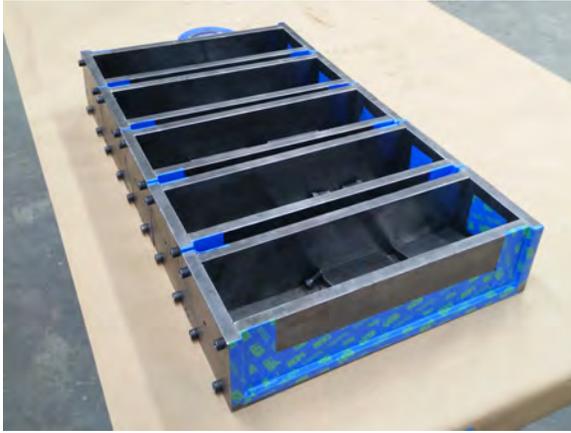
(a)
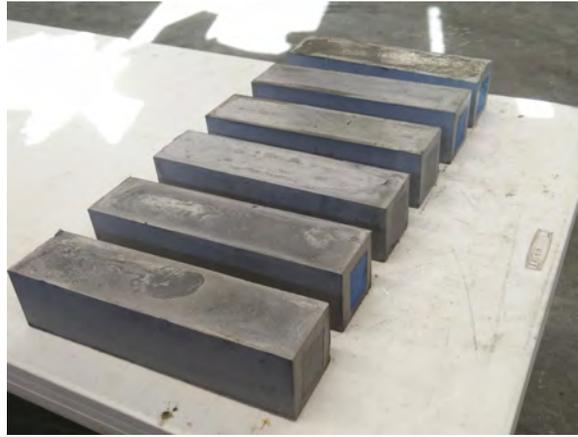
(b)
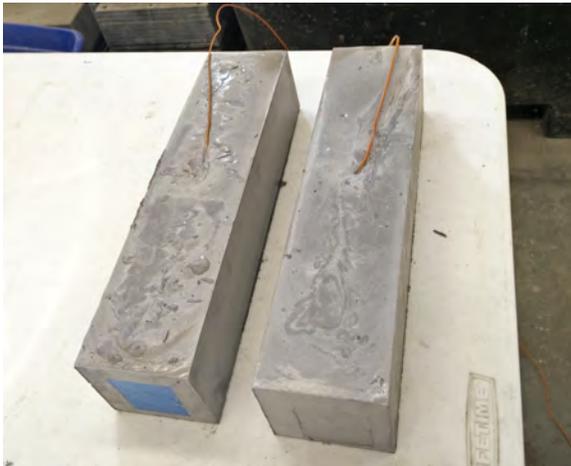
(c)

(d)

(e)

(f)

Figure 2.5: Photographs of various steps during the FT resistance testing procedure.
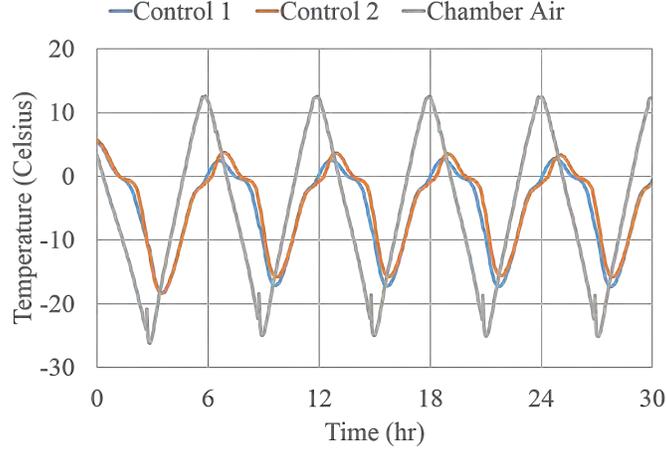
Figure 2.6: Typical cycles of the two control specimen temperatures and the environmental chamber air temperature.

RDME and the ratio E_N/E_0 have been used interchangeably throughout this report.

$$E_D \propto f^2 \qquad (2.2)$$

$$\frac{E_N}{E_0} = \frac{f_N^2}{f_0^2} \qquad (2.3)$$

where,

E_D = Dynamic Elastic Modulus

E_N = Dynamic Elastic Modulus after N cycles

E_0 = Initial Dynamic Elastic Modulus

f_N = Fundamental natural frequency after N cycles

f_0 = Initial fundamental natural frequency

Measurement of the fundamental natural frequency of prismatic specimens was carried out according to ASTM C215 [3]. The setup is shown in Figure 2.5f. An accelerometer was attached to one of the ends of the specimen. The specimen was then placed on a damping mat and was impacted at the center with a hammer. The acceleration response of the specimen was recorded by an oscilloscope (Figure 2.7a). This time domain response is then

Table 2.5: Grout mixtures tested under ASTM C666.

Mixture Code	Water Content per bag (lbs.)	Durability Factor (DF)	Concluding Remarks
CG1	8.5	100%	Good Performance
CG1	9.0	100%	Good Performance
CG2	8.4	100%	Good Performance
CG3	6.6	100%	Good Performance
CG4	9.3	46%	Poor Performance
PG1	w/c=0.46	<10%	Extremely Poor Performance

converted computationally into the frequency domain (Figure 2.7b) to obtain the frequency corresponding to resonant peak, i.e., the fundamental natural frequency.

ASTM C666 defines a dimensionless number to be used as a parameter to compare different materials, called the durability factor. The durability factor (DF) according to ASTM C666 is defined as:

$$DF = \frac{P \times N}{M} \tag{2.4}$$

where P is the relative dynamic modulus of elasticity at N cycles (E/E_0) in %, N is the number of cycles at which P reaches the specified minimum value for discontinuing the test or the specified number of cycles at which the exposure is to be terminated, whichever is less, and M is the specified number of cycles at which the exposure is to be terminated.

ASTM C666 Procedure A was performed on four different high-strength commercial cementitious grouts and one conventional concrete mix. Table 2.5 provides a summary of the results obtained for different materials. CG1-CG4 stand for cementitious grouts one to four, and PG1 stands for pea-gravel concrete.

Oscilloscope output

(a)
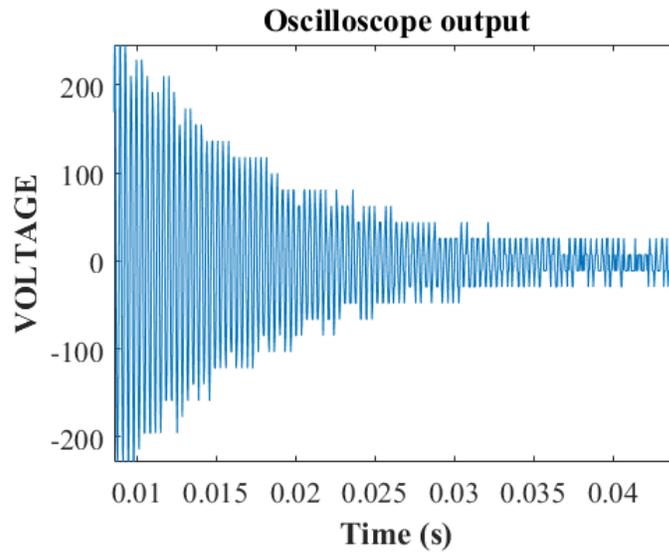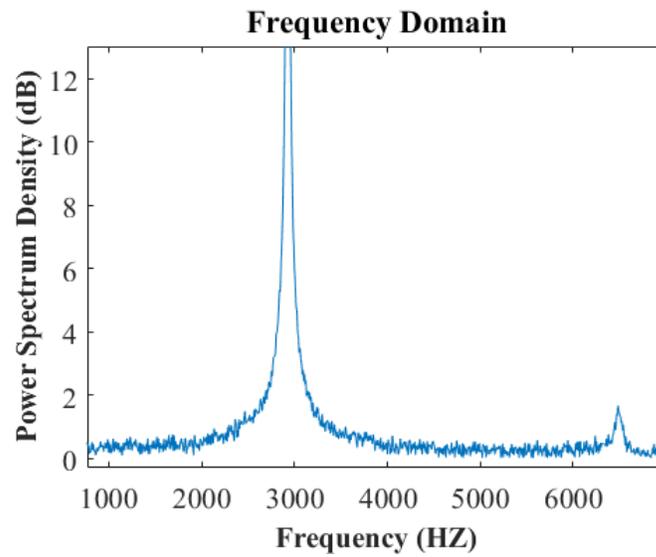
Frequency Domain

(b)

Figure 2.7: A typical time domain and frequency domain pair of specimen acceleration responses.

2.4.2 Exploratory Investigation

To form some basis for detailed testing of different commercial grout materials, a series of specimens of the material labeled CG1 in this report was tested under FT cycling. Grout CG1 was chosen since it was the same material used in the fabrication of large scale structural test specimens by Fulmer et al. [16]. These CG1 specimens were divided into different batches depending on variables such as curing conditions and total water content per bag. Not all of these batches could be tested to completion due to unforeseen technical issues. Only those batches that were completed are discussed here.

Since w/c ratio is an important parameter for FT resistance, an initial choice had to be made regarding the amount of water per bag of grout. Note that for commercial grouts, the mix proportion in a bag is proprietary. Therefore, it is impossible to ascertain the w/c ratio for a mixture. Accordingly, the water content per bag of grout was used as an indirect measure of the w/c ratio. The manufacturer specified range of water content per bag for CG1 was 9.0 lbs. to 10.5 lbs. Since FT resistance increases with reduction in total water content per bag, the minimum specified amount of 9.0 lbs. was chosen. The first batch of specimens E1 to E6 (not shown here) were terminated prematurely due to widely inconsistent behavior between specimens. These cured for more than the ASTM C666 specified 14 days. The inconsistency may have been due to poor quality of grout in that bag, or poor mixing quality. This was corroborated by subsequent results discussed later.

The second batch of specimens E7 to E11 was tested according to ASTM C666 and the results are shown in Figure 2.8a. The y-axis shows the E/E_0 ratio which is an indicator of damage. E is the elastic modulus of the specimen at the time (cycle number) of measurement and E_0 is the baseline elastic modulus of the same specimen before start of FT cycling. A higher reduction in elastic modulus is an indicator of a larger amount of damage due to cracking. The reduction in RDME was consistent among the specimens and all but one of the specimens completed 300 FT cycles above 60% RDME (ASTM C666 specified cut off). In hindsight, the drop in RDME is thought to be caused by another instance of poor bag of

grout and mixing quality. Although, at the time, it was thought that the reason for material degradation could have been the severe nature of ASTM C666 Procedure A. To test this hypothesis, the next batch of specimens was cured in a sealed condition.

The third batch of specimens E12 to E16 was cured in sealed plastic bags after demolding. It was believed that curing in water may have been too severe of a condition. Curing in a sealed condition alleviates this issue by reducing the degree of saturation below the critical degree of saturation thereby improving the FT resistance. Sealed curing also more closely represents actual environmental conditions of the GSS connection since it is open only from one side and is rarely under water. Results of this batch are shown in Figure 2.8b. Clearly, they behaved contrary to expectations of better performance compared to the second batch. All specimens showed rapid deterioration within the first 100 cycles. Hence, the hypothesis that the second batch degraded due to the specimens being at a high degree of saturation due to curing under water before FT cycling, can be rejected. Consequently, new questions arose as to why the sealed cured specimens performed worse. One reason could have been a still high degree of saturation due to the high initial water content of 9.0 lbs. This was rejected upon obtaining more results that are discussed later in this report. Batches four and five were cast with a reduced 8.5 lbs. of water per bag. Note that this amount of water is slightly less than minimum amount of 9 lbs of water per bag, as recommended by the manufacturer. Due to an equipment malfunction, the testing of these specimens was terminated very early and hence are not discussed here.

Upon the conclusion of this exploratory investigation, the following observations were noted. The material behavior under FT cycling was highly inconsistent. Reasons for this were thought to have been poor quality of grout material and/or poor mixing resulting in poor air void distribution. Good air void distribution is essential for good resistance to freeze and thaw damage. Poor mixing could have been caused due to an old mixer or inexperienced labor. Results of sealed cured specimens performed significantly worse than water cured specimens which goes against general expectation. These issues were addressed
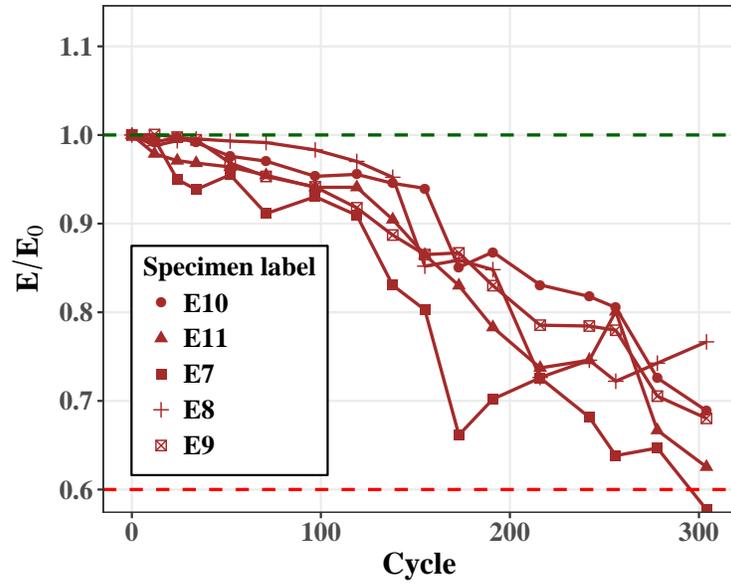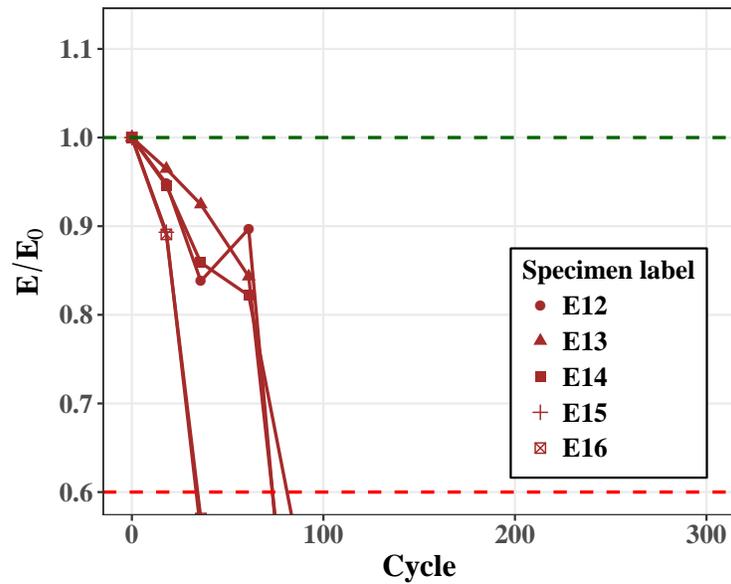
Figure 2.8: Results from exploratory investigation of FT resistance of grout material CG1: (a) with 9 lbs. water, and cured under water (b) with 8.5 lbs. water, and sealed cured.

in later tests and are discussed subsequently.

2.4.3 Freeze-Thaw Tests on Multiple Commercial Grouts

After the exploratory experiments on grout material CG1, additional grout materials were tested according to ASTM C666. These materials were labeled CG2, CG3, CG4 and PG1. A new batch of CG1 was also tested along with the other grout materials. PG stands for pea-gravel concrete which can be understood to represent the class of conventional flowable concrete ordered from a local ready-mix producer. The water content per bag used for each grout material (CG series) was chosen based on the amount specified by the manufacturers. These water contents are provided in Table 2.5, presented earlier. Note that the water content chosen for CG1 was 8.5 lbs. which is less than the 9.0 lbs. used in the exploratory study. All the specimens were cast using a concrete drum mixer of a larger capacity than that used earlier. This larger mixer was also more robust with regard to speed of rotation and drum tilt angle. Results from this series of tests is discussed next.

It is clear from Table 2.5 that most materials performed well and others performed poorly. Figures 2.9 to 2.11 show the results of all the materials that were tested. Five repeated specimens were cast for each material (CG1 to CG4, and PG1). For example, in CG1 results, these are labeled as CG101 to CG105. Figure 2.9 shows the result from specimens of CG1 with 8.5 lbs. water per bag of grout. In Figure 2.9, as no reduction in E/E_0 is observed, there is minimal or no damage due to FT cycles. This is a different behavior from that observed during the exploratory study for the same material. The consistency of results in Figure 2.9 introduced the possibility that earlier poor results from tests of CG1 may have been an exception rather than the norm. Since a reduced water content was used for this new batch of CG1, another possibility for previous poor performance was the effect of excess water within the microstructure. In later tests discussed in the next section, it was observed that this is not the case.

CG2 and CG3 also showed similar resistance to freeze and thaw as that of CG1. Figures
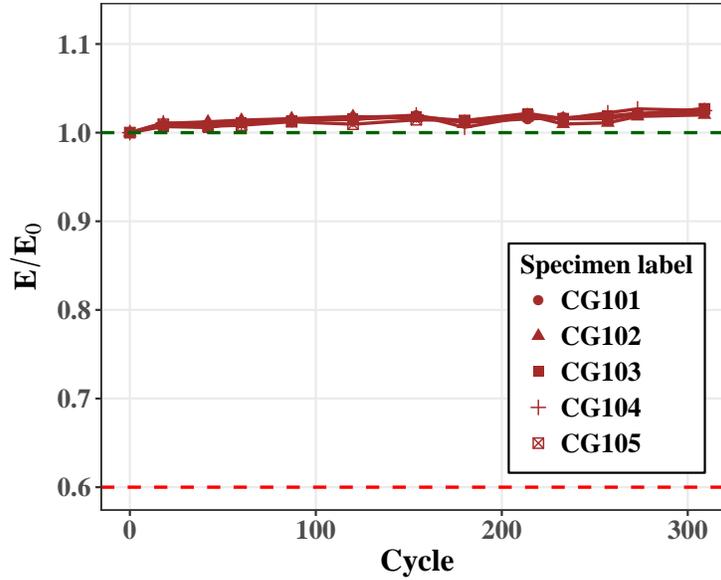
Figure 2.9: Results from ASTM C666 FT tests on multiple commercial grout (Good performance). Grout: CG1, Water per bag: 8.5 lbs.

2.10a and 2.10b show the results from tests of CG2 and CG3, respectively. Apart from a single specimen showing a slight dip in E/E_0 for CG2, all of the other specimens retained 100% of their initial elastic modulus throughout the 300 cycles. It was concluded that grouts CG1, CG2 and CG3 show good FT resistance and were selected to proceed to the next phase of durability tests. Questions still remained concerning the poor results obtained for CG1 in the exploratory study which were addressed by two more FT tests that were performed on CG1. These are discussed in the next section.

Not all the materials that were tested showed good performance. For example, in CG4 (Figure 2.11a), there is significant reduction in E/E_0 over time. CG4 is hence more prone to damage due to FT cycles. Figure 2.11b shows the results for PG1. All specimens of PG1 failed consistently within the first 10 cycles of freeze and thaw. Behavior of PG1, flowable pea-gravel concrete, merits some discussion. The water-cementitious ratio for this concrete was 0.46. According to the Powers' model [31, 32], a w/c ratio of 0.42 results in all the water being consumed for the hydration reaction. This implies that a w/c ratio of 0.46 would leave excess water within the microstructure forming capillary pores. In addition,
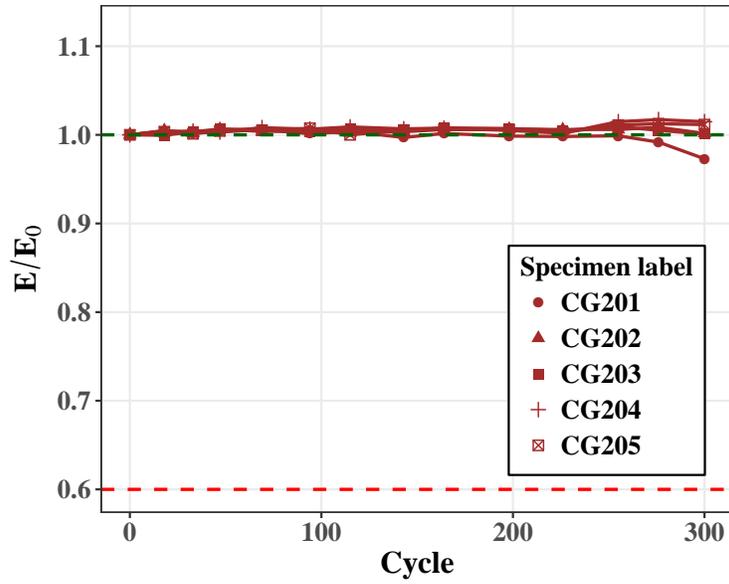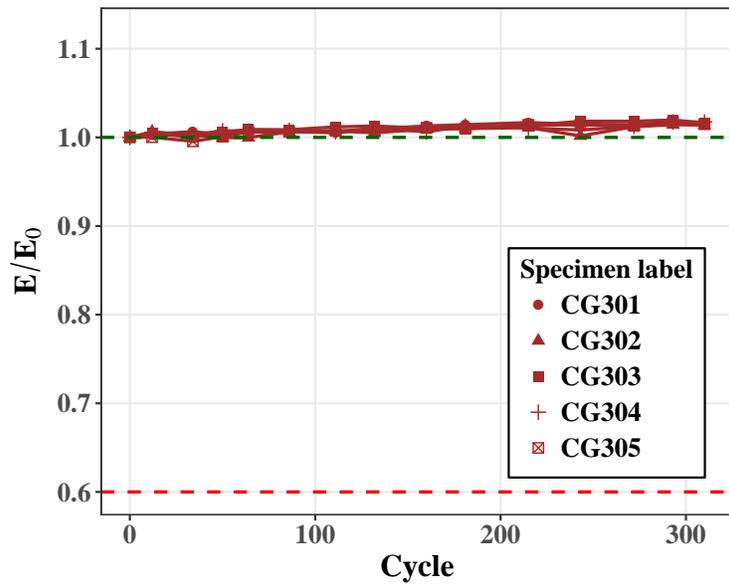
Figure 2.10: Results from ASTM C666 FT tests on multiple commercial grout materials (Good performance).: (a) Grout: CG2, Water per bag: 8.4 lbs., (b) Grout: CG3, Water per bag: 6.6 lbs.
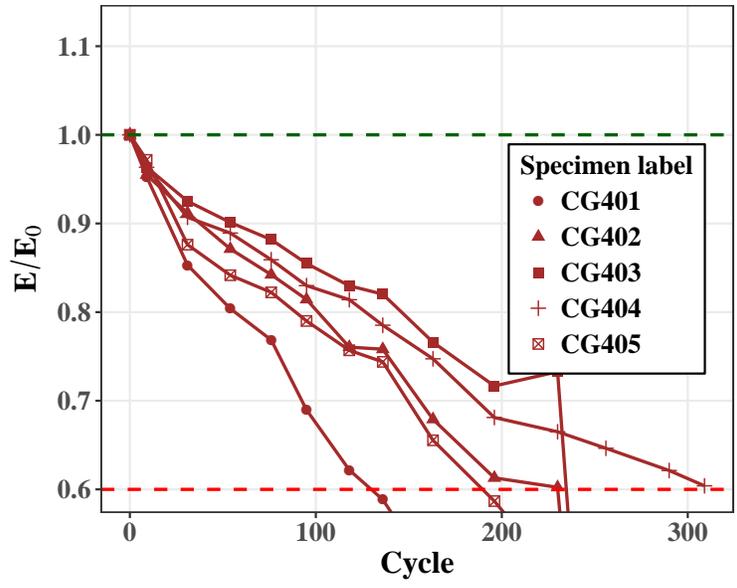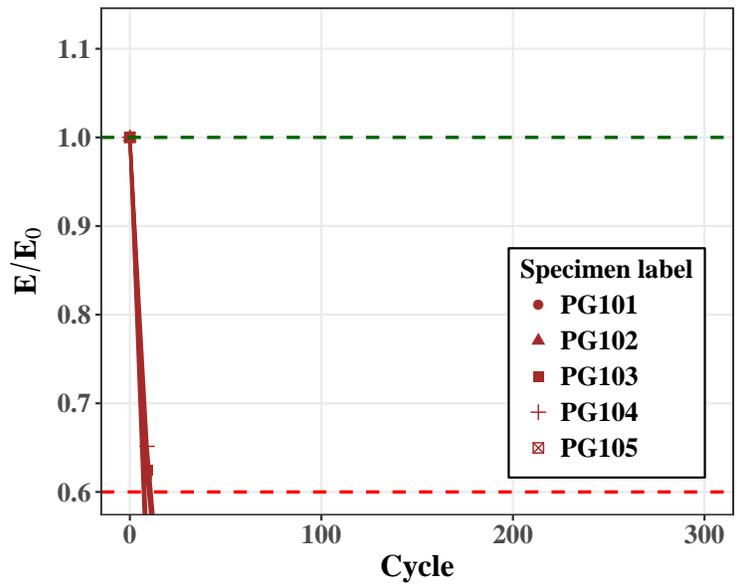
Figure 2.11: Results from ASTM C666 FT tests on multiple commercial grout materials (Poor performance).: (a) Grout: CG4, Water per bag: 9.3 lbs., (b) Grout: PG1, w/c ratio: 0.46

the cementitious particles that contributed to the water-cementitious ratio included fly ash, which is pozzolanic in nature and only contributes to the strength of the microstructure in the long term. Hence, the effective early w/c ratio would have been some value higher than 0.46 resulting in larger a amount of water filled pores. This may have resulted in early attainment of the critical degree of saturation of the material. Although a 6% air content was specified within the mixture, the mixing may not have achieved good dispersion of air. A combination of all of the above could have caused the extremely poor results that were observed. Nevertheless, it was decided not to pursue further inquiry into pea-gravel concrete.

2.4.4   Closure to Freeze and Thaw testing

Insofar as the results of the ASTM C666 tests on multiple grout materials are concerned, CG1, CG2, and CG3 showed good FT resistance. However, results from exploratory investigations on CG1 had shown some poor results that still needed to be addressed. Two more FT tests on CG1 were planned to provide some closure on this issue. The two new batches of CG1 specimens were:

1. CG1 with 9 lbs. of water per bag mixed in the old mixer (the same mixer used in the exploratory study), cast, and cured under saturated lime water for 14 days. This batch was chosen to isolate the effect of mixing on the performance of FT specimens. Specimens in the exploratory study where mixed using the same mixer and had yielded poor results.

2. CG1 with 8.5 lbs. of water per bag mixed in a new mixer, cast, and cured in sealed plastic bags for 14 days. This batch was chosen to isolate the effect of sealed curing on the performance of FT specimens. In the exploratory study, sealed cured specimens had performed poorly.

Results of both tests are shown in Figures 2.12 and 2.13. For the first batch of CG1 (Figure 2.12b) with 9.0 lbs. of water mixed with the old mixer the specimens are consistently
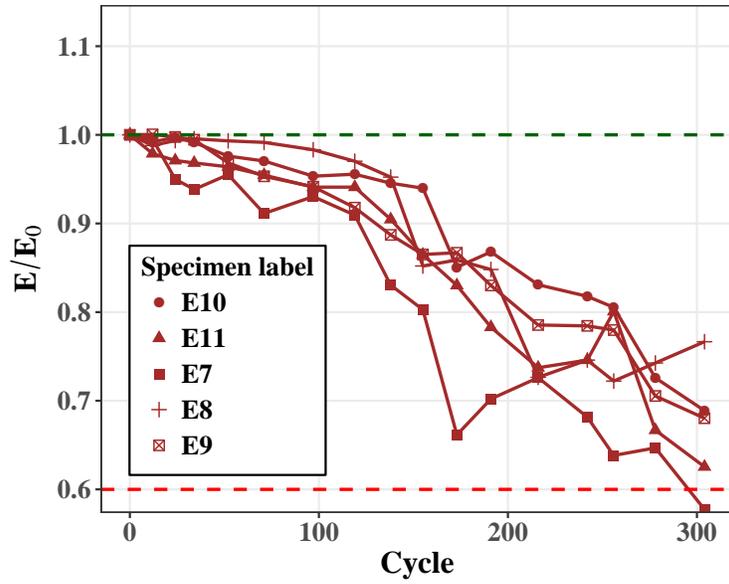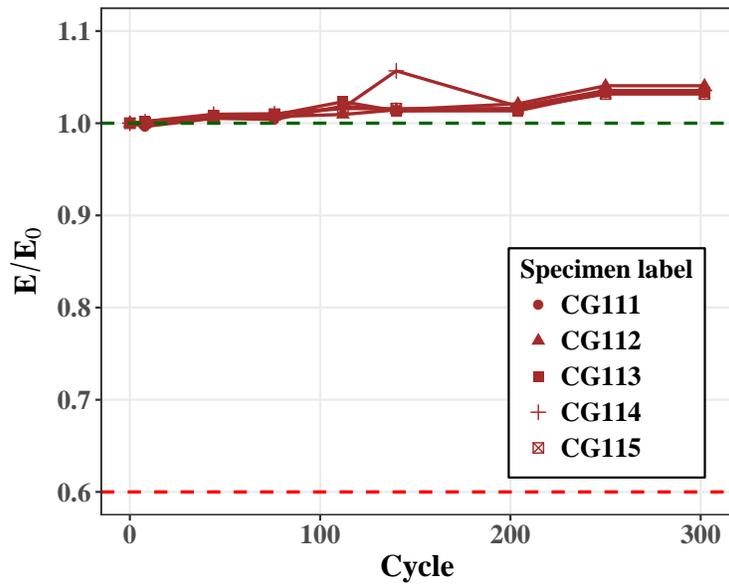
Figure 2.12: A comparison of results of the exploratory study performed on CG1 with 9 lbs. water per bag, and cured under water to the results of the same when repeated: (a) Exploratory (b) Repeat.
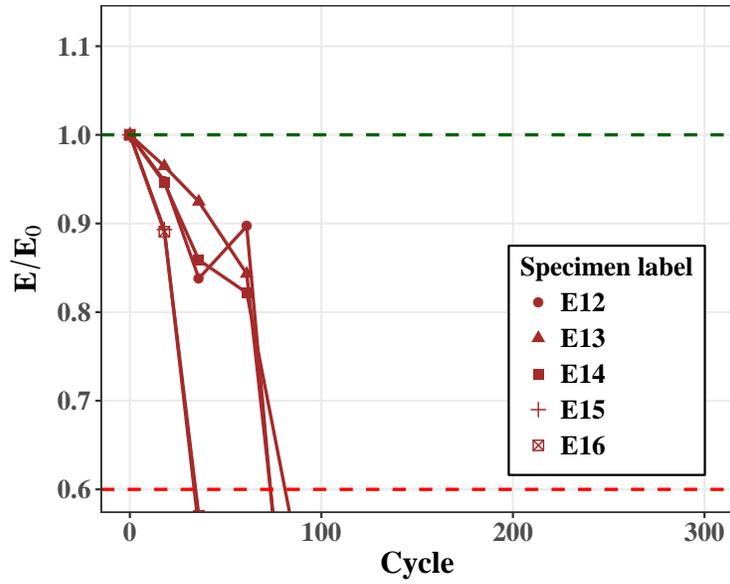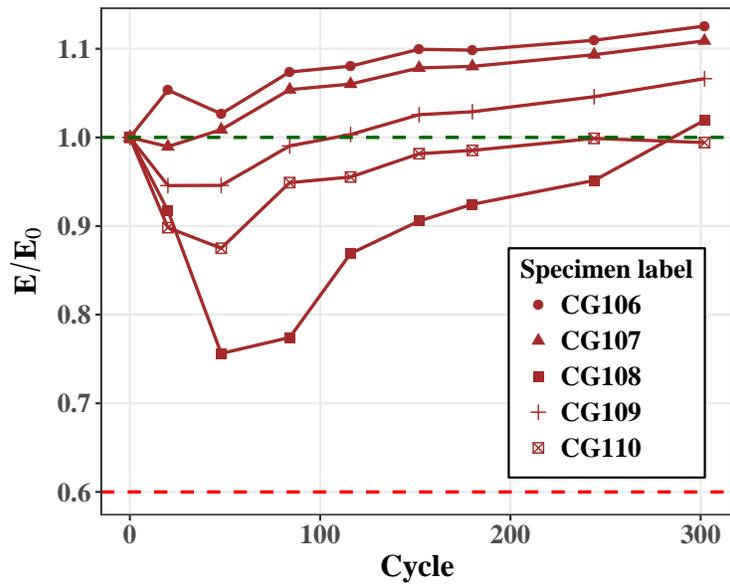
Figure 2.13: A comparison of results of the exploratory study performed on CG1 with 8.5 lbs. water per bag, and cured under sealed conditions to the results of the same when repeated: (a) Exploratory (b) Repeat.

at a 100% or above the initial elastic modulus. This is different from the CG1 specimens tested in the exploratory study mixed with the same amount of water (Figure 2.12a). The results are exactly as the CG1 specimens with 8.5 lbs. water discussed in the previous section. An increase in the amount of water did not seem to affect the results in these specimens. Hence, it was concluded that the poor results obtained for CG1 during the exploratory study could have been either due to a poor quality batch of grout or due to inexperienced labor or both.

For the CG1 specimens that were sealed cured (Figure 2.13b), an initial drop in E/E_0 was observed. Note that the amount of water in these specimens was 8.5 lbs. per bag, the same as that for specimens which showed good FT resistance when cured under water. After the initial drop, the curves showed a reversal in direction. They reached the same value or even exceeded the initial elastic modulus before any FT cycling. Delayed hydration of the material could be one reason for such behavior. This hypothesis is strengthened by the curves exceeding the initial values of elastic moduli. Further studies are required to ascertain the true mechanism. For the purposes of GSS connection durability, this observation does not pose a serious issue because within the early period that the grout hydration progresses, a GSS connection in practice would see few FT cycles.

To summarize, as part of the study on FT resistance of cementitious grouts, multiple commercial grouts were tested according to ASTM C666 Procedure A. A comparison of results from these tests yields that some commercial grouts show good resistance to frost damage while others do not. Hence, it is important for engineers to choose the grout filler for the GSS connection with caution. Even a good choice of grout does not guarantee long service life with respect to FT resistance.

2.5 Shrinkage Cracking in Cementitious Grouts

2.5.1 Introduction

Portland cement-based materials undergo volume change as a result of the hydration process and consequent loss of moisture. This is called shrinkage. When allowed to shrink freely with no external restraint, no stresses develop within the material. However, concrete or grout materials are commonly restrained against free shrinkage. This restraint causes stress development in the material. If these stresses exceed the tensile strength of the material, cracking ensues. The potential for cracking depends on the magnitude of these stresses and the tensile strength of the material.

The shrinkage characteristics of the grout are important in the overall performance of the GSS connection because the force transfer occurs through multiple mechanisms dependent on the grout. The size and shape of the annular grouted zone, as well as the restraint provided by the inner steel pipe, play a role in the long-term performance of the GSS connection.

The standard test to determine the cracking age and the induced tensile stress under restrained shrinkage is ASTM C1581-18a [2] which is also known as the "restrained ring test" or simply the "ring test". The core aim of the test is to determine the early age cracking tendency of concrete. The concrete material is cast as an annular ring around a circular steel ring. Due to shrinkage of the concrete ring, the imposed strain on the inside steel ring is measured as a function of time. When a crack forms, the tensile stress in the grout is released and a sudden reduction in the compressive strain in the steel ring is observed. The steel strain can be used as an indicator of the risk of cracking. When comparing different materials, the earlier a material cracks, the higher is its cracking potential. Similarly, the higher the rate of strain development for a material, the sooner the material will crack. It should be noted that the ring test does not measure a fundamental material property. It rather measures the response of the material to a stimulus under a specific boundary condition. This means that if the boundary conditions (e.g., degree of restraint, drying rate,

surface-to-volume ratio) change, the results of the test will also change.

2.5.2   A Literature Review of the Ring Test

In general, the ring test only provides the time to cracking and the steel strain at cracking. However, methods to obtain more information from the test results have been developed. Hossain and Weiss [19], obtained stresses in concrete from the measured steel strain and geometric properties of the ring. For this purpose, they used specimens with a sealed circumferential surface, allowing drying only from the top and bottom surface of the concrete ring. Top and bottom drying results in a simpler stress profile which simplifies the analytical calculations. Calculating the residual stress provides an estimate of the cracking potential for materials that do not crack during the test, by comparing the maximum residual stress developed to the tensile strength of the material. Hossain and Weiss also formulated an expression for the degree of restraint (Ψ) for a test specimen based on the elastic modulus, test geometry, and Poisson's ratio of the materials.

Hossain and Weiss [20] discussed the effects of specimen geometry and boundary conditions on stress development and cracking in the ring test. When allowed to shrink freely, specimens with larger drying surface to volume ratio had a higher shrinkage strain. Larger shrinkage strains arise because more water can leave the material during a certain period of time.

In addition to top and bottom drying, a different exposure condition that has been studied is circumferential drying. In circumferential drying, the crack initiates from the outer circumference and propagates inward. This behavior is opposite to what is observed in specimens with top and bottom drying. The reason for the inward propagation of cracking in circumferential drying is the development of a complex stress profile as shown in Figure 2.14. Because of this complex stress profile, conventional stress analysis does not yield results for this boundary condition, and the need for a different approach was recognized. The degree of restraint also has a significant role on the cracking age. Rings with smaller degrees of

restraint (thinner steel wall) cause concrete cracking at later times as compared to thicker steel rings.

Moon et al. [28] quantified the influence of specimen geometry on the results of the ring test with the goal of tailoring the ring geometry for specific applications. They studied three different drying conditions:

1. Uniform shrinkage of the concrete ring (completely sealed specimens),

2. Shrinkage caused by top and bottom drying, and

3. Shrinkage caused by circumferential drying.

The role of moisture gradients, thickness of the concrete and the restraining rings, and the stiffness of concrete were considered in a series of numerical simulations. A direct result of this study was an expression in terms of the geometry of the test specimen, Equation 2.5, to check if it satisfied a given criterion which would yield good results for calculating the residual stress:

$$\frac{\epsilon_{st}(t)}{\epsilon_{SH}(t)} = \frac{E'_c}{E_s} \frac{2}{1-\left(\dfrac{R_{IS}}{R_{OS}}\right)^2} \frac{1}{\dfrac{E'_c}{E_s} \dfrac{\left[(1+\nu_s)\left(\dfrac{R_{IS}}{R_{OS}}\right)^2+(1-\nu_s)\right]}{1-\left(\dfrac{R_{IS}}{R_{OS}}\right)^2} - \dfrac{\left[(1+\nu_c)\left(\dfrac{R_{OC}}{R_{OS}}\right)^2+(1-\nu_c)\right]}{1-\left(\dfrac{R_{OC}}{R_{OS}}\right)^2}}$$

(2.5)

where ϵ_{st} = measured steel strain on the inner surface,

ϵ_{SH} = free shrinkage strain of the concrete,

E'$_c$ = effective elastic modulus of concrete (considering the creep effect),

E$_s$ = elastic modulus of steel,

R$_{IS}$ = inside radius of the steel ring,

R$_{OS}$ = outside radius of the steel ring,

47
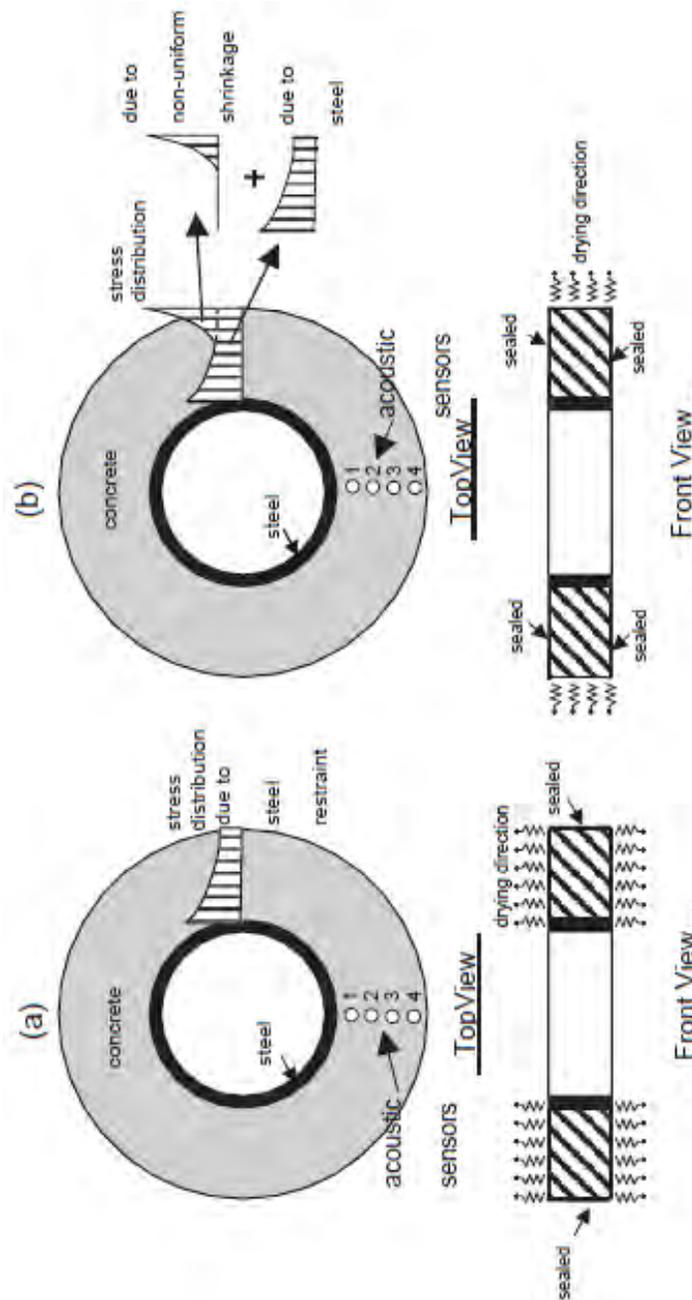
Figure 2.14: Restrained ring specimens: (a) top and bottom drying, and (b) circumferential drying, and their corresponding stress profiles as shown in [20]

R_{OC} = outside radius of the concrete ring,

ν_s = Poisson's ratio of steel,

ν_c = Poisson's ratio of concrete.

The stipulated criterion was that $\dfrac{\epsilon_{st}}{\epsilon_{SH}}$ should be greater than 0.125 for a specific test set up to achieve good results. This result is followed by the expression for the degree of restraint (Ψ) shown in Equation 2.6.

$$\Psi = 1 - \frac{E_c'}{E_s} \frac{1}{\dfrac{E_c'}{E_s} - \dfrac{1 - \left(\dfrac{R_{IS}}{R_{OS}}\right)^2 \left[(1+\nu_c)\left(\dfrac{R_{OC}}{R_{OS}}\right)^2 + (1-\nu_c)\right]}{1 - \left(\dfrac{R_{OC}}{R_{OS}}\right)^2 \left[(1+\nu_s)\left(\dfrac{R_{IS}}{R_{OS}}\right)^2 + (1-\nu_s)\right]}} \tag{2.6}$$

Moon and Weiss [29] followed this study to try to analytically formulate an expression for the complex stress profile developed along the thickness of the concrete ring during circumferential drying. They superimposed the stress due to the external ring restraint ($\sigma_{\theta\theta,rest-ring}$) and the stress due to the self-restraint from differential shrinkage ($\sigma_{\theta\theta,diff-shr}$). These stress contributions were formulated separately and then superimposed to give the overall stress ($\sigma_{\theta\theta}$) at any point in the concrete ring,

$$\sigma_{\theta\theta}(r, \gamma) = \sigma_{\theta\theta,rest-ring} + \sigma_{\theta\theta,diff-shr} \tag{2.7}$$

$$\sigma_{\theta\theta}(r, \gamma) = -\epsilon_{steel}(t) \cdot E_s \cdot \frac{R_{OS}^2 - R_{IS}^2}{2\left(R_{OC}^2 - R_{OS}^2\right)} \left(1 + \frac{R_{OC}^2}{r^2}\right)$$
$$+ \frac{\epsilon_{SH-const} E_c}{r^2} \left[\frac{r^2 + R_{IC}^2}{R_{OC}^2 - R_{IC}^2} \cdot (f(R_{OC}) - f(R_{IC})) + f(r) - f(R_{IC}) - erfc(A) \cdot r^2\right] \tag{2.8}$$

where

$$f(r) = \gamma^2 \cdot \left[\frac{1}{2} erfc(A) \cdot A^2 + erfc(A) \cdot \frac{R_{OC}}{\gamma} \cdot A + \frac{2}{\sqrt{\pi}} \left(\frac{-A}{4e^{A^2}} + \frac{\sqrt{\pi} \cdot erfc(A)}{8} + \frac{R_{OC}}{2e^{A^2}\gamma} \right) \right] \quad (2.9)$$

r = the radial distance of the point from outer surface, $erfc$ is the complementary error function, A and γ are constants defined as,

$$A = \frac{(R_{OC} - r)}{\gamma} \quad (2.10)$$

$$\gamma = 2\sqrt{Dt} \quad (2.11)$$

where D is the aging moisture diffusion coefficient of concrete and t is the drying time. This expression makes it possible to calculate the cracking potential of a material under non-uniform drying.

2.6 Restrained Ring Test on Cementitious Grouts

To investigate shrinkage cracking potential in this study, the same cross sectional geometry of the GSS connection was used rather than the size specified by ASTM C1581. The degree of restraint of the ASTM C1581 ring is 72.5% while that of the GSS connection is only 64%. It is important to model the degree of restraint in determining the shrinkage cracking potential. The complete test matrix for the restrained ring test is given in Table 2.6. Three grout materials that performed well in FT tests CG1, CG2, and CG3 were used in the first six ring tests. Each material was subjected to both circumferential drying and sealed (no drying) conditions. The schematic in Figure 2.15 shows the two different drying conditions that the specimens were subjected to. In circumferential drying, the grout ring 3.5" thick, is cast around a 6" tall steel ring of 16" diameter and 0.5" wall thickness, with the top and bottom sealed. To eliminate friction, the grout is separated from the steel ring by an acetate

50

Table 2.6: Test matrix and results for restrained shrinkage ring tests

Test No.	Material	Number of specimens	Drying Condition [1]	Shear Studs	Avg. age of cracking (days)	Avg. crack width (mm)	Avg. steel strain at cracking ($\mu\epsilon$)
1	CG1	3	CD	No	3.2	1.70	28
2	CG2	3	CD	No	6	1.00	23
3	CG3	3	CD	No	5.9	1.08	38
4	CG1	3	ND	No	9.5	0.40	68
5	CG2	3	ND	No	15.3	0.30	40
6	CG3	3	ND	No	N/A	N/A	N/A
7	CG1	2	ND	24-3/4" dia.	7.5	0.10	139
8	CG1	2	ND	8-1" dia.	9.9	0.10	134

[1] CD - Circumferential Drying; ND - Sealed (No Drying)

sheet oiled on both sides. The outside surface of the grout ring is exposed to the environment which is controlled at 23°C and 50% relative humidity (RH). Four strain gages are placed on the inside of the steel rings around 90°, apart. For specimens under sealed or no drying conditions, the only difference in the setup to that of circumferential drying specimens is that their outer surface is no longer exposed. An outer steel ring covers the grout ring rendering the specimens fully sealed. Again, acetate sheet and oil layers separate the outer ring from the grout. Note that this outer ring does not influence any other characteristics of the test setup. Three specimens of each material (CG1, CG2 and CG3) were tested. The rings were placed inside an environmental chamber for temperature and humidity control. Figure 2.16 shows a photograph of a sample test setup. The rings in the figure are under circumferential drying conditions.

Figures 2.17, 2.18, and 2.19 show the results for the first six ring tests. It is divided into two columns and three rows based on the two drying conditions and three grout materials. The sub-figures have time in days on the x-axis. This is the elapsed time from the moment of casting the material. Strain readings averaged over all of the strain gages on one specimen are given on the y-axis. The readings are in micro-strain ($\mu\epsilon$) units. The negative values of strain indicate compression on the inside ring. As time progresses from casting, the strains
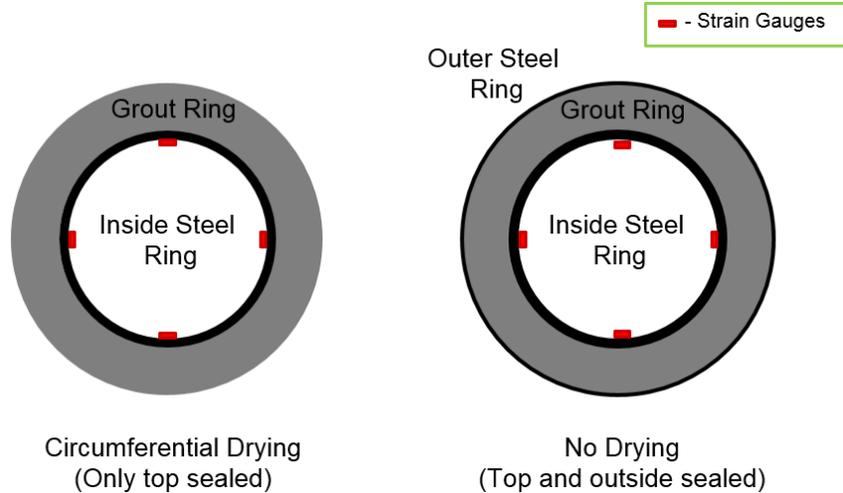
Figure 2.15: Restrained ring test specimen cross section schematic: Circumferential drying specimen (Left) and sealed specimen (Right).

increase until the point where the grout material cracks. The formation of a crack plane is accompanied by a release of stress which manifests itself in the figures as an instantaneous decrease in steel strain level. It is clear that the circumferential drying condition (left) is more severe than no drying (right). All the materials crack earlier under circumferential drying conditions compared to no drying. This matches expectations since the stress development inside the material due to restrained shrinkage is proportional to the amount of drying which in turn is proportional to the exposed surface-to-volume ratio of the specimen. Since no surface is exposed for drying in the case of sealed conditions, the stress development is slower.

However, most of the specimens under no drying still crack, but at a later time. All specimens of CG1 and two specimens of CG2 cracked under no drying. None of the specimens of CG3 cracked. In comparison therefore, CG3 performed better than the other two, while CG1 had the highest potential for cracking. The strain at cracking is also an indicator of cracking potential. CG1 has a higher strain accumulation rate and also cracks at strains much higher than the other two. Since CG1 specimens accumulated high strains even under no drying conditions, it may be concluded that the autogenous shrinkage component is high for CG1. Autogenous shrinkage is the component of shrinkage that occurs without any

Figure 2.16: Restrained ring test specimens under circumferential drying conditions in the environmental chamber.

exposure to the environment [27]. This happens within the grout microstructure as a result of the hydration reaction of cement. Autogenous shrinkage is comparatively lower for CG2 and CG3.

Along with age of cracking and the steel strain at cracking, the crack width of each specimen at 10 days post cracking was also measured. The crack widths are of interest since wider cracks facilitate more ingress of water and chemicals and can have more deleterious effects. For circumferential drying conditions, the crack widths were large for all three materials. CG1 had the highest crack width of 1.70 mm. When tested under no drying, the crack widths reduced drastically. This is reassuring since the connection geometry of the GSS connection results in conditions closer to no drying. Resulting data of average age of cracking, average crack width and average steel strain at cracking have been tabulated in
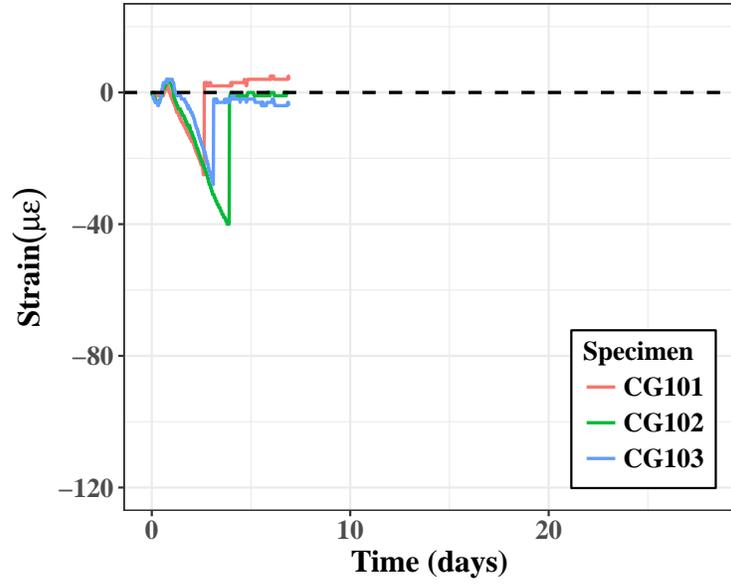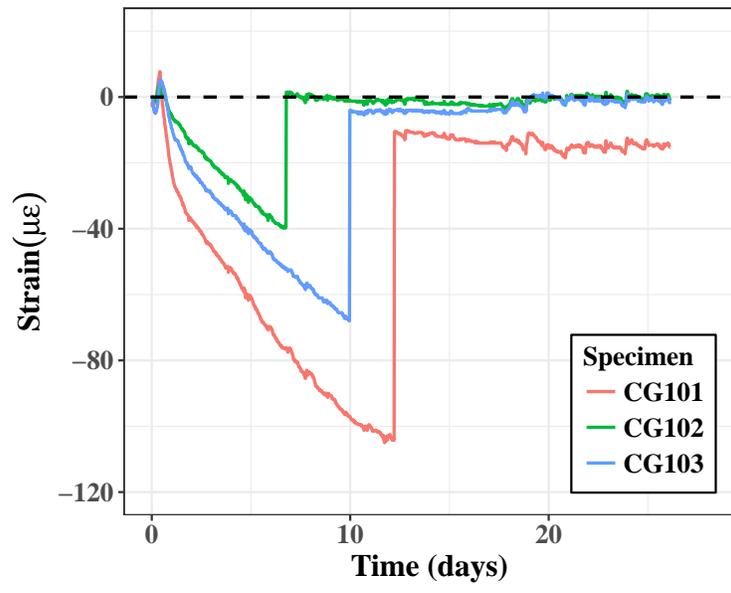
Figure 2.17: Results from restrained ring tests tests on CG1 under two different drying conditions: Circumferential drying (Left) and Sealed (Right) conditions.
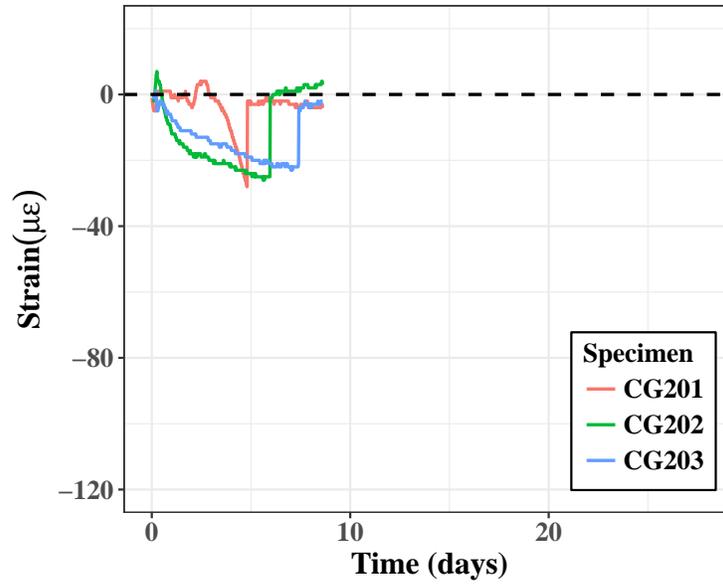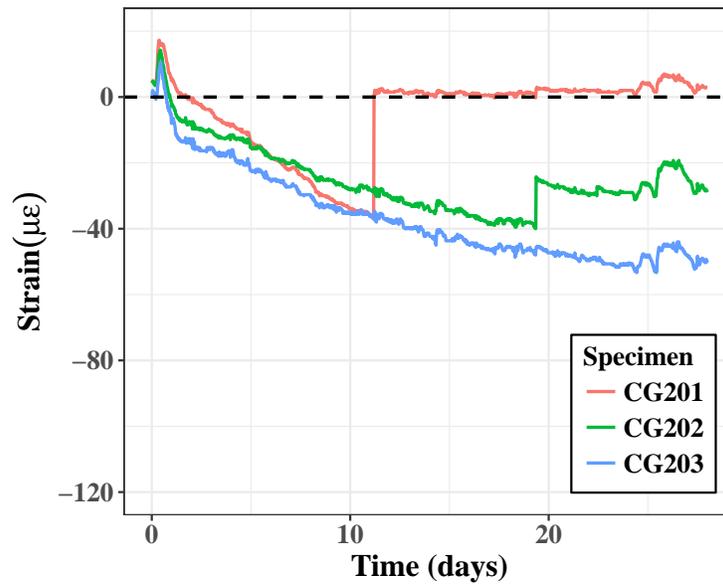
Figure 2.18: Results from restrained ring tests tests on CG2 under two different drying conditions: Circumferential drying (Left) and Sealed (Right) conditions.
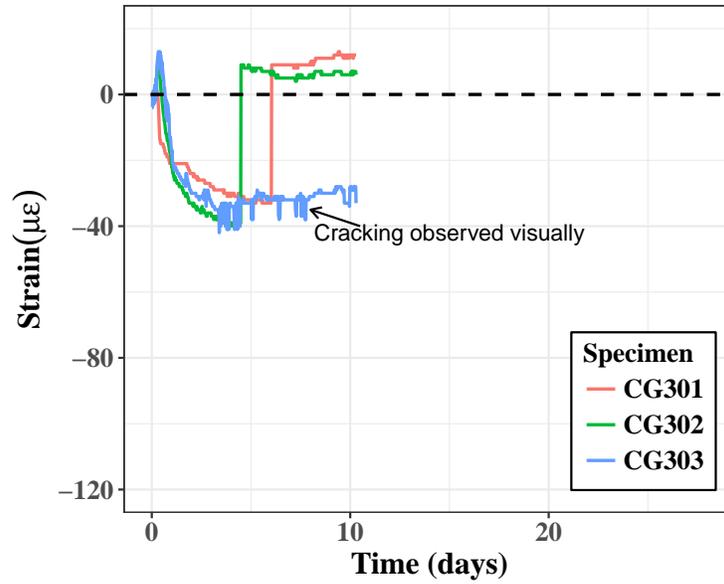
(a)
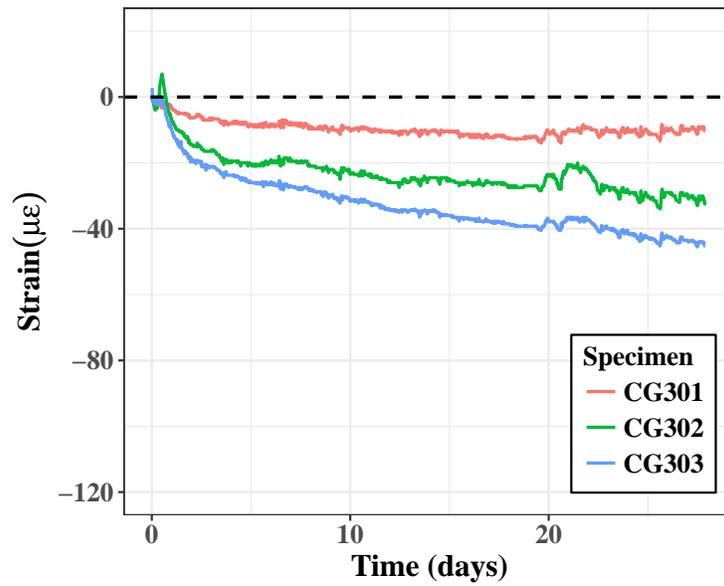
(b)

Figure 2.19: Results from restrained ring tests tests on CG3 under two different drying conditions: Circumferential drying (Left) and Sealed (Right) conditions.

Table 2.6.

It must be noted that the results obtained are only indicative of the cracking potential for the degree of restraint provided by the boundary conditions in the geometry used for these tests. This degree of restraint is 0.64 using Equation 2.6. In practice, the bridge columns making use of the GSS connection would have different degrees of restraint. One way to extrapolate results such as those obtained herein to practice is to use figures that plot degree of restraint versus the column radius, for given outer diameter to inner diameter ratios of the GSS connection. An example of such a figure is shown in Figure 2.20. The lines are calculated using Equation 2.6 for different input geometric parameters. Different lines indicate different column thicknesses. The dotted line shows the degree of restraint corresponding to the tests discussed here. Any degree of restraint below the dotted line can be understood to be less severe than that used for the ring tests in this study. This can be made use of when making decisions regarding the connection geometry for an actual bridge connection. For example, all the results obtained in this study are valid for a degree of restraint of 0.64 or higher. In practice therefore, any combination of column diameter and wall thickness that equals to a degree of restraint less than 0.64 will result in lesser grout cracking potential.

The next tests in the series of ring tests were done to identify the effect of shear studs on cracking potential. Grout material CG1 was chosen to perform these tests as it performed poorest among the three that were tested previously. Even under no drying condition, all specimens of CG1 cracked with an average crack width of 0.40 mm. Upon discussion with personnel from Alaska Department of Transportation and Public Facilities (AKDOT), it was learned that a crack width of 0.30 mm is an acceptable upper bound because it can be repaired by epoxy injection. The presence of shear studs within the grout produces two opposing effects with respect to cracking potential of the grout. Shear studs increase the degree of restraint thereby hastening cracking, but simultaneously can create redundant load paths to distribute the cracking thereby reducing crack widths.
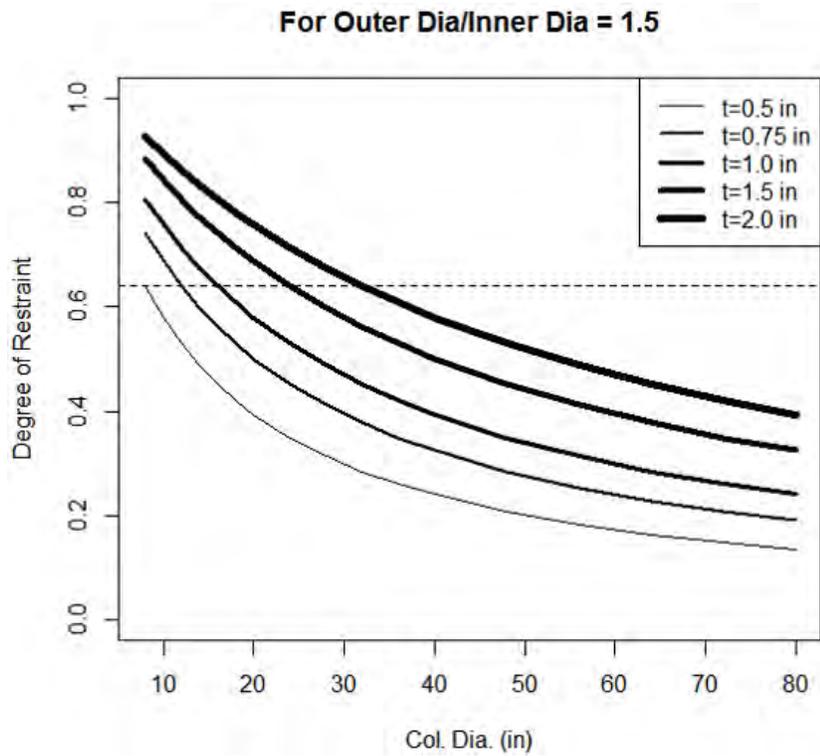
Figure 2.20: Degrees of restraint plotted against column diameter for a GSS connection outer-to-inner diameter ratio of 1.5.
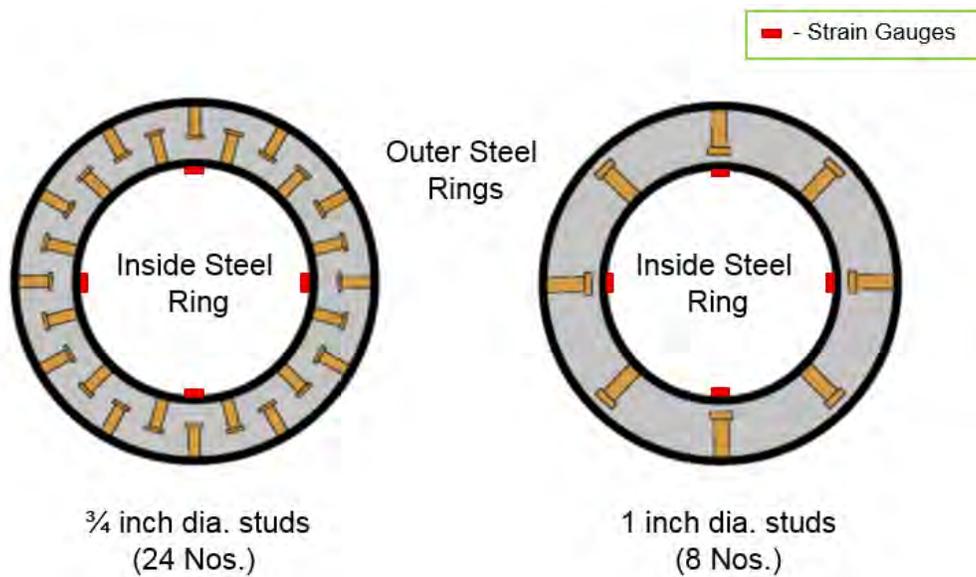
Figure 2.21: Restrained ring test specimen cross section schematic: 3/4" dia. shear studs (Left) and 1" dia. shear studs (Right).
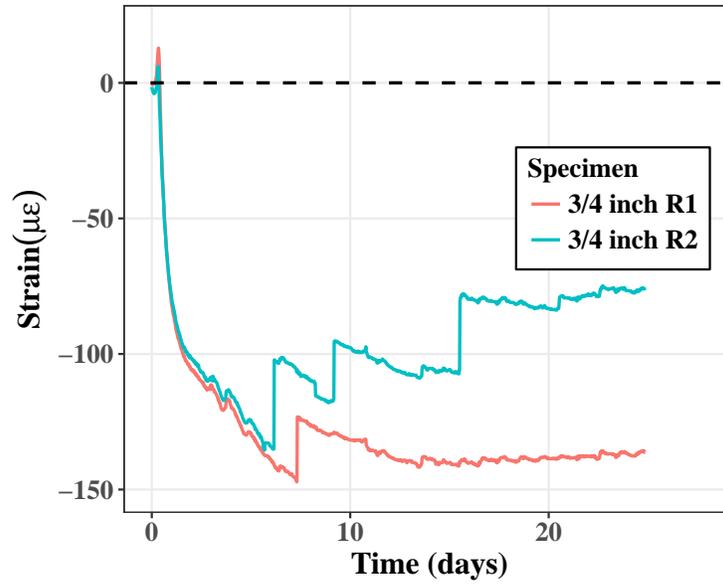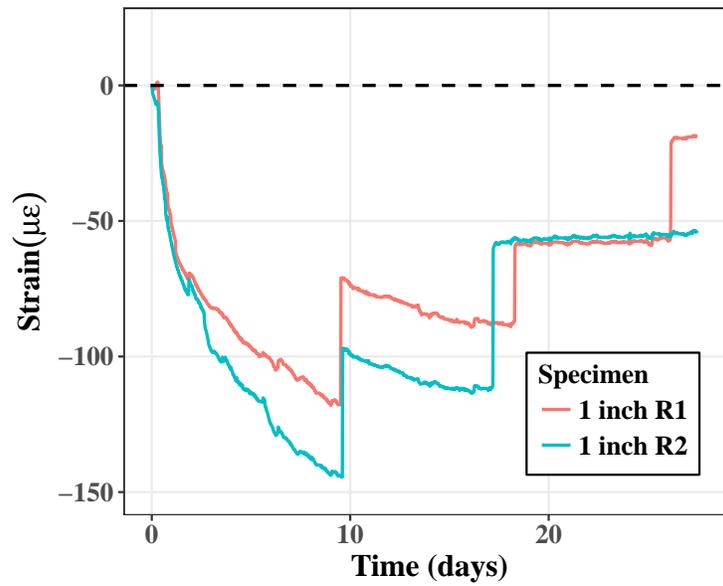
Figure 2.22: Results from ring tests performed on specimens with shear studs: (a) 3/4" dia. shear studs (b) 1" dia. shear studs.

Two tests were planned to investigate the effect of shear studs. Each test was performed under no drying conditions with shear studs of different sizes. The first test (Test 7 in Table 2.6) had 24 shear studs of 3/4" diameter within the grout ring, while the second test (Test 8 in Table 2.6) had 8 shear studs of 1" diameter. The cross section schematic of both tests is shown in Figure 2.21. Strain gages were attached on the inside of the steel rings in the regions in between the welded studs. The presence of shear studs likely creates a non-uniform distribution of stress (and hence strain) in the steel ring, but it is thought that an average over all strain gages may still provide meaningful results.

Specimens with both 3/4" diameter and 1" diameter studs show a release of strain at an average of 7.5 days and 9.9 days, respectively. However, this observation did not correspond to visual cracking on the top surface. Since the release of strain was not to zero, it can be concluded that the shear studs contribute to resistance to cracking. Cracks started to appear on the surface not long after the first instance of stress drop. Instead of a single crack that was observed in earlier tests without shear studs, multiple cracks formed when shear studs were present. Moreover, these cracks were smaller compared to the wide single cracks observed earlier. This observation led to the conclusion that the shear studs play an important role in reducing crack widths. Further research is required to quantify the effect of shear studs on shrinkage cracking. A detailed investigation of this mechanism is beyond the scope of this study.

Among the tests that were conducted under sealed/no drying conditions, the results follow an expected trend. The ring specimens with the most number of shear studs (24) cracked the earliest. This result is due to the highest degree of restraint among the three different types of specimen. The rings with the second highest degree of restraint cracked later and those with the lowest degree of restraint among the three cracked last. A separate observation is that the rings with 24 shear studs cracked at relatively higher stresses in the grout. This can be an indication of the contribution of shear studs to the tensile strength of the ring. More tests are needed to confirm this hypothesis.

In summary, the ring tests to investigate early age cracking potential of multiple commercial grouts yielded the following results:

1. All tested grout materials cracked early under circumferential drying conditions.

2. Sealing the specimens delayed cracking in two materials (CG1 and CG2) and eliminated cracking in one (CG3). Sealing also reduced the crack widths.

3. Presence of shear studs (as in the GSS connection) helps reduce the cracking potential of grouts. Shear studs distribute the cracks and reduce crack widths by providing redundant paths for stress redistribution.

2.7 Chapter Summary, Recommendations, and Concluding Remarks

2.7.1 Chapter Summary

Previous studies have used cementitious grout to fill the annular space in the GSS connection. The grout serves an important function of force transfer for the satisfactory performance of the GSS connection. Our primary objective was to determine the long term durability of grout in the GSS connection. Cementitious grouts from four different manufacturers, all meeting AKDOT requirements, were chosen to assess their strength and durability characteristics. All four grouts developed high early age strength compared to normal concrete, some having much higher strength than the others.

Durability here means the potential of the grout material in the GSS connection, to provide a long service life in extreme cold climates. Two major durability concerns in this study were cracking due to freeze and thaw cycles, and cracking due to early age restrained shrinkage. Freeze and thaw cracking occurs due to cyclic expansion and accumulation of water in the grout microstructure causing internal stresses. Upon testing the freeze thaw

resistance of the chosen grouts, some grouts are durable and some are not. Hence, one must choose grout for cold climate applications with caution. Early age shrinkage is an inherent characteristic of cementitious materials. Under restrained conditions such as those in the GSS connection, tensile stresses are developed as a result of shrinkage and lead to cracking. All the grouts chosen for restrained ring tests cracked within the first few days after casting. This means that the geometry of the GSS connection provides a high enough restraint to crack high-strength grouts. However, when shear studs were added in the rings, the cracking was delayed and upon cracking, the grout rings formed multiple cracks of smaller widths. This result is, of course desirable. Hence, in addition to the structural requirement, shear studs serve a secondary function of distributing shrinkage cracks and reducing crack widths.

2.7.2 Recommendations

We suggest the following for choosing and mixing cementitious grouts for applications in cold climates. Note that these recommendations are qualitative, based on observations during experimental testing of a set of different cementitious grouts.

Choosing a durable grout

Durability tests, especially those pertaining to cold climatic environmental conditions, are time consuming and require a significant amount of work. ASTM C666 Procedure A is a good testing standard to compare the freeze-thaw resistance of available grouts. We recommend choosing grouts that meet a Durability Factor (DF) of at least 95% measured according to ASTM C666 Procedure A.

Mixing grout

We want to re-emphasize the importance of water in both strength and durability characteristics of cementitious grouts. We suggest the use of the minimum manufacturer specified water content per bag of grout for flowable consistency. Good grout products generally have

different specified water contents per bag for different consistencies such as plastic, flow-able, or fluid. Note that each consistency label will give different strength and durability characteristics.

We found that grout durability is largely independent of the mixing process. However, grout consistency (flowability) is dependent on the mixing process. For example, mixing a large amount of grout in a drum mixer provides better consistency than mixing smaller amounts in the same mixer, provided the time of mixing remains the same. This improved consistency results from larger amounts of grout revolving in a drum mixer, which provides more weight of grout to fall on top of itself, facilitating better mixing. Grout consistency can also vary based upon mixer type. When we mixed the same amount of grout in a drum mixer and with a screw mixer, the screw mixer took less time to reach the same level of consistency than the drum mixer. This result may be because of the higher shear rate of the screw mixer, compared the slow process of gravity aided mixing in a drum mixer. However, given enough time, both processes can achieve the same level of consistency. Therefore, it is important that the contractor is aware of this dependence so as to prevent the addition of excess water to increase flowability. We also suggest to be cautious of the setting times of the grout being used. We recommend grouts that have longer setting times for better workability.

2.7.3   Concluding Remarks

Through a series of durability tests on commercially available cementitious grouts, we found that some grouts are good while some are bad for use in the GSS connection in cold climates. A simple method to separate good ones from the bad ones does not exist. Developing such a method requires further studies. However, before proceeding in this direction, it is worth going back to the main objective of this project which is to answer the question: *Can the GSS connection be used in cold climates with no loss in the structural integrity of the lateral load resisting system?* Therefore, as the next step, it was necessary to consider the second

part of the question: *How much impact does grout deterioration have on the consequent structural performance of the lateral load resisting system?* We tried to answer this question in Phase 2 of the project discussed in the next chapter.

Chapter 3

Simulating Grout Deterioration for Large Scale Tests

3.1   Introduction

Years of exposure to a cold and wet climate tend to reduce the structural properties, such as compressive strength (f'_c) and elastic modulus (E) of cementitious grouts. Simulating this reduction in grout properties to effectively represent the long-term damage state of grout was essential to define the levels of deterioration (LoD) for the large scale tests. Ideally, physical damage simulation must be achieved by subjecting the specimens to multiple accelerated freeze-thaw cycles. However, this is difficult to achieve for specimens that are of the scale to be tested.

Alternate methods of reproducing damaged states of grout were explored. Ravindrarajah and Tuck [33] investigated properties of hardened concrete containing aggregates called expanded polystyrene (EPS). EPS is a stable low density foam and consists of discrete air voids in a polymer matrix [33]. They found that the water-cement (w/c) ratio is an important factor upon which the compressive strength of EPS concrete is dependent. They also provided an empirical expression (Equation 3.1) to calculate the static elastic modulus of
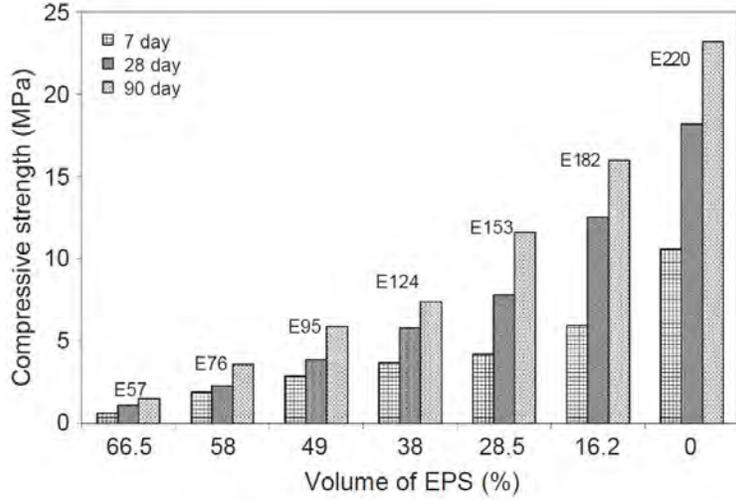
Figure 3.1: Variation of compressive strength with age and EPS volume for concrete added with fly ash [9].

EPS concrete, when the density (D), and cylinder strength (f'_c) are known.

$$E = 1.146 D^{1.1} \sqrt{f'_c} \tag{3.1}$$

EPS has been used as ultra lightweight aggregate suitable for developing concretes for both structural and non-structural applications, by varying its volume percentage in mortar or concrete [11, 30]. Babu et al. [8, 9] investigated the possibility of producing good quality lightweight concrete using volume replacement of aggregates by EPS aggregates. The mixtures they studied also included fly ash. During their study, Babu et al. [9] observed that the compressive strength of EPS concrete reduced with increasing volume fraction of EPS, as shown in Figure 3.1 [9]. They also observed the variation of the split tensile strength of EPS concrete with compressive strength (Figure 3.2) and provided the following expression:

$$f_t = 0.358 f_{cu}^{0.675} \tag{3.2}$$
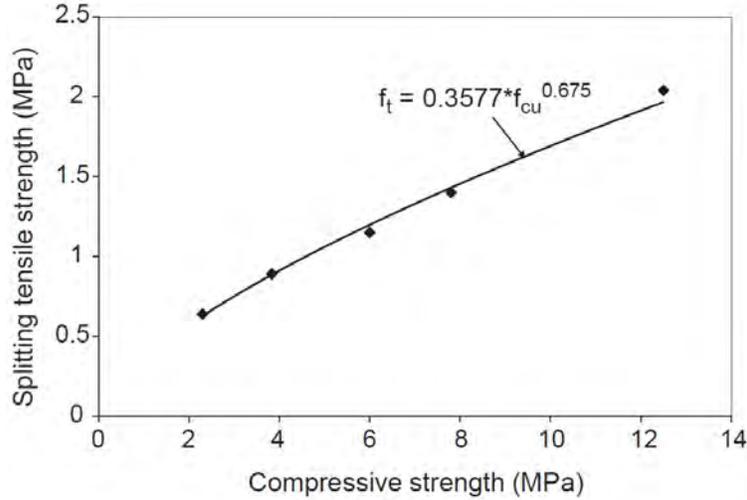
Figure 3.2: Variation of split tensile strength with compressive strength for EPS concrete added with fly ash [9].

where f_t and f_{cu} is the split tensile strength and compressive strength in MPa, respectively. The study validated the expression for static elastic modulus (Equation 3.1) provided by Ravindrarajah and Tuck [33]. The authors also noted that the EPS mixes showed good flowability and no segregation was observed in any mix, although they did not explore the results beyond an EPS replacement volume of 40%.

Later, Bucher [13] investigated the possibility of using what he called Lightweight Synthetic Particles (LSP) to reduce the potential for restrained shrinkage cracking in concrete. Aggregates in concrete and mortar provide restraint against deformations of the cement paste. The degree of restraint, discussed in Chapter 2, is not only a function of the boundary conditions of concrete, but also of the aggregate content and distance of cement paste from aggregate. Bucher claims that LSPs can be used as low stiffness aggregates that lower stress concentrations at the aggregate, thereby decreasing the propensity for early-age cracking of mixtures.

In all of the studies above, the authors observed that adding EPS (synonymous to LSP) to a cementitious mixture can reduce its structural properties E and f'_c. In this study, these results are used for a different purpose, i.e., simulating the state of damaged grout, termed LoD herein. EPS beads of 0.15-0.20 inch diameter (Figure 3.3) with a density of 1.40-1.50

lbs/ft^3 were used. Although this material achieves the required reduction in E and f'_c, some quantification was required to enable reproducible levels of deterioration (LoDs).

3.2   Physical Damage Simulation

3.2.1   Exploratory Study

Many trial grout mixtures were used to obtain a simple linear predictive model that relates the reduction in E to the percentage volume replacement of EPS in the grout mixture. Grout was mixed using a drum mixer. During mixing, EPS aggregates were added gradually, in parts. After mixing, prismatic grout samples of size 3"×3"×12" were taken. Relative Dynamic Modulus of Elasticity (RDME) discussed in Chapter 2 was used as a measure of reduction in the elastic modulus. However, the baseline E_0 in the now familiar E/E_0, is the elastic modulus of the specimens with 0% EPS. RDME was measured on the 3rd day from the day of casting.

Table 3.1 shows the full matrix of the trial and error tests that were performed along with average values of measured RDME. Figure 3.4 shows the results of the trial and error tests. A negative trend can be seen in the normalized elastic modulus with increasing volume replacement of EPS. A simple linear model has been fit to be used as a guideline to control the LoD.

Since E and f'_c are positively correlated, reducing the former to predefined values also results in the latter being reduced. The modulus of elasticity, E, was chosen as the primary variable to be reduced for two reasons. One is that between the two, E is the parameter that is more difficult to reduce, i.e., a 40% reduction in E will result in a significantly higher percentage reduction in f'_c. Second, durability studies, especially those pertaining to freeze and thaw resistance, utilize E as the parameter that defines the failure limit states.

Figure 3.3: Expanded Polystyrene (EPS) beads [13].

Table 3.1: Trial and error test matrix to determine required EPS volume percentages.

Test No.	EPS by Volume	Number of Specimens	RDME (3 day)
1	0%	3	100%
2	5%	3	96%
3	10%	3	87%
4	15%	3	82%
5	20%	3	76%
6	25%	3	72%
7	30%	6	70%
8	35%	6	62%
9	40%	6	53%
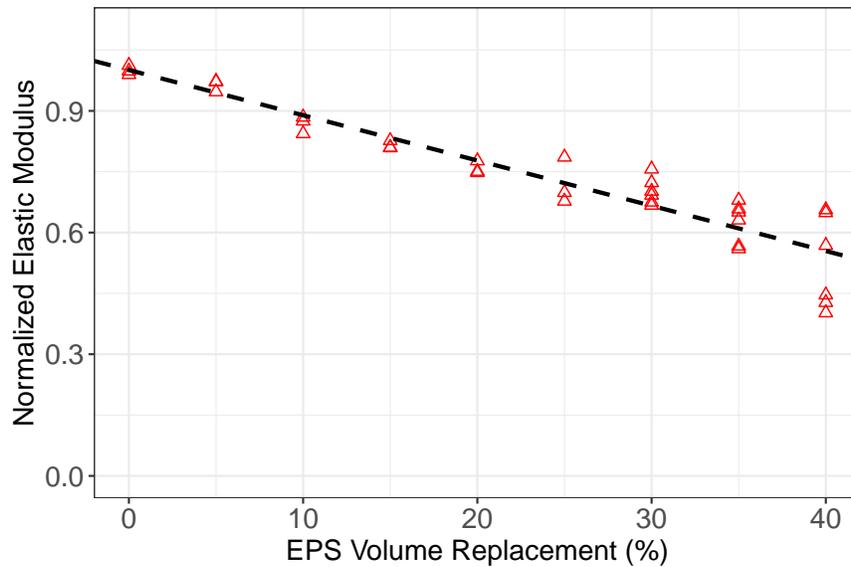
Figure 3.4: Elastic modulus normalized to value at 0% EPS plotted against EPS volume replacements for trial and error mixtures.

Figure 3.5: Migration of EPS aggregates observed in cylindrical grout samples.

3.2.2 Preventing EPS migration

Although it was not observed in prismatic samples of grout with added EPS, the cylindrical samples after demolding showed signs of EPS aggregates migrating to the top. In Figure 3.5, this can be seen externally as a change in color between the top and bottom layers. Some samples have greater migration than others, indicated by the different levels at which this change in color is observed. This migration can be attributed to the extremely low density of the EPS beads in the wet grout mix. When such samples are tested under a compressive load, they display premature failure, a shown in Figure 3.6.

The migration of EPS aggregates was undesirable for the purpose of simulating reduced structural properties. In real bridges with the GSS connection, the deterioration, such as cracking, scaling etc., initiates at the bottom, since only the bottom surface is exposed, and progresses to the top. Hence, at all points of time, properties such as the elastic modulus and strength will be lower at the bottom compared to the top of the connection. EPS migration to the top would result in the opposite trend. Therefore, it was essential to solve this problem.

To solve the problem of EPS migration to the top of the cylindrical samples, new samples

(a)   (b)

Figure 3.6: Premature failure observed in two different samples of grout mixed with 18% EPS. This corresponds to a 20% reduction of elastic modulus compared to standard grout.

(a)   (b)

Figure 3.7: Compressive strength cylindrical specimens cast in 2" layers with 18% EPS.

<div style="text-align:center">(a)   (b)</div>
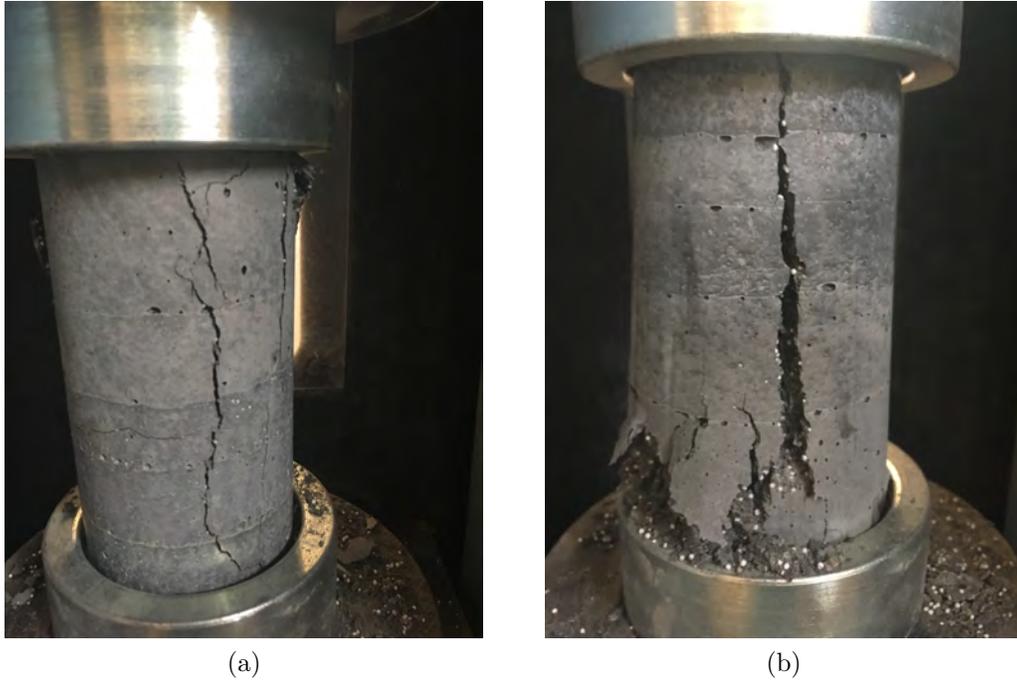
Figure 3.8: Compressive strength cylindrical specimens cast in 1" layers with 18% EPS.

were cast in 2" thick layers. A 4"×8" cylindrical sample contained 4 layers of 2" thick pours. After each layer was cast, 30 minutes elapsed before casting the next layer. The assumption was that this strategy would provide enough time for each layer to achieve sufficient viscosity to prevent the beads from migrating upward. Figure 3.7 shows the samples after compressive strength testing. Although migration to the top of the samples were prevented, there was still migration of the aggregates within each layer. This migration created weak planes along the height of the samples resulting once again in premature failure. This result was also deemed as a failure to effectively simulate grout deterioration.

Subsequently, the layer thickness in the cylindrical samples was reduced from 2" to 1". This resulted in eight 1" layers in a 4"×8" cylinder. Figure 3.8 shows the 1" layered samples after compression testing. The cylinders failed by cracking through the entire height, which was typical of normal concrete cylinders. No premature failure was observed, and the sample strengths were consistent. One half of a failed sample is shown in Figure 3.9. The EPS aggregates have a uniform distribution along the height of the sample. The layered casting scheme with 1" layers was therefore chosen as the method to physically simulate

Figure 3.9: Uniform distribution of EPS aggregates observed in cylindrical grout samples under the 1"-layered casting scheme.

deterioration.

3.2.3 Mock Connection

In addition to ensuring uniform distribution of EPS aggregates in the GSS connection, it was required to generate a reproducible level of deterioration for the large scale tests. To investigate reproducibility of elastic modulus and compressive strength measurements, a mock connection was cast. This mock connection was a replica of the grout ring in the GSS connection without the shear studs. The formwork for this connection was prepared using 24" dia. and 16" dia. sonotubes, as shown in Figure 3.10. The top was closed with a plywood sheet with two holes (one to pump in grout, the other to let air out) to replicate actual pumping conditions. The annulus between these concentric sonotubes was pumped with a grout mixture with 18% volume replacement of EPS to simulate the first LoD. The grout mixture was cast in a layered scheme shown in Figure 3.11. The entire connection was 24 inches deep. For the first 9 inches from the bottom, 1" thick layers of grout were cast at

Figure 3.10: Formwork for the mock GSS connection.

intervals of 30 minutes. This wait-time allowed enough time for the fluid mixture to develop partial setting that prevented migration of EPS. The next 6 inches were cast in layers of 2" thickness with the same wait time. The last 9 inches were cast in layers of 3" thickness. This region will have some EPS migration. However, the forces during the test in this region are low and hence this region was less important than the lower half of the connection, from a damage simulation standpoint. Grout mixture samples were collected in round and square PVC pipes that were cut to 2' lengths. The sample collection followed the same layering scheme as the actual connection. Samples in round PVC pipes were later cut into discs to measure the elastic modulus (E) profile along the height of the connection [23]. Samples in square PVC pipes were cut into cubes to measure the cube compressive strength (fc).

After setting, the distribution of EPS was assessed qualitatively. Ultrasonic pulse velocity (UPV) measurements were made along the height of the mock connection to determine the time required for the ultrasonic wave to travel through the thickness. The locations of UPV measurements are shown in Figure 3.12. The elastic modulus is directly proportional to the square of the travel time; therefore a profile of elastic modulus along the height of the connection was obtained (Figure 3.13). In addition, samples were cast in round PVC pipes
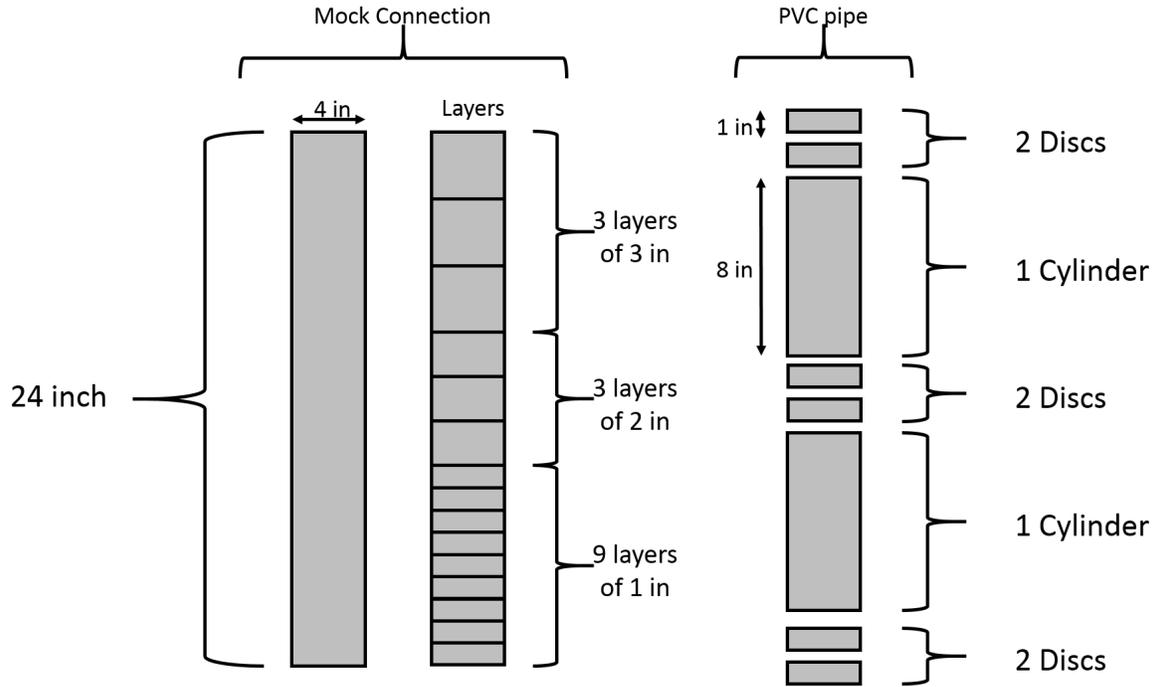
Figure 3.11: The layered scheme used to cast the mock connection and the corresponding 4"×24" PVC pipes.
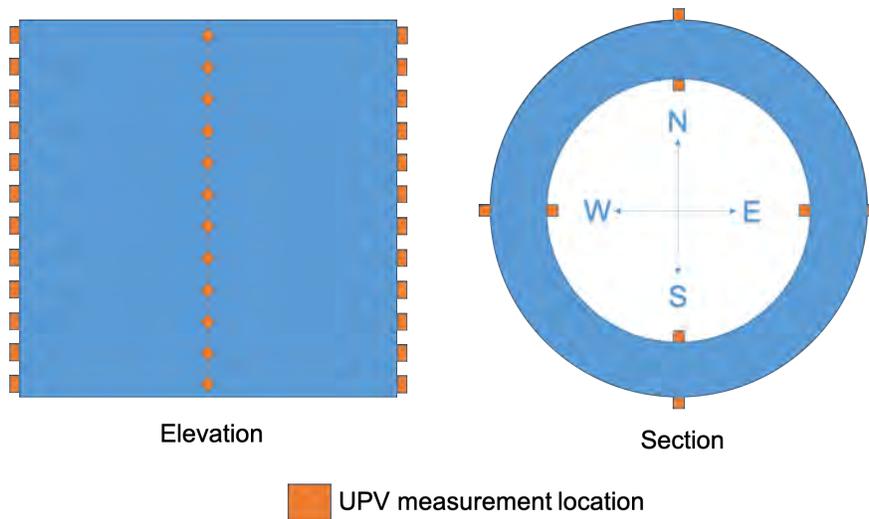
Figure 3.12: The locations of ultrasonic pulse velocity measurements along the height and around the section of the mock connection.
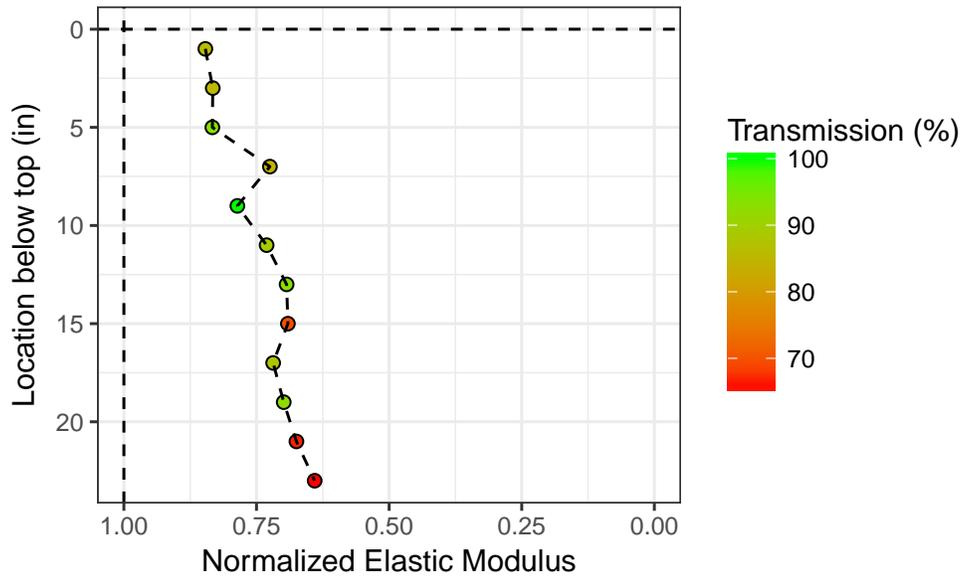
Figure 3.13: Results of the UPV test to measure relative elastic modulus along the height of the mock connection.
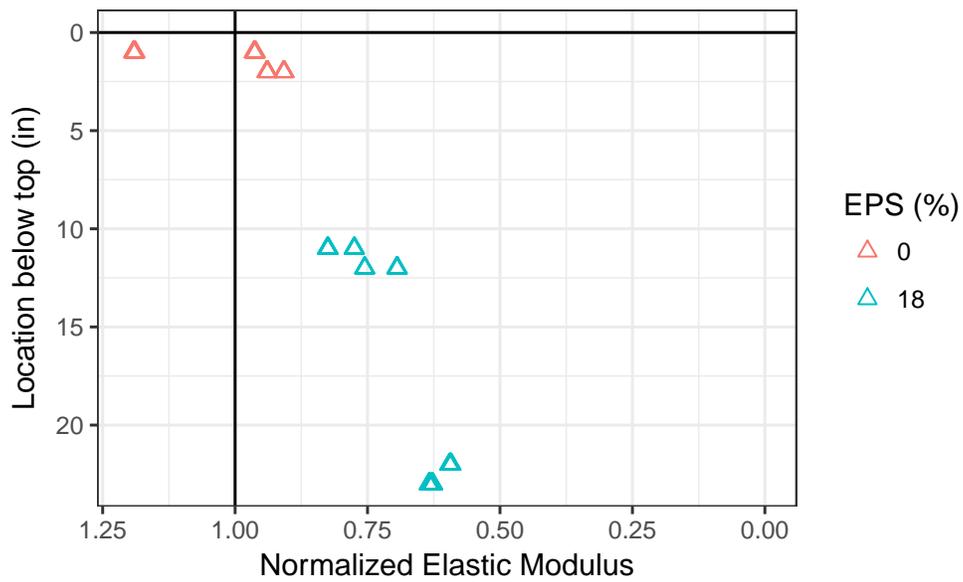
Figure 3.14: Results of elastic modulus measurements using disc samples along the height of the mock connection.
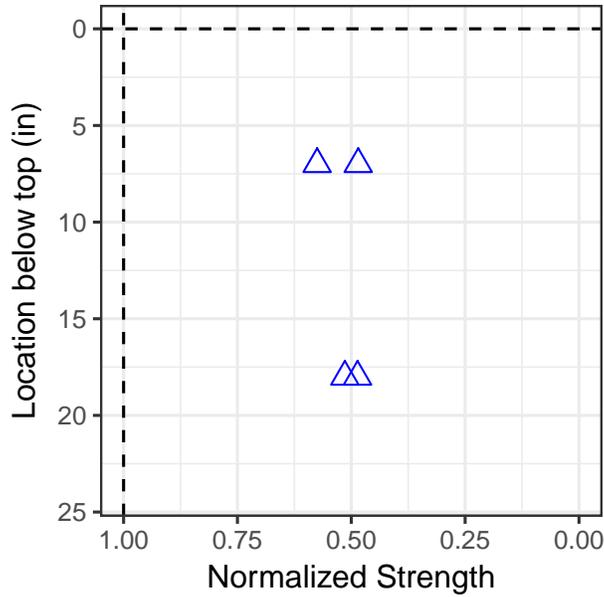
Figure 3.15: Results of compressive strength measurements using cylindrical samples along the height of the mock connection.

of the same height as the connection (Figure 3.11). These samples also followed the layered pouring scheme utilized in the mock connection. Cylinders and discs were cut from these samples to measure f'$_c$ and E (Figure 3.14 and 3.15). The compressive strength was measured according to ASTM C39-18 [4] and the elastic modulus was measured utilizing the method proposed by Leming et al. [23]. Although obtained using two different non-destructive testing methods, Figures 3.13 and 3.14 show similar results.

3.2.4 Level of Deterioration for Large Scale Tests

The mock connection produced valuable information. The primary concern regarding the method of EPS addition for damage simulation was the upward migration of EPS beads because of their low density. This migration would have resulted in a reduced strength and elastic modulus closer to the top half of the connection rather than in the bottom. This distribution would have been unacceptable since in reality, the bottom half of the GSS connection will experience deterioration first, while the top remains essentially unaffected. Figure 3.14 shows the lowest values of elastic moduli at the bottom with an approximately

linear increase with height. This trend is what one would expect in a real GSS connection exposed to a few years of freeze-thaw cycles. The mock connection was able to achieve an LoD with average reduction in elastic modulus of approximately 30% and strength of about 50%.

The same process of grout casting was repeated for the construction of the specimens for large scale tests 2, 3, and 4. Grout samples were poured into round and square PVC pipes to obtain discs and cubes for E and f'$_c$ measurements. Results from the testing of grout properties of the real specimens of tests 2 and 3 are shown in Figures 3.16 and 3.17, respectively. Results are shown separately for the two connections, North and South side of each specimen. Below the mid-depth of the connection, the elastic modulus profile shows the same trend as that shown in Figure 3.14 which indicate reproducibility. While there is some scatter, the GSS connections in tests 2 and 3 had, on average, a reduction in strength of 60% and in elastic modulus of 30% compared to those in test 1.

3.3   Chapter Summary

This chapter discussed the method that was followed to achieve a simulation of deteriorated GSS connections in the large scale tests. The objective of simulating deterioration was to be able to compare the structural performance of the deteriorated GSS connection to that of a standard undeteriorated connection. A literature search revealed that expanded polystyrene (EPS) aggregates when mixed with grout can reduce its compressive strength and elastic modulus. Therefore, EPS addition was chosen as the method through which damage simulation was achieved, since long term exposure to cold climates also results in reductions in the aforementioned structural properties.

EPS beads are extremely lightweight aggregates which tend to migrate upward in a grout mixture. This behavior was undesirable since a realistic simulation of damage must have a more uniform distribution of EPS near the bottom of the connection. A layered casting
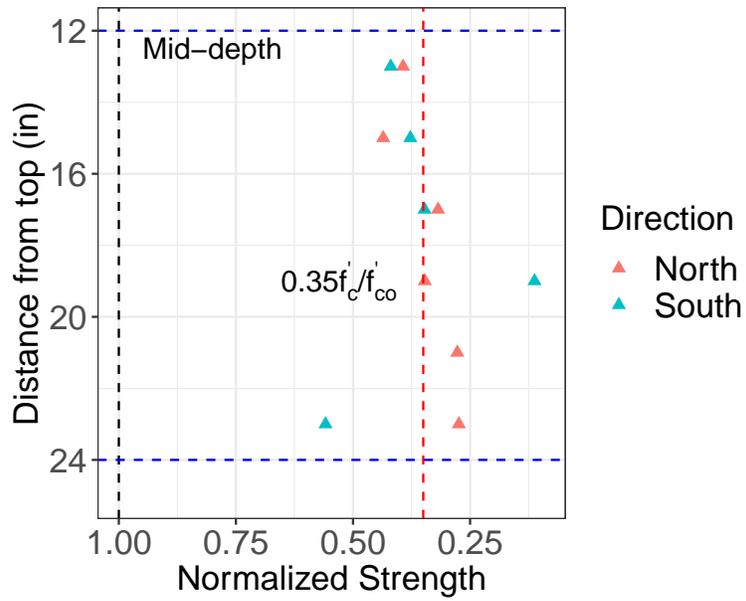
(a)
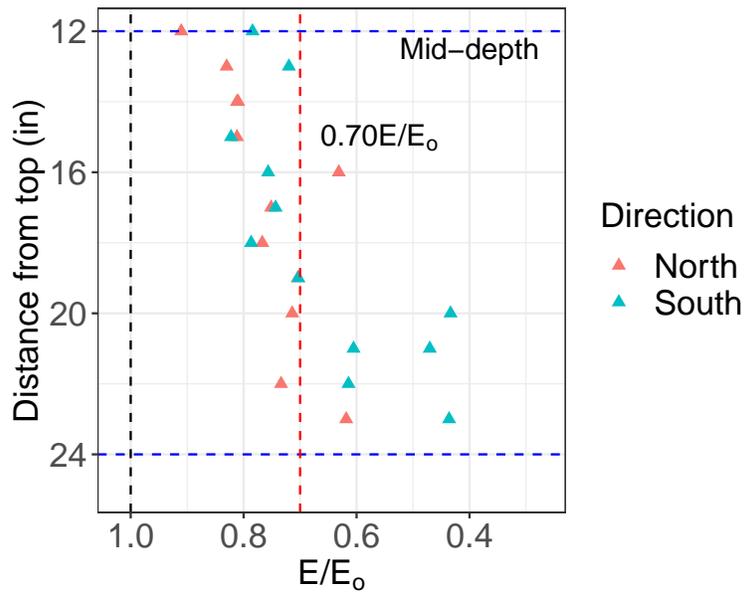
(b)

Figure 3.16: Results of grout properties from the GSS connection of **test 2** (a) Compressive strength profile obtained from cubic samples (b) Dynamic elastic modulus profile obtained from disc samples.
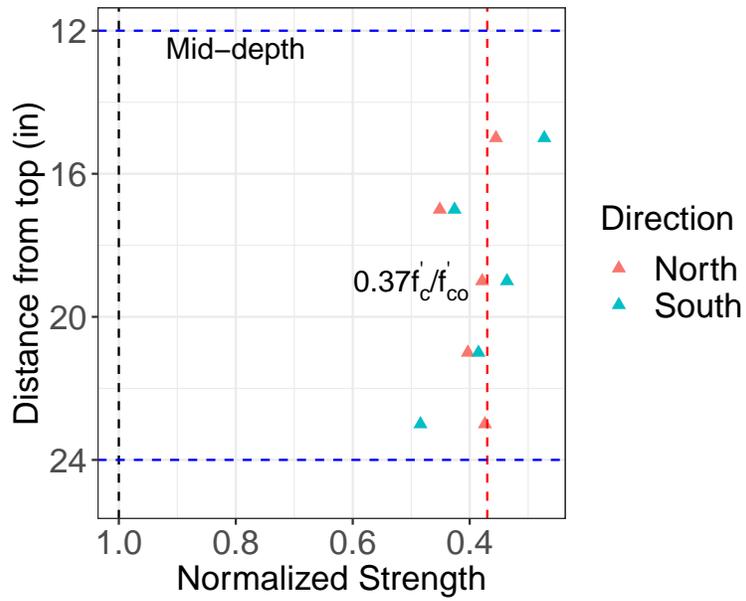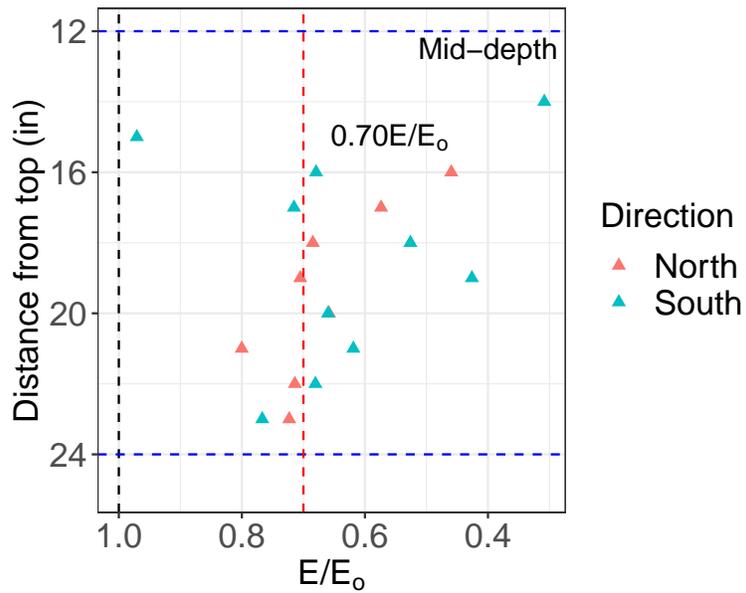
Figure 3.17: Results of grout properties from the GSS connection of **test 3** (a) Compressive strength profile obtained from cubic samples (b) Dynamic elastic modulus profile obtained from disc samples.

scheme was developed to overcome this problem. Practice casts were performed to ensure reproducibility of damage simulation. Finally, a grout mixture with enough EPS to simulate moderate-to-high levels of damage due to cold climate exposure was developed.

Chapter 4

Consequences of Grout Deterioration on Structural Performance of the GSS Connection

4.1 Introduction

This project began with the motivation of determining whether the GSS connection could be used in cold climates. Phase 1 of this project, discussed in Chapter 2, investigated the state of commonly available high-strength cementitious grout from the perspective of cold climate durability. This study was able to show that while all high-strength cementitious grouts do not possess good durability, some do, and testing samples of selected grouts for their durability can potentially separate the good ones from the bad. Before emphasizing the need for further study of cementitious grouts, it was worth determining the consequences of grout deterioration on the structural performance of the GSS connection. If grout deterioration does not significantly diminish the structural integrity of the lateral load resisting system, investigating additional commercial grouts may not yield significant further knowledge, from the GSS application standpoint. However, if grout deterioration does compromise the ability

of the system to successfully function under lateral loading, further studies optimizing the grout material would likely be required.

The approach was to perform large scale structural tests on specimens having deteriorated GSS connections and compare the results to those of specimens having fresh non-deteriorated GSS connections. Theoretically, any effect of grout deterioration would be evident from the comparison of the results of these experiments. Each structural test utilized a certain level of deterioration (LoD) for the grout in its connections. We simulated a damage (or deteriorated) state for the GSS connections in each test specimen by using an additive known as expanded polystyrene (EPS) aggregates. Differences in their performance under cyclic quasi-static lateral loading were investigated. The GSS connections in the first test specimen were initially "undamaged". The subsequent tests had GSS connections that had reduced grout compressive strength (f_c) and elastic modulus (E), representative of a moderate-to-high level of damage due to freeze-thaw exposure. We found that despite a substantial reduction in grout strength of approximately 60%, and grout elastic modulus of about 30%, no significant differences were observed in the global system behavior, including hysteretic characteristics, maximum strength, and maximum ductility. This result suggests that grout durability is likely of little concern in the long term performance of the GSS connection in cold climates.

The remainder of this chapter elaborates on our experiments to determine the structural consequences of grout deterioration. To understand this part of the project, it is necessary to follow the chronological order of experiments. We discuss each large scale test in detail. Important choices pertaining to several variables involved in each test were made at different points of time based on the most recent information. Decisions were made with due consideration of input from AKDOT engineers. To put these decisions into context, each test is described one after the other stating prior expectations and post implications of each.

4.2 Large Scale Experiments on Two-Column Bridge Bents - I

4.2.1 Research Approach

The objective of the large scale tests was to investigate the effect of GSS connection durability damage on the seismic behavior of the lateral load resisting system. An ideal procedure to determine the consequences of connection deterioration would be to cast multiple specimens with the GSS connection, test one of them as a control and subject the others to severe cold climate environment (real or simulated), and subsequently test them one by one at different points of their service life. Due to obvious constraints, this procedure was not adopted.

The approach was to artificially simulate different levels of deterioration (LoD) in the connection without environmental exposure. To elaborate, an LoD represents the effective state of the grout after years of service. As discussed in earlier chapters, the durability detriments, namely freeze and thaw, thermal gradients, and restrained shrinkage act on the GSS connection to produce cracking within the grout. The grout properties that are adversely affected by environmental exposure in cold climates are its compressive strength (f'_c) and elastic modulus (E). Incidentally, the grout properties that contribute to the integrity of the structural system are also its f'_c and E. By producing a grout mixture with the effective properties of deteriorated grout, an LoD could be achieved that would be an adequate substitute for a deteriorated connection.

The test specimens were large scale two-column bridge bents. These consist of two steel columns connected to a steel cap-beam using the GSS connection. The procedure by which different LoDs were achieved was discussed in detail in Chapter 3. The idea was to introduce expanded polystyrene (EPS) beads to the grout mix by part replacement of grout. The EPS material is extremely lightweight and when distributed within the grout microstructure, it can take up space simulating air pockets. The larger the volume fraction of these beads in the hardened grout, the lesser will be the grout's compressive strength and elastic modulus.

To achieve a controlled reduction of grout properties, many trials were carried out with different amounts of EPS mixed in grout.

Table 4.1 provides a summary of the results from all of the large scale experiments that were performed. Note that test 0 was not performed as part of this project. It was one of the tests performed by Fulmer et al. [16], but is provided here because of its relevance to this project. In Table 4.1, tests 0 and 1 represent bridge bents that are new and hence have GSS connections that are undamaged. Tests 2 and 3 represent bridge bents exposed to multiple years of service in a cold climate. The connections in these bridge bents exhibit a moderate-to-high level of simulated grout deterioration. As seen in the table, all the tests from test 0 to test 3 show good structural behavior, i.e., ductile failure via plastic hinge formation in the columns just below the GSS connection. Soon after test 2, a meeting with AKDOT led to a change of scope of the project. Consequently, test 3 was adjusted to assess the impact of a reduced number of shear studs. This impact is discussed in Chapter 5. However in hindsight, it can also be used as another data point to determine the effect of grout deterioration, because the effect of shear studs on global response was later found to be insignificant. In this chapter therefore, test 3 results serve as a repeat of test 2. Each test and its implications are discussed later in detail.

Table 4.1: Test matrix used to determine consequences of grout deterioration on the structural performance of the GSS connection.

Test No.	Test ID	LoD (E and f'$_c$)	Number of Shear Studs	Result
0	SG-96	NA and 0.7f'$_{c0}$	96	Good
1	SG-32	E$_0$ and f'$_{c0}$	32	Good
2	DG-32	0.7E$_0$ and 0.4f'$_{c0}$	32	Good
3	DG-16	0.7E$_0$ and 0.4f'$_{c0}$	16	Good

4.2.2 Large Scale Experimental Setup

Large scale experimental tests were conducted at North Carolina State University's Constructed Facilities Laboratory (CFL). In all cases, the test specimens were a large scale

two-column steel bent as shown in Figure 4.1. The columns were 1/2" thick, 16" diameter round API 5L X52 PSL2 pipes while the short stub pipes were 1/2" thick, 24" diameter round sections of the same material. The cap-beam was a double-wide HP14x117 section. The height of the center of the cap-beam from the pin was 11'2", and the center-to-center distance between the two columns was 12'. The steel bent was supported by two base shoes through pinned connections. The steel pins were 5" in diameter. Such a boundary condition mimics the point of contraflexure that develops in the moment profile of an actual bridge system. The base shoes themselves were prestressed to the laboratory strong floor utilizing 1-3/8" diameter Dywidag bars, with a force of 150 kips per bar.

A 440-kip actuator mounted on the laboratory strong wall was used to apply cyclic quasi-stating lateral loading. We used a three-cycle set loading history, as shown in Figure 4.2. The definition of this loading history consists of an initial elastic portion based on the anticipated yield force of the system, and a second section based on the experimentally determined yield displacement of the system. The elastic portion consisted of double reverse cyclic load-controlled cycles of 1/4 first yield force increments until the full first yield force cycle was completed. The first yield force (F_y) for the two-column bent was determined as

$$F_y = \frac{2f_y S}{X} \tag{4.1}$$

where S represents the elastic section modulus of the pipe pile members, f_y represents the anticipated yield stress of the pipe material, and X represents the shear span from the pinned supports to the critical pile hinging section.

The second section of the load history was defined by displacement controlled incremental ductility levels where displacement ductility 1, or equivalent yield displacement, is defined by Equation 4.2 and subsequent displacement ductility levels are defined by Equation 4.3,

$$\mu_1 = \Delta_y = \Delta'_{y,exp} \frac{M_p}{M_y} \tag{4.2}$$
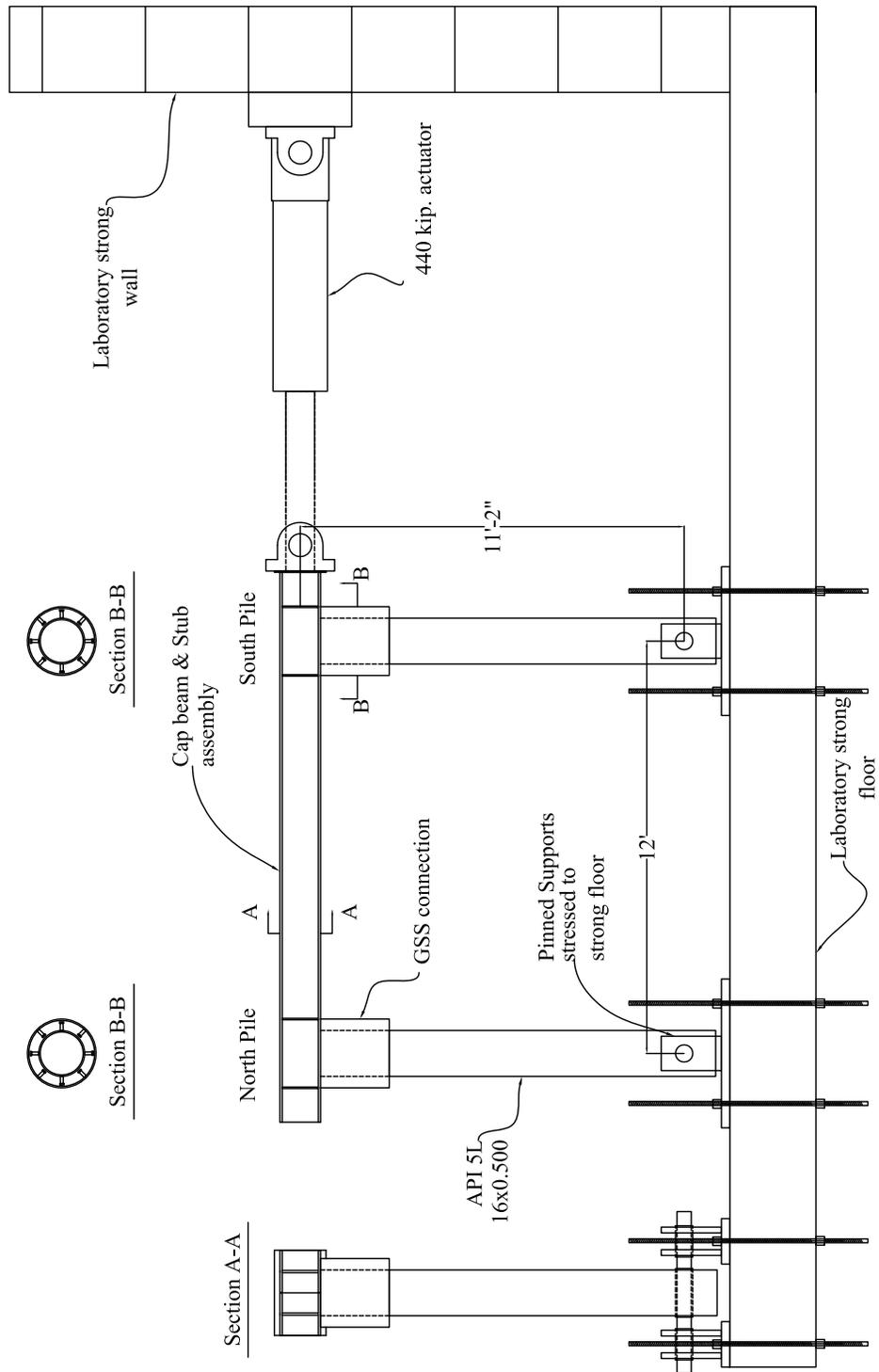
Figure 4.1: Laboratory large scale experiment setup
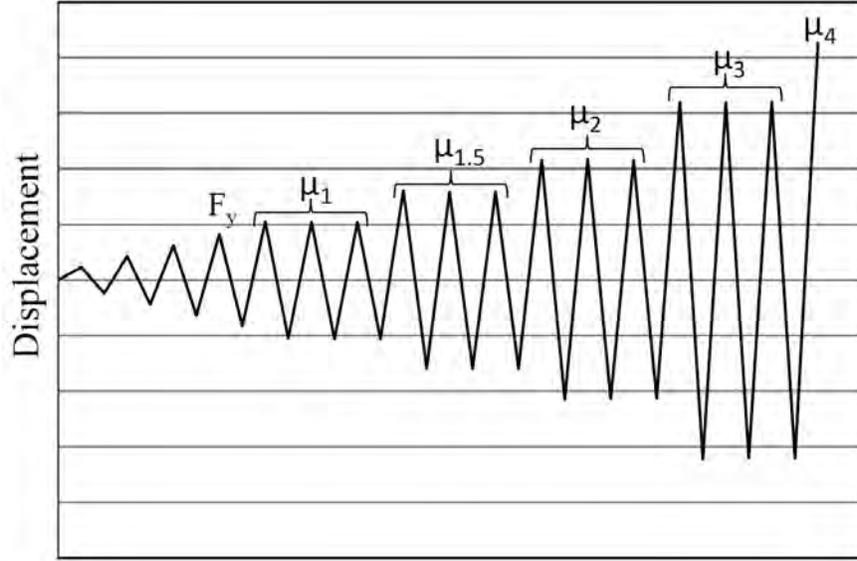
Figure 4.2: A typical three cycle set loading history.

$$\mu_i = i\mu_1 \tag{4.3}$$

where $\Delta'_{y,exp}$ represents the experimentally determined first yield displacement, and M_p and M_y represent the full plastic moment capacity and the first yield moment capacity of the column section, respectively.

The instrumentation scheme for the test consisted of conventional electrical resistance strain gages and string potentiometers. Also utilized were NDI Certus OPTOTRAK sensors that detect LED markers attached to the specimen. This system allowed the monitoring and recording of the three dimensional coordinates of each marker in real time. This coordinate data was post-processed to obtain displacement fields at locations of interest. Strains were then calculated from this data.

The construction process of the specimens in tests 1 through 4 was consistent. The process differed slightly from that of test 0 [18]. The differences are mentioned subsequently wherever relevant. Fabrication of the cap-beam/pipe-stub assembly was performed in the shop by a certified welder and inspected by a certified weld inspector. Figure 4.3 shows the fabrication details. The shear stud welding on the columns and stubs was also performed by

the same welder. A lower number of larger sized shear studs was chosen for this test. These studs were cut (as they were too long), and hand welded. Shear studs were also welded to the top of the two pipe columns as shown in Figure 4.4.

The next step of the construction process was erecting the two pile columns on top of their pin supports. This was achieved by tying the erected piles to the floor using ratchet straps and D-rings (Figure 4.5). The cap-beam/stub assembly was then brought in and lowered onto the two columns (Figure 4.6a). The columns were inserted into the sockets created by the pipe stubs, and the cap-beam rested on top of the columns (Figure 4.6b). No additional welding was performed to connect the columns to the cap-beam.

Once the cap-beam was in place, the annular regions surrounding the column tops were filled with grout to complete the GSS connections. We used a manual grout pump to achieve this casting (Figure 4.7a). It is worth noting that the grout was pumped through an opening in the beam flange (bottom flange of the beam) at the top of the connection (Figure 4.7b). This casting process differed from that used in test 0 where the grout was pumped from the bottom.

4.2.3   Large Scale Test 1

Introduction

Recall that the motivation for Phase 2 of this project was to ascertain the consequences of deteriorated GSS connections on the global structural performance of bridge bents. Also, recall that the approach to achieve this objective was to compare structural response of bridge bents with deteriorated connections to those with undamaged connections. Test 1, discussed here, acted as a control test to provide a baseline for the comparison of the results of deteriorated connections (Tests 2, 3, and 4). Test 0 may also be considered to act as secondary control test. However, a one to one comparison of the results of tests 2, 3, and 4 to that of test 0 cannot be made because of some important changes made to the experimental setup of Tests 1 through 4, as discussed next.
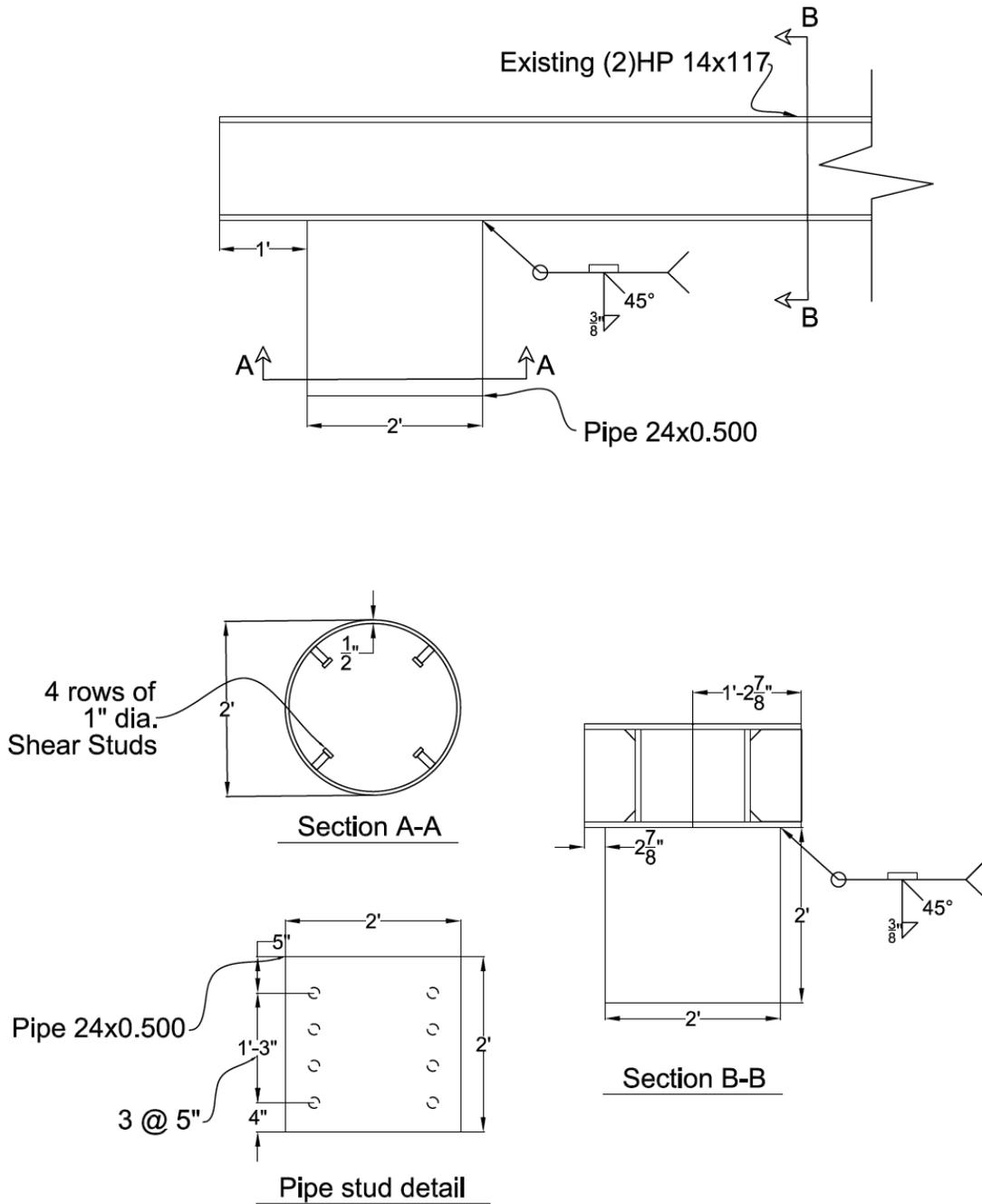
Figure 4.3: Fabrication details for the cap-beam stub assembly of Tests 1 through 4.

Figure 4.4: Fabrication details for the hollow circular columns used in Tests 1 through 4.

Figure 4.5: Columns erected and ready for cap-beam assembly.

(a)   (b)

Figure 4.6: Photographs showing (a) the cap-beam stub assembly being lowered onto the columns and (b) one of the columns afterwards.

<div align="center">(a)   (b)</div>

Figure 4.7: Photographs showing (a) the grout pump and (b) the pumping process.

Experimental Setup

AKDOT prefers to use steel pipe material API 5L X52 PSL2 for the construction of new bridges compared to conventional ASTM A500 Gr. B material. API 5L PSL2 is a steel material with better quality control. American Petroleum Institute (API) standards require this material to meet the following specifications. For pipe grade X52, a minimum and maximum material yield strength of 52.2 ksi and 76.9 ksi, respectively, must be met. This requirement is useful from a seismic design standpoint because material overstrength is better controlled and more importantly, defined. PSL2 rated material is required to be tested for its Charpy V-notch (CVN) energy absorption values. Typically, the CVN toughness of this material is above 200 ft-lb at 32°F (0°C). The high toughness provides the material with high ductility capacity even at low temperatures. Therefore, all columns and stub pipes used in tests 1 to 4 of this project were API 5L X52 PSL2 material. The geometry of the test setup remains the same as that in test 0.

(a)   (b)

Figure 4.8: Photographs showing the arrangement of shear studs in (a) the stub pipe on the cap-beam, and (b) the pile columns.

Yet another difference from test 0 is that while it had a total of 96 shear studs of 3/4" diameter, per GSS connection, the specimens in tests 1 and 2 consisted of connections with a total of 32 shear studs of 1" diameter (16 on each column and 16 in each stub). Furthermore, Tests 3 and 4 consisted of a total of 16 shear studs of 1" diameter, per GSS connection. A detailed discussion of the reasons for this change is presented in Chapter 5. A shorter version is as follows. The design of the number of shear studs in test 0 was accomplished using an excessively high axial force demand versus what realistically develops. In addition, the capacity of shear studs embedded in confined grout may have been underestimated. AKDOT wanted to explore the possibility of using a smaller number of larger diameter shear studs for economy and ease of construction. In test 1, a total of 32 (16 each on the column and stub pipe) 1" dia. shear studs were welded inside each GSS connection. A symmetrical condition was generated by 4 lines of 4 shear studs at 90 degrees center to center as shown in Figure 4.8.

Experimental Summary

The structural test was performed 30 days after casting the grout in the GSS connections. Cyclic quasi-static loading was applied to the two-column steel bent initially in the force control mode at a rate of 10 kips/min. The two columns of the test specimen were from different heats of manufacturing. The measured average yield strengths of the North and South columns were 63.8 ksi and 69.6 ksi, respectively. The calculation of F_y used the lower yield strength of the two columns. Two cycles to each force level ($0.25F_y$, $0.50F_y$, $0.75F_y$ and F_y) were applied first. Within the first two cycles, there were audible sounds of grout cracking. These sounds continued until the force level of F_y. The force-displacement response of the system is provided in Figure 4.9.

After two cycles at yield force, the actuator control was changed from load control to displacement control. A load rate of 1 in/min was used for ductilties 1 and 2. The rate was changed to 2 in/min for subsequent ductilities. Three cycles at each ductility level (μ_1, $\mu_{1.5}$, μ_2, μ_3 and μ_4) were performed. The pipes showed minor slip and detachment from the surrounding grout rings during the first positive cycle of ductility 1.5. The maximum force at this stage was 143.7 kips. No strength drop was observed. Within the second negative cycle of ductility 1.5, large pieces of grout started spalling from the north GSS connection. The spalling continued for the next few cycles in the north GSS connection. The grout below the first row of shear studs spalled out in the north GSS connection after three cycles at ductility 1.5, as shown in Figure 4.10. This observation is a different behavior from that of test 0. Grout did not spall from the specimen in test 0 until ductility 4 cycles. A combination of factors could have contributed to this difference in test 1.

First, the number of shear studs in each GSS connection in test 1 is only one-third the number used in test 0. Therefore in test 0, a larger number of compression struts and tension ties are formed under loading. The larger number of these truss-like members help distribute the forces more efficiently, resulting in a reduced stress demand per unit volume of grout.

Second, under cyclic loading, a gap starts to open in the GSS connection between the

95
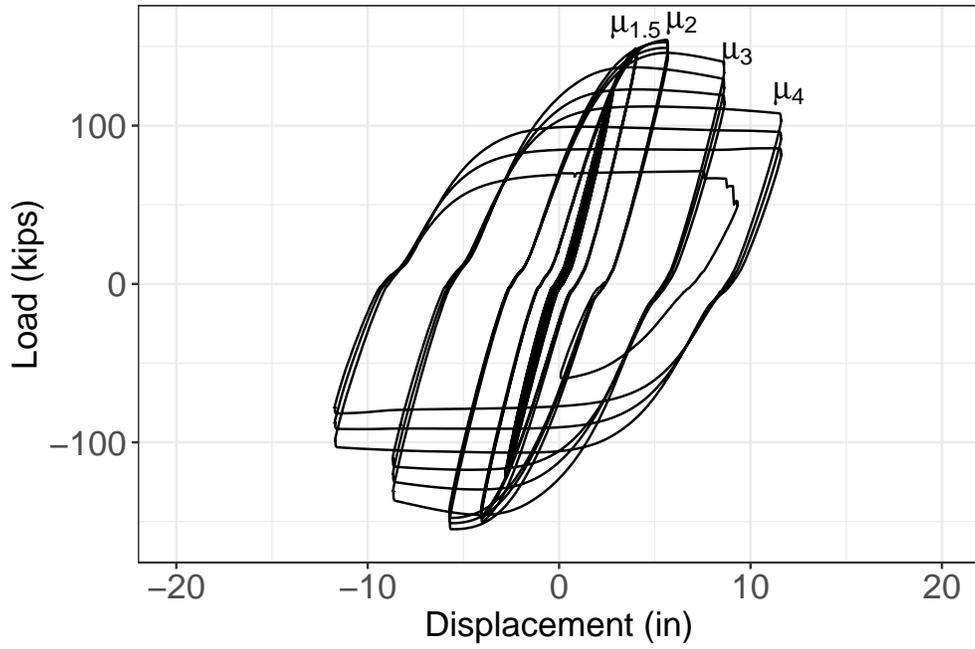
Figure 4.9: The force-displacement hysteretic response of Test 1.
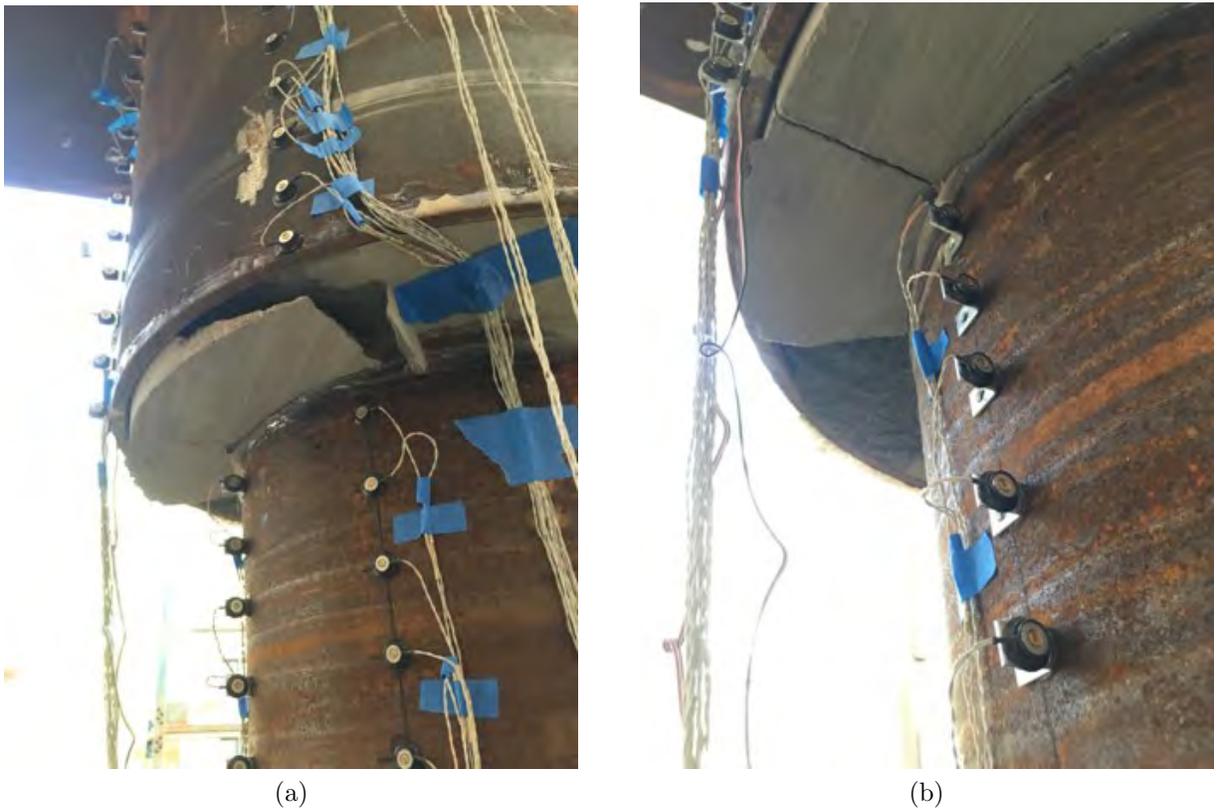
Figure 4.10: Grout spalling observed at (a) North column, South side, and (b) South column, South side (Ductility: 1.5, Cycle: -3, Force: 143.7 kips, Displacement: -4.1 in.).

outside surface of the grout ring and the inside surface of the stub pipe. The magnitude of this gap is dependent on the number of shear studs present near the bottom of the connection. When the grout ring tries to detach from the inside of the stub pipe, the shear studs prevent this detachment by mobilizing tensile stresses in them. The magnitude of the tensile stresses developed depends on the number of shear studs that help resist the demand. In test 1, the number of shear studs mobilizing this mechanism was much lower than that in test 0. The excessive tensile stresses thus developed, crack the grout near the bottom of the connection. Thus, the grout below this spalls out.

The mechanism of force transfer within the GSS connection, which is the topic of the next chapter, is complicated. In addition to the possible causes mentioned above, the location of the bottom row of studs in test 1 is much higher into the connection compared to test 0. In other words, there is a much larger amount of plain grout cover in test 1 than in test 0. This large cover may also be unable to resist excessive tensile stresses developed as a result of the second mechanism mentioned above.

During the first positive cycle of ductility 2, minor local buckling was observed in the south face of the north pile section, just below the GSS connection. This is the same column and face where high grout spalling was observed earlier. The bottom row of shear studs was further visible. The GSS connection on the south pile started showing grout spalling during the third negative cycle of ductility 2. The bent showed slight drops in strength for each subsequent cycle of ductility 2. The maximum force during the ductility 2 cycles was 150.6 kips.

The first positive cycle of ductility 3 induced outward pile wall local buckling in the south face of the north pile, as shown in Figure 4.11a. On the subsequent negative cycle, similar local buckling was observed on the north face of the south pile (Figure 4.11b). Initially, the outward curvature of buckled pipe walls reduced and "straightened up" upon load reversals. The curvatures increased with each successive cycle and showed permanent buckling. The strength of the specimen continued to drop on each successive cycle. The maximum force
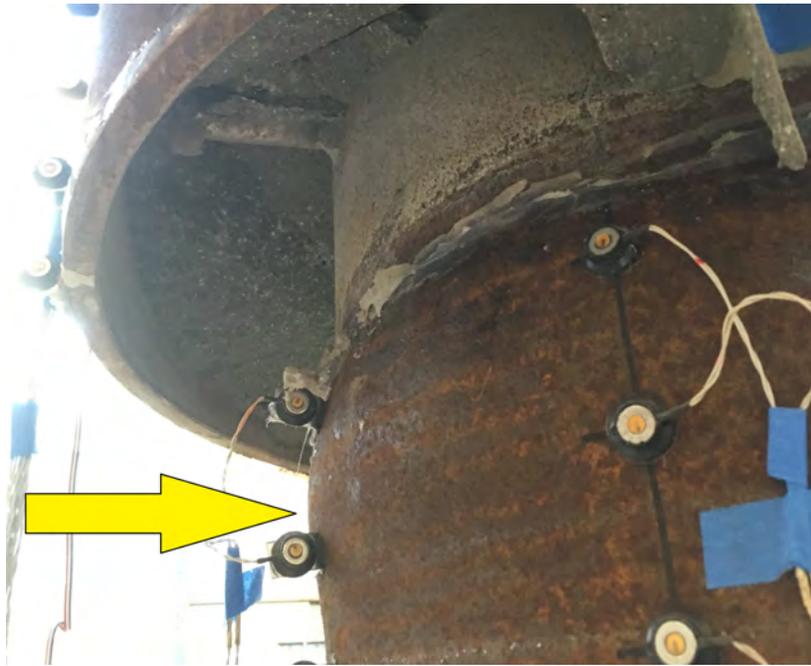
(a)

(b)

Figure 4.11: Pile wall outward local buckling on the (a) south face of north pile (Ductility: 3, Cycle: +1, Force: 136.3 kips, Displacement: 8.62 in.) and, (b) north face of south pile during the first negative cycle of ductility 3 (Ductility: 3, Cycle: -1, Force: -132.2 kips, Displacement: -8.65 in.).

Figure 4.12: Pile wall rupture in the plastic hinge region on the north face of south pile during the first positive cycle of ductility 5 (Ductility: 5, Cycle: +1, Force: 51.0 kips, Displacement: 9.32 in.).

during the ductility 3 cycles was 136.3 kips.

Three positive and three negative cycles of ductility 4 were completed successfully without rupture. Further grout spalled from both the connections. The plastic hinge length was observably small, with large curvatures evident in the buckled regions. Wall local buckling progressed around the circumference of the pile sections. The reductions in strength became larger. The maximum force during the ductility 4 cycles was 104.3 kips.

During the first positive cycle of ductility 5, the north face of the south pile experienced rupture in the plastic hinge region. This is shown in Figure 4.12. The specimen was deemed to have failed and the test was terminated. The specimen experienced a maximum displacement of 11.7 in before failure which corresponds to 9% drift (Figure 4.13).

Results and Discussion

Plastic hinge relocation was successfully achieved in test 1. A comparison of the force-displacement response of tests 0 and 1 is shown in Figure 4.14, in which the load on the y-axis is the normalized load. The load values were normalized to their respective peak loads

Figure 4.13: The test specimen experienced a maximum drift of 9% (Ductility: 4, Cycle: +3, Force: 82.2 kips, Displacement: 11.60 in.).

for each test. This was to eliminate the effect of the difference in yield strengths of the steel used in each test. Note that the hysteretic behavior of the two specimens is similar. A reduction of the number of shear studs did not seem to significantly affect the response.

Close to zero load at all ductility levels, a slip was observed in test 1, indicated by a small kink in the force-displacement response. This slip is absent in test 0. This slip also seems to increase in magnitude at higher ductilities. From results of later tests, it was possible to conclude that this was caused by the opening of a gap between the pipe and the grout ring on the tension side of the connection, as shown in Figure 5.31a. When the column bears on the grout ring on the compression side, the round section deforms, and is no longer round. This behavior reduces the diameter of the column orthogonal to the neutral axis, pulling the tension side off of the grout ring. In test 0, however, the number of shear studs was larger compared to test 1. This large number of shear studs prevented the column from detaching from the grout ring, resulting in an insignificant gap. Therefore, the force-displacement
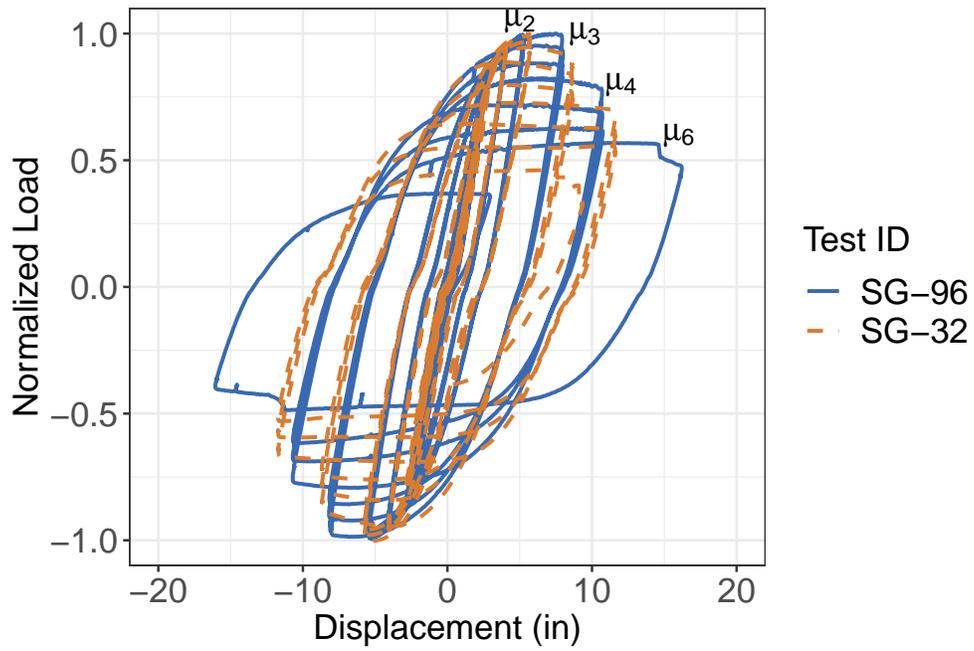
Figure 4.14: Comparison of the force-displacement response of Test 0 (SG-96) and Test 1 (SG-32).

Figure 4.15: Detachment of the column from the surrounding grout ring on the tension side of the connection.

response of test 0 does not exhibit slip. This slip in force-displacement response is of little concern.

4.2.4 Large Scale Test 2

Introduction

Test 1 results serve as a control to which the results of the tests with deteriorated GSS connection may be compared, to make inferences about the effects of grout deterioration on the structural performance of the connection. In test 2, EPS beads were added to the grout to reduce its elastic modulus and compressive strength to about 70% and 35% of that in test 1, respectively. The profile of the elastic modulus and compressive strength along the height of the connection below mid-depth is shown in Figure 4.16. The values have been normalized to the corresponding value of standard grout used in Test 1. It is assumed that these profiles are representative of GSS connections that have been exposed for many years in cold climates. The results of test 2, therefore, provided us information useful to determine the structural consequence of grout deterioration.

Experimental Setup

The test specimen was a large scale two-column steel bent similar to the one used in test 1. Test 2 followed the same displacement history as that of test 1. The entire test was performed in displacement control mode. After elastic cycles, three cycles at each ductility level were applied until test termination. The instrumentation scheme consisted of electrical resistance strain gages, string potentiometers, and OPTOTRAK sensors, the same as test 1.

A lower number of larger sized shear studs was used for this test. The only difference from test 1 was the position of these studs with respect to the connection. In test 1, there was 5" thick grout ring cover that was unreinforced with shear studs. In this test, this was reduced to 2.5" to mitigate early grout spalling. These studs were cut (as they were too long), and welded by hand rather than by a stud gun.
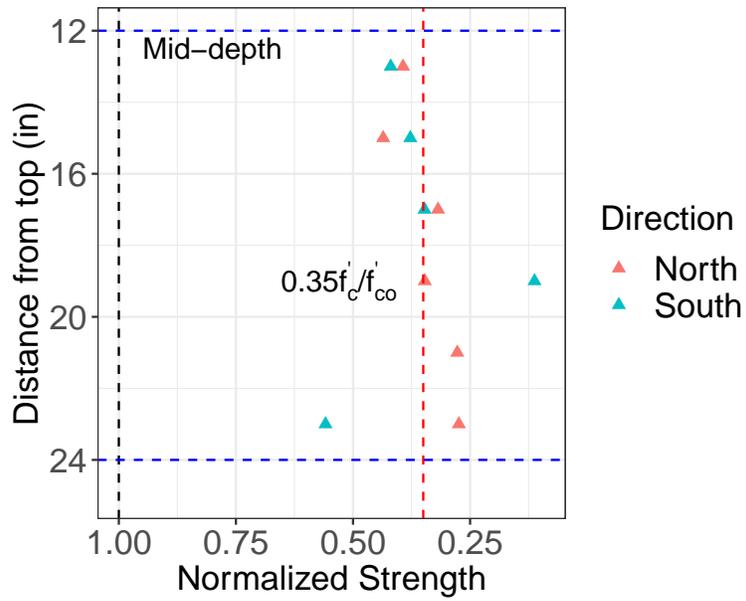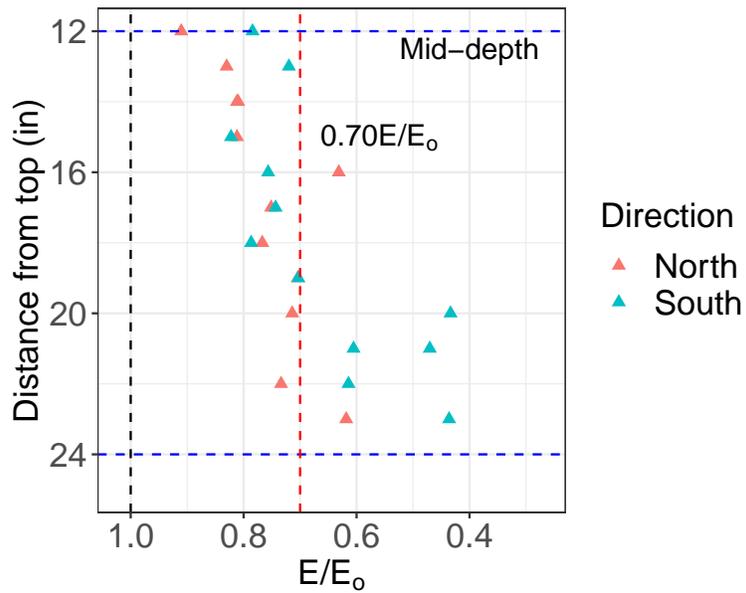
Figure 4.16: Results of grout properties from the GSS connection of **Test 2** (a) Compressive strength profile obtained from cubic samples (b) Dynamic elastic modulus profile obtained from disc samples.
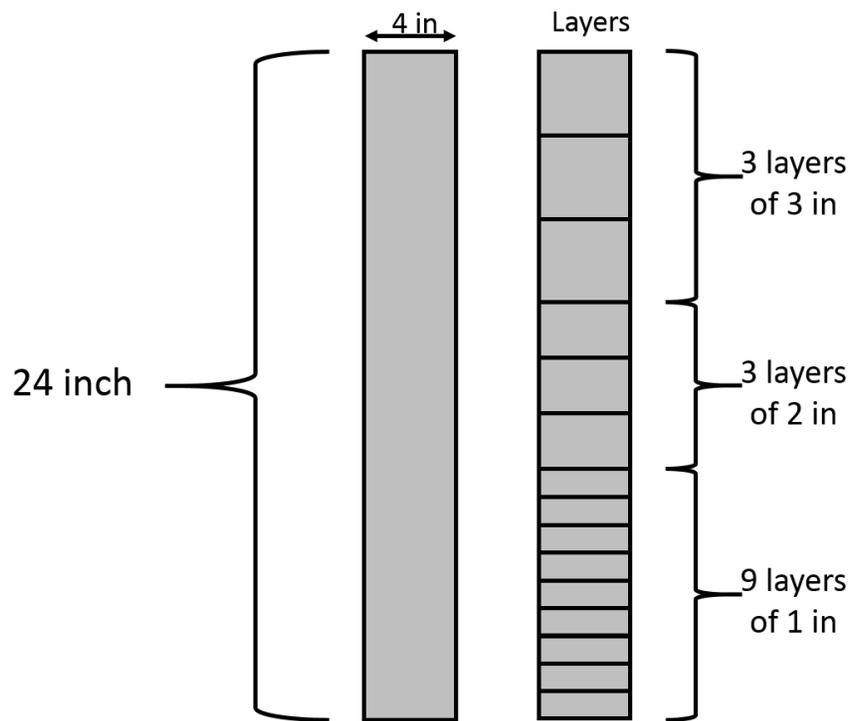
Figure 4.17: Layering scheme used to obtain uniform EPS distribution in GSS connections for physical damage simulation.

The GSS connections were filled with the grout mixture that was developed to simulate deterioration (Chapter 3). EPS beads were added to the grout mixture for this purpose. To prevent segregation and migration of the EPS beads, the connections were cast in layers as shown in Figure 4.17. For the first 9 inches from the bottom, 1" thick layers of grout were cast at intervals of 30 minutes. This wait-time allowed enough time for the fluid mixture to develop partial setting that prevented migration of EPS beads. The next 6 inches were cast in layers of 2" thicknesses with the same wait-time. The last 9 inches were cast in layers of 3" thickness. Grout mixture samples were collected in round and square PVC pipes that were cut to 24" lengths. The sample casting followed the same layering scheme as the actual connection. Samples in round PVC pipes were later used to cut into discs to measure the elastic modulus profile along the height of the connection. Samples in square PVC pipes were cut into cubes to measure the cube compressive strength.

Experimental Summary

The structural test was performed 15 days after casting the grout in the GSS connections. Cyclic quasi-static loading was applied to the two-column steel bent in the displacement control mode. The initial load rate was 1.5 in/min which was later changed to 4 in/min in the inelastic cycles. Two cycles at each force level ($0.25F_y$, $0.50F_y$, $0.75F_y$, and F_y) were applied first. Within the first two cycles, there were sounds of grout cracking. These sounds continued to occur until the force level of F_y was reached. Visible separation of the grout ring from the pile wall was observed at about $0.75F_y$. Radial cracks near the neutral axis of the connection started to develop in both connections, as shown in Figure 4.18a. The cracks multiplied during the second cycle of F_y.

After three cycles at ductility 1, the gap between the grout ring and the pile column opened to nearly 0.1". The outer circumference of the grout ring also started to slip inside the stub pipe. At the second cycle of ductility 2, minor spalling was observed in the south column. Major spalling occurred in the same column on the first push cycle of ductility
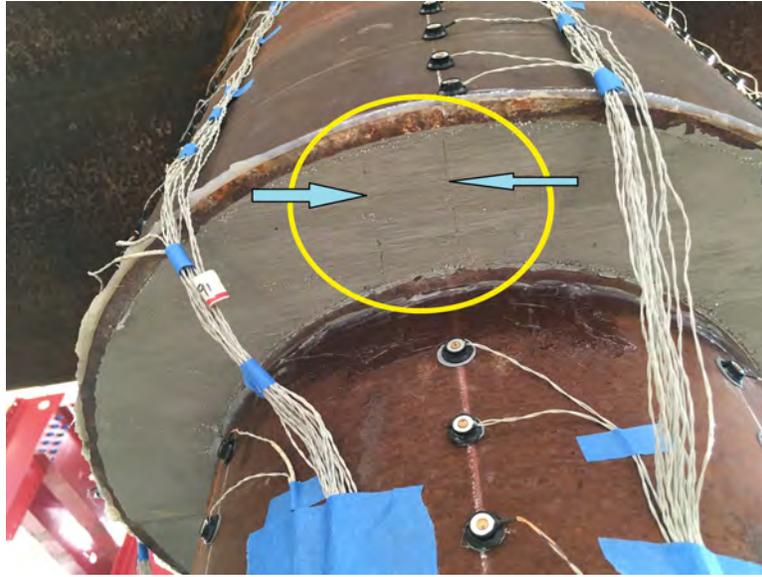
(a)

(b)

Figure 4.18: (a) Transverse cracking observed at the neutral axis of the GSS connection (Ductility: F_y, Cycle: +1, Force: 97.8 kips, Displacement: 2.53 in.), and (b) the observed gap between the column and surrounding grout ring (Ductility: 3, Cycle: +1, Force: 142.1 kips, Displacement: 8.64 in.).
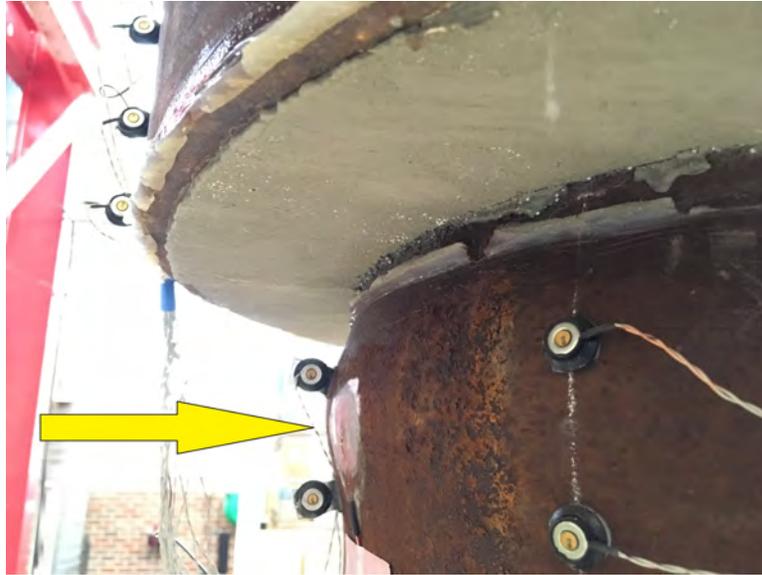
Figure 4.19: Pile wall local buckling (Ductility: 3, Cycle: +1, Force: 142.1 kips, Displacement: 8.64 in.)

3. The separation between the grout and the column increased to about 0.5" on the north column, as shown in Figure 5.32b. Pile wall local buckling was observed on the south side of the north column on the same cycle (Figure 5.34b). On the subsequent pull cycle, the north side of the south column also experienced pile wall local buckling. On the second push cycle of ductility 3, there was further grout spalling on the north side of the south column and the first row of shear studs was visible. The separation between the pile and the grout ring on the south side during the same cycle increased to 0.7".

On every subsequent cycle, the load in the system dropped. During the first push of ductility 4, significant local buckling was observed in both columns, as shown in Figure 5.35b. All three cycles at ductility 4 were then completed without any sign of tear or rupture. After the first push cycle of ductility 5, some tear marks developed on the north column (Figure 5.37b). The specimen was then subjected to the first pull cycle at ductility 5. During this cycle, a loud popping sound was heard. Upon investigation, no pipe rupture had occurred yet. It is thought that the shear studs on the columns were bearing against the stub wall and consequently slipped with a sudden release of stored strain energy causing the popping sound. The specimen was then brought back to zero force. By this point, the
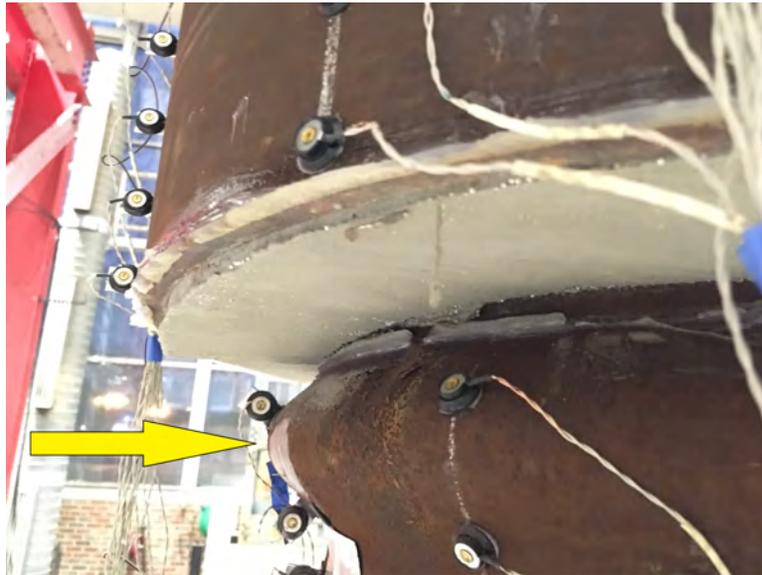
Figure 4.20: Pile wall local buckling (Ductility: 4, Cycle: +1, Force: 112.2 kips, Displacement: 11.50 in.)

Figure 4.21: Pile wall local buckling (Ductility: 5, Cycle: +1, Force: 84.1 kips, Displacement: 14.21 in.)

Figure 4.22: Structure drift of 11% (Ductility: 5, Cycle: +1, Force: 84.1 kips, Displacement: 14.21 in.)

load had dropped by 60% and the specimen had attained a drift of 11% as shown in Figure 4.22. The test was terminated at this point because of stability concerns.

Results and Discussion

A comparison of the force-displacement responses of tests 1 and 2 is shown in Figure 4.23. In the figure, the notation SG-32 is the code for standard grout with 32 shear studs in the GSS connections of the corresponding test. Similarly, DG-32 is the code for deteriorated grout with 32 shear studs in the GSS connections of that test. Hence, Figure 4.23 shows the effect of deteriorated grout on overall structural response.

During the elastic cycles, test 2 specimen had a slightly reduced stiffness compared to Test 1 (Figure 4.24a). This was expected since the grout in test 2 had a reduced elastic modulus or stiffness. However, this reduction is barely noticeable on the complete force-displacement hysteresis curve. In ductility 1 and 2 cycles, the curvature demand in the plastic hinge region
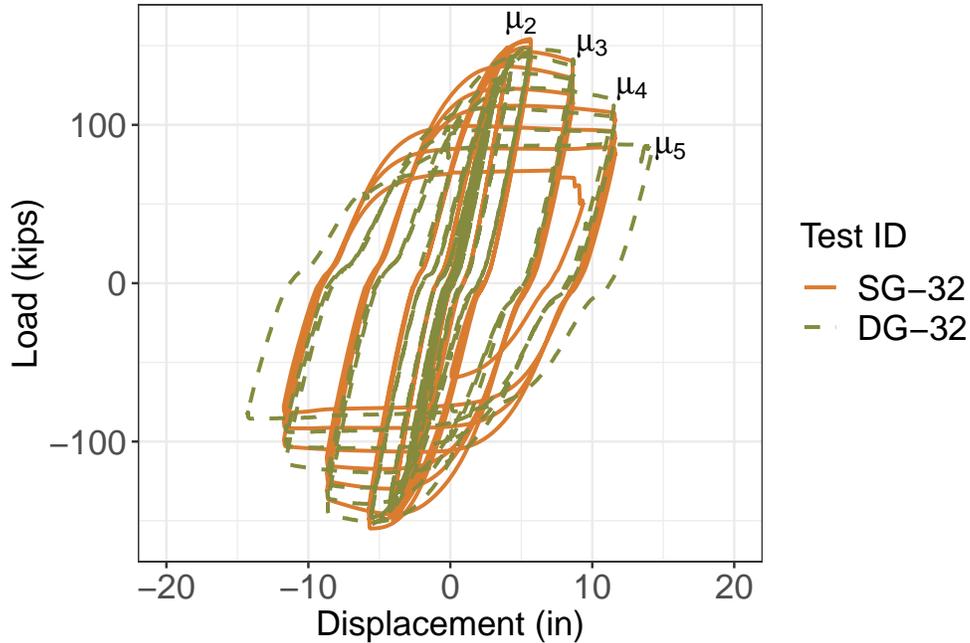
Figure 4.23: A comparison of the force-displacement hysteretic responses: Test 1 (SG-32) v Test 2 (DG-32)

for test 1 columns was higher than that of test 2. This larger curvature resulted in a slightly larger energy dissipation by test 1 specimen compared to test 2 specimen (Figure 4.24b). The reduction in curvature demand in Test 2 specimen may be attributed to the higher flexibility of the grout as well as the gap that opens between the column and the grout ring.

During ductility 3 cycles, test 1 specimen had already started to lose the its load carrying capacity as the plastic hinge was fully developed, and there was minor local buckling, as shown in Figure 4.25a. The section just below the plastic hinge pinched and thereby reduced the section modulus. test 2 specimen only started to lose strength at subsequent cycles, albeit at the same ductility. During ductility 4 cycles, both test 1 and test 2 started to show similar behavior once again (Figure 4.25b). Some differences here include a slightly higher load carrying capacity and a reduced reloading stiffness of test 2 specimen.

The observed differences between the global force-displacement response of the two specimens in tests 1 and 2 are minor from the perspective of satisfactory structural performance in an earthquake. Despite the grout properties being reduced considerably, the difference
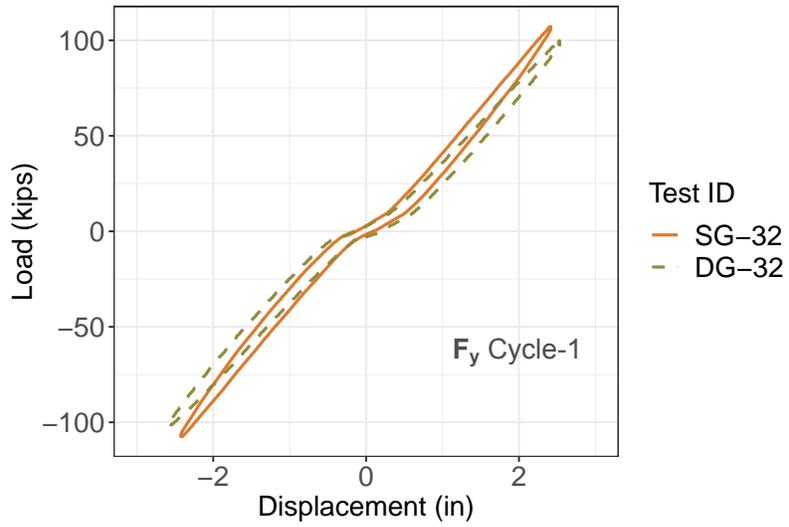
(a)
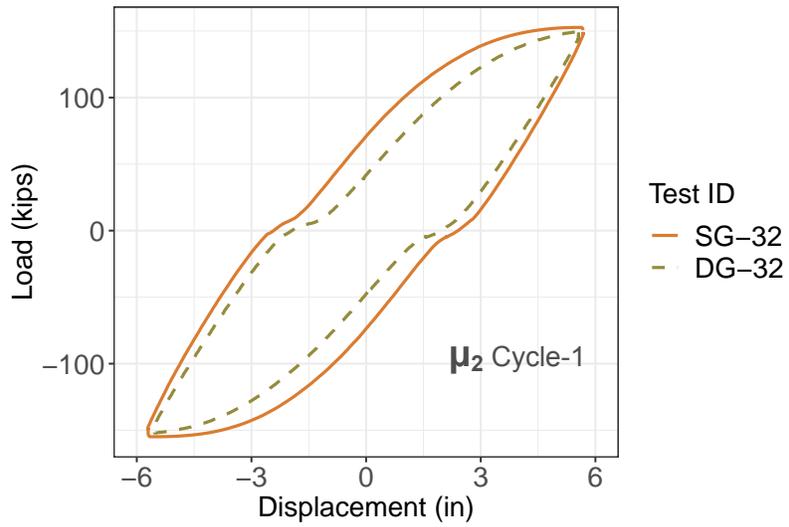
(b)

Figure 4.24: Comparison between hysteretic loops of Test 1 (SG-32) and Test 2 (DG-32) at different ductilities: (a) F_y (b) μ_2.

(a)

(b)

Figure 4.25: Comparison between hysteretic loops of Test 1 (SG-32) and Test 2 (DG-32) at different ductilities: (a) μ_3 (b) μ_4.

in the overall structural behavior of the two-column bent specimen is insignificant. These results suggest that a moderate to high level of durability damage is unlikely to compromise the structural integrity of the lateral load resisting system.

The force-displacement hysteretic curves of two tests (1 and 2) show a kink close zero force. Recall, that this kink or slip was not observed for test 0. The hypothesis of the gap opening between the column and the grout ring causing this "slip" in the hysteresis curve was corroborated in test 2. As discussed earlier, the gap that opened between the column and the grout in test 2 was much larger than that in test 1. This observation corresponds to the larger kink in the force-displacement response. Later (tests 3 and 4) produced further support for this hypothesis.

4.3 Chapter Summary and Conclusions

4.3.1 Summary

In this chapter, we discussed the large scale structural tests that were performed to determine whether grout deterioration in cold climates could cause significant problems for satisfactory performance of the GSS connection. Our approach was to test two large scale specimens that incorporated the GSS connection. While standard grout was used for the fabrication of the GSS connections in the first specimen, a grout mix designed to simulate representative conditions of cold climate deterioration was used in the fabrication of the connections in the second. The specimens used were two-column steel bridge bents connected to the floor by pin supports. The specimens were subjected to cyclic quasi-static lateral loading that simulated the demand on the real bridge bent from an earthquake. The global response of both specimens was measured and compared. The results suggest that a moderate to high level of grout damage due to cold climate exposure is unlikely to cause any significant deficiencies in the satisfactory structural performance of the GSS connection.

4.3.2   Concluding remarks

After large scale tests 1 and 2, the research team met with AKDOT on February 1, 2019, to discuss project direction. In this meeting, it was decided to not pursue testing more specimens with further reduced grout properties in the connections. The subsequent tests would be used to determine the force transfer mechanism occurring within the GSS connection. This new path is discussed in detail in Chapter 5. However in hindsight, the results of the third large scale test (test 3) provide information relevant to this chapter. A short discussion follows.

4.3.3   Relevant results from Large Scale Test 3

Test 3, discussed in detail in Chapter 5, was performed on a two-column bent specimen that closely represented the test 2 specimen. The only difference between the specimens of tests 2 and 3 was the number of shear studs per GSS connection of each test. While the test 2 specimen had 32 shear studs in each of its connections, test 3 had only 16. However, this difference in the number of shear studs did little to affect the global structural behavior. A full description of the reasons for this behavior is provided in Chapter 5.

Since the difference in the number of shear studs was inconsequential, in hindsight, test 3 can be construed as a repeat of test 2. Comparing the results of test 3 to those of the control test (test 1) can either corroborate or invalidate the conclusions that were made based on the comparisons of test 1 and test 2. Figure 4.26 shows the comparison of the global force-displacement response of tests 1 and 3. The comparison looks strikingly similar to that of test 1 and test 2 in Figure 4.23. Force-displacement hysteretic loops at different ductility levels were also compared, as shown in Figure 4.27 and 4.28. The results show a similar trend as that seen in Figure 4.24 and 4.25, discussed earlier.

Test 3 did not invalidate any of the conclusions made after test 2. Therefore, it can be said with a higher certainty that grout deterioration within the GSS connection may be inconsequential from its structural performance standpoint.
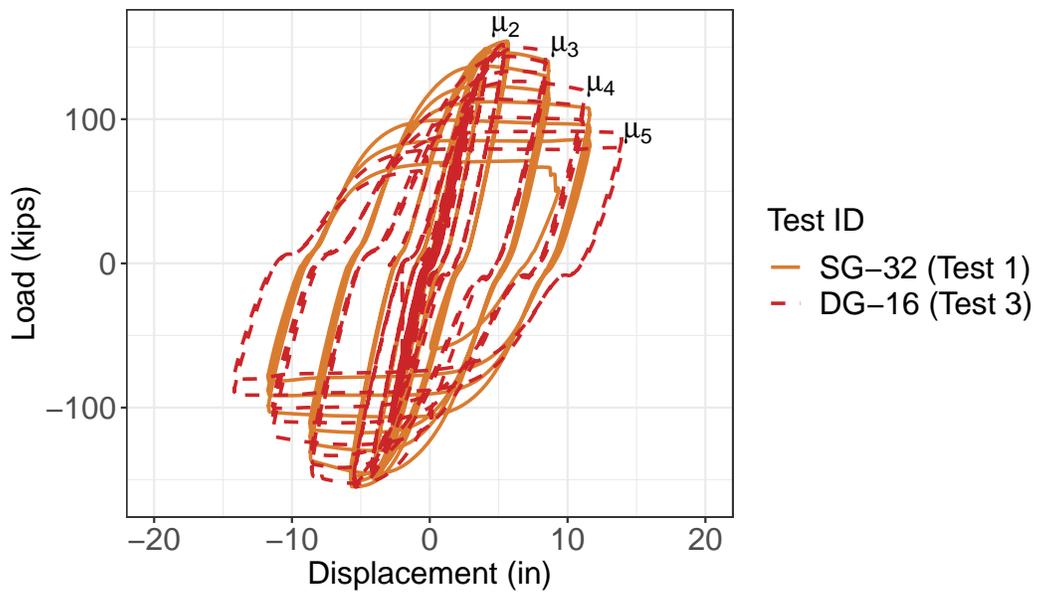
Figure 4.26: A comparison of the force-displacement hysteretic responses: Test 1 (SG-32) v
Test 3 (DG-16)
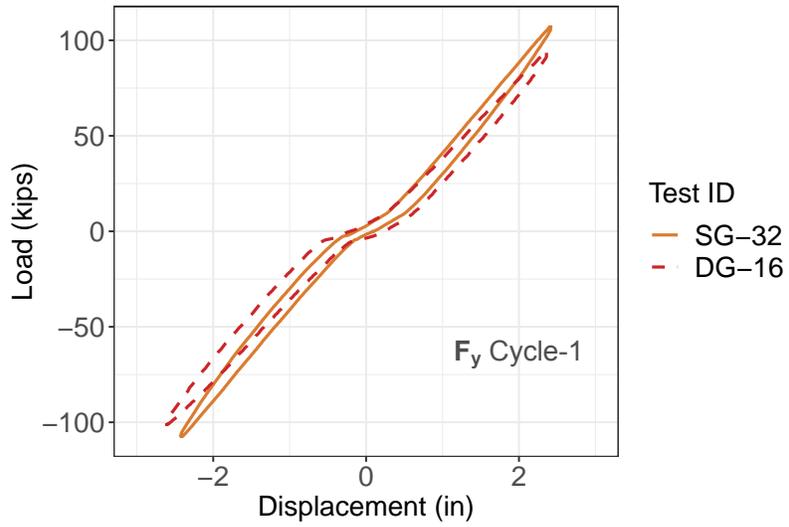
(a)
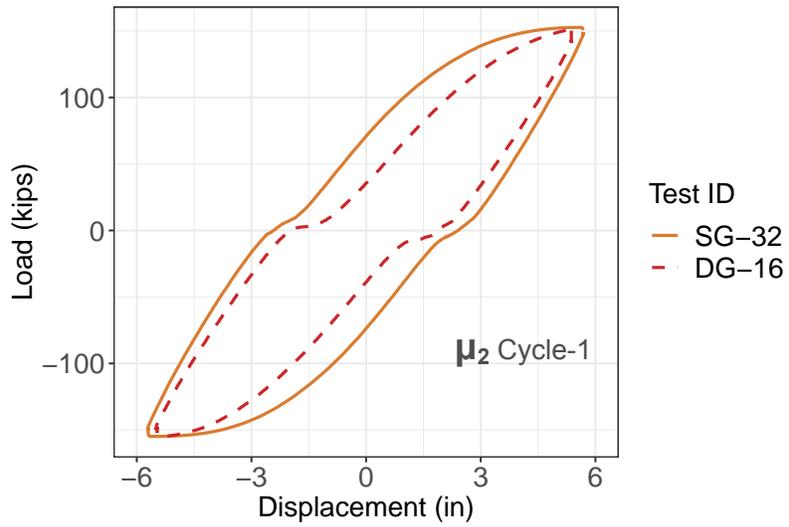
(b)

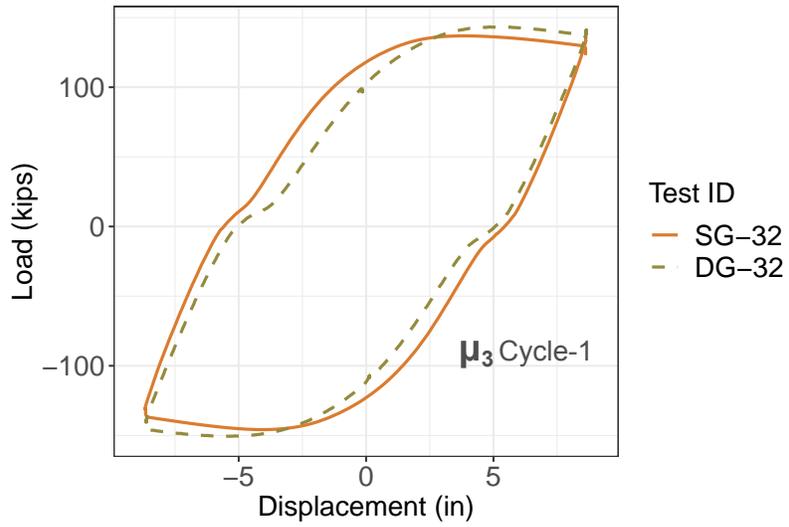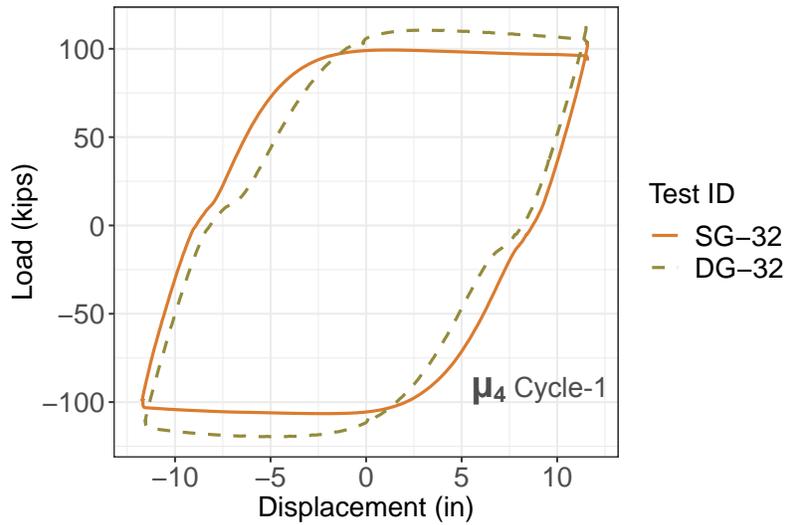Figure 4.27: Comparison between hysteretic loops of Test 1 (SG-32) and Test 3 (DG-16) at different ductilities: (a) F_y (b) μ_2.
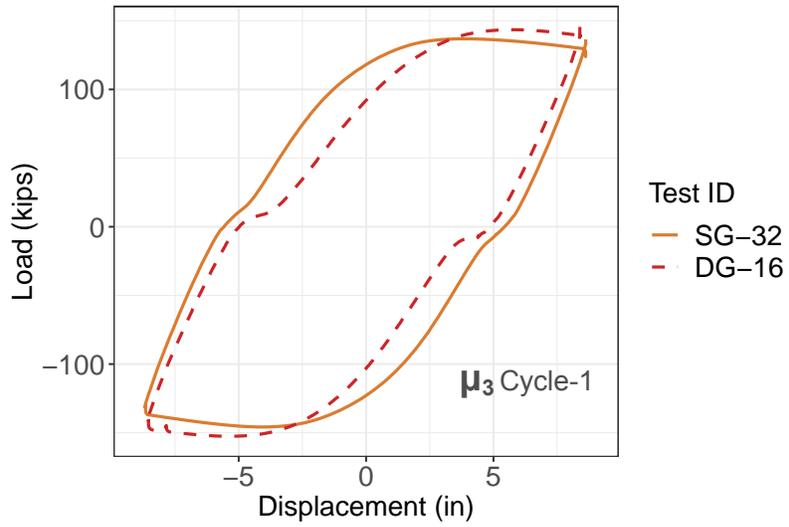
(a)
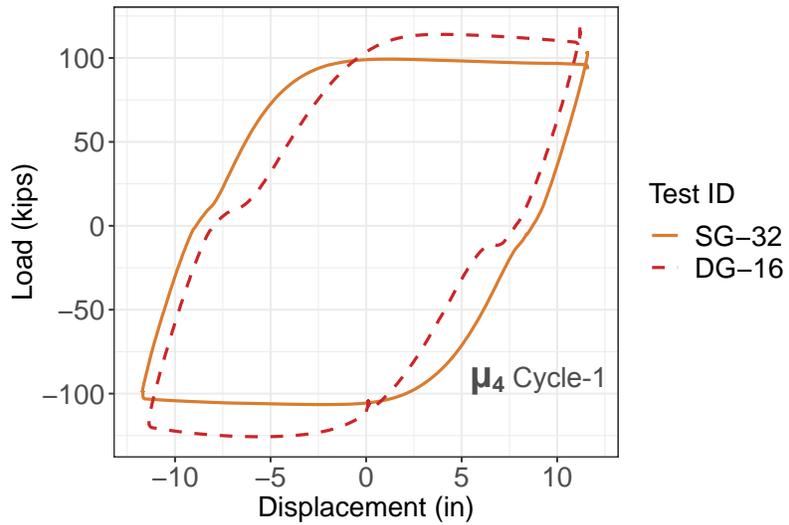
(b)

Figure 4.28: Comparison between hysteretic loops of Test 1 (SG-32) and Test 3 (DG-16) at different ductilities: (a) μ_3 (b) μ_4.

Chapter 5

Force Transfer Mechanism in the GSS Connection

5.1   Introduction

The second large scale test which showed similar global behavior as the first, despite having weaker GSS connections, indicated that a moderate to high level of durability damage might not be a significant concern for design. According to the original plan for the large scale tests, the third and fourth tests were to contain even weaker grout within their GSS connections. However, after a meeting with AKDOT, it was concluded that there was likely no new knowledge to be gained by following this plan. An alternative plan was suggested by AKDOT for carrying out the remaining two large scale tests.

Since tests 1 and 2 revealed that GSS connections with a much lower number of shear studs could satisfactorily protect the weld and relocate the plastic hinge to the column, AK-DOT engineers were interested in determining the minimum number of shear studs required for a reliable design. AKDOT was also interested in investigating the repercussions of a lower socket depth (length of the stub pipe) on the structural performance. Information to help answer these questions, either wholly or partially, was important from a design perspective.

Ideally, if the force transfer mechanism within the GSS connection can be described with a mechanics based mathematical model, this model can be used by engineers to better design steel bridge substructures through performance based and capacity design principles.

This chapter describes the approach to obtain more information regarding the force transfer mechanism within the GSS connection. Tests 3 and 4 were carried out to serve this purpose, and they provided valuable information regarding potential mechanisms involved within the connection during earthquakes. Although making conclusive recommendations regarding a design model would require computational studies, planned to start soon (as part of the first author's dissertation), the observations made during Tests 3 and 4 helped form a qualitative picture of the dominant mechanisms that contribute.

5.2   Background

To better understand the approach, it is useful to discuss the background of large scale testing of the GSS connection, and how an understanding of the connection has evolved over time.

In 2015, Fulmer [17] investigated multiple design details for steel bridge column-to-cap-beam connections. The takeaway from this study was that among the connection details tested, the GSS connection was the most efficient in forcing the lateral load resisting system to predictably fail in a ductile manner. The study successfully showed the proof of concept of the GSS connection. The authors were only interested in achieving plastic hinge formation in the columns by capacity protecting the connection. Therefore, they followed a conservative design procedure for the GSS connection with available data on the capacity of shear stud connectors.

The mechanism of force transfer within the GSS connection was thought to be through a formation of complex compression struts between the shear studs on the column and the stub. The connection under tensile axial loading resulting from lateral loads in a two-column

bent was considered as the critical connection. The column in such a connection is under the danger of being pulled out of the socket, if nothing resists the pull out. Given the capacity of a single shear stud, calculated according to Equation 5.1, they calculated the total number of shear studs required to resist the axial tension demand in the connection using Equation 5.2. The tensile axial demand in the connection was in turn calculated as the full axial yield force in the column section, per Equation 5.3.

$$Q_n = 0.5 A_{sc} \sqrt{f'_c E_c} \leq A_{sc} F_u \tag{5.1}$$

$$N_{req} = \frac{T_y}{Q_n} \tag{5.2}$$

$$T_y = f_{y,exp} A_{g,col} \tag{5.3}$$

In Equations 5.1 to 5.3,

Q_n = Capacity of a single shear stud, kips

A_{sc} = Cross-section area of a shear connector, in^2

f'_c = Compressive strength of surrounding grout, ksi

E_c = Elastic modulus of surrounding grout, ksi

F_u = Ultimate tensile strength of the shear connector, ksi

N_{req} = Required number of shear connectors

T_y = Axial tension demand on the GSS connection, kips

$f_{y,exp}$ = Expected yield strength of the column steel, ksi

$A_{g,col}$ = Gross cross-section area of the column, in^2

This design procedure lead to a total of 96 shear studs in a single GSS connection, 48 on the column and 48 on the stub pipe. All of the structural tests of two-column bridge bents with this connection lead to successful outcomes. Plastic hinge relocation was achieved and the column section failed by rupture well after local buckling. One of the large scale tests performed by Fulmer et al. [16] is discussed here. This test is referred to as Test 0 in this report and is relevant to the discussion of understanding the force transfer mechanism within the connection.

5.2.1 Large Scale Test 0

Introduction

As part of evaluating alternate steel column to cap-beam connections, Fulmer et al. [16, 18] performed four large scale tests on two-column bent specimens incorporating the GSS connection. Out of all of the modified connection details, the GSS connection stood out in its ability to aid and relocate the plastic hinge formation to the columns in a predictable, and reproducible manner. One of the four tests performed by Fulmer et al. [18] is discussed in detail here because of its relevance to the problem at hand. It is referred to as Test 0 (or SG-96) to differentiate it from the the four new tests performed as part of this project. The new tests are referred to as Tests 1 through 4 (or SG-32, DG-32, DG-16, and DG-16-SS).

Experimental Setup

ASTM A500 Gr.B HSS16×0.500 piles were chosen as the column elements of the bent specimen. The construction of the cap-beam consisted of double ASTM A572 HP14x117 sections to provide both a capacity protected cap beam as well as adequate bearing seat width for single span girders, should a designer choose not to utilize continuous spans. Furthermore, in the case of the grouted shear stud connection, a multi-wide HP cap beam was necessary to accommodate the size of the 24" diameter stub pipe sections. The 24"×0.500" pipe sections were manufactured to the material standards of ASTM A500 Gr. B specification. The

diameter of the stub pipe was selected to provide an adequate gap for the placement of shear studs as well as to accommodate construction tolerances.

A total of 96 3/4" dia. mild steel shear studs were welded inside each GSS connection. Forty eight were welded on the outside of the column and inside of the stub pipe. The design calculation of this requirement is interesting, but is not relevant to this chapter. This calculation will be revisited in the next chapter in further detail. To generate a symmetrical condition, 12 vertical lines of 4 shear studs each, at 30 degrees on center, were used as shown in the photograph in Figure 5.1.

To complete the connection, a high-strength cementitious grout material was then placed in the annular ring formed by to the pipe sections. This grout material was the same as that with the designation CG1 in the durability study discussed in Chapter 2. To assist in minimizing the possibility of air voids within the annular grout pocket, the grout was pumped vertically from the bottom of the connection to the top, where 1" diameter holes had been drilled in the cap beam flange to allow air to escape. A hand operated pumping system was utilized along with shut off valves that were attached onto the formwork and later removed to facilitated pumping of the grout. Note that this process was different from the one that was followed in the construction of specimens in tests 1 to 4. For tests 1 to 4, the grout was cast from the top of the connection through a larger hole on the cap-beam bottom flange.

Results and Discussion

The material yield stress was found to be 56.5 ksi for the A500 Gr. B columns. This yield stress resulted in a calculated first yield force of 93.3 kips, according to Equation 4.1. The experimentally determined yield displacement was 2.15 in and the equivalent yield or ductility 1 displacement was calculated to be 2.82 in, according to Equation 4.2. The measured average compressive strength of the grout material at 19 days (time after casting) was 6.85 ksi. Note that this is much lower than the strengths measured during the durability study as

Figure 5.1: Shear stud detail and constituent elements of the specimen in Test 0.

part of the current project. Measured 7-day strengths in excess of 8.8 ksi for the same grout material were obtained in this study. This reduced strength could be because the amount of water used by Fulmer et al. [16] was much larger than bag labelled specifications. Therefore, it is recommended that AKDOT be mindful of contractors not following manufacturer specifications. Specific directives can go a long way in controlling grout durability.

The force-displacement hysteretic response of Test 0 is shown in Figure 5.2. Initiation of pile wall local buckling was observed as early as the third positive cycle of ductility 2 as shown in Figure 5.3. However, no strength loss was observed at this point. The second and third cycles of ductility 3 level produced propagation of the pile wall local buckling which consequently led to strength reductions of approximately 10% and 15%, respectively. It was during these cycles that significant grout spalling was observed, as shown in Figure 5.4. The grout located below the first row of shear studs began to spall out. Cycles at ductility 4 level started to produce tears in the buckled region of the pile walls. The test was terminated at the first negative cycle of ductility 6 when the pile wall finally ruptured at the buckled region (Figure 5.5). This mode of failure was the expected mode, i.e., the plastic hinge being relocated to the columns allowing high ductility cycles with gradual strength loss before failure. The specimen achieved a maximum drift of 12% as shown in Figure 5.6.

123
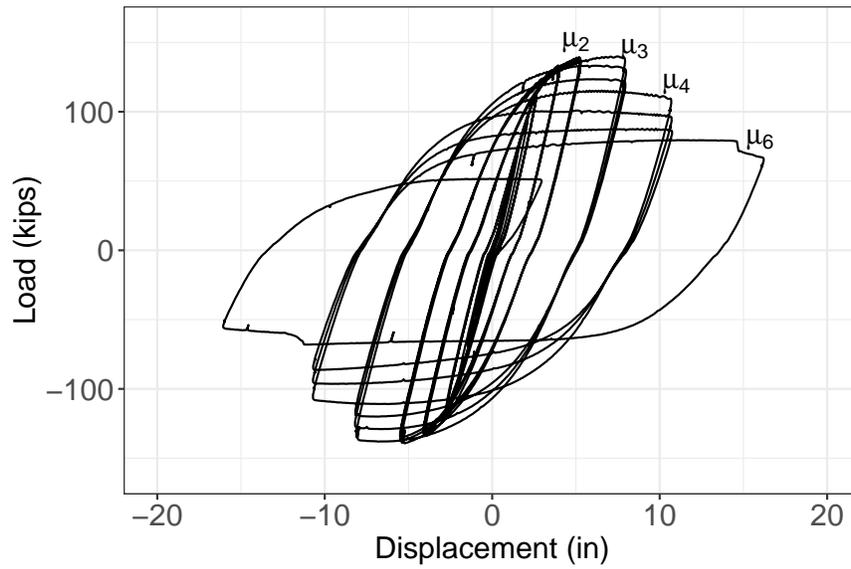
Figure 5.2: Force-displacement hysteresis of the two-column bridge bent specimen tested by Fulmer et al. [18], referred to as Test 0 in this report
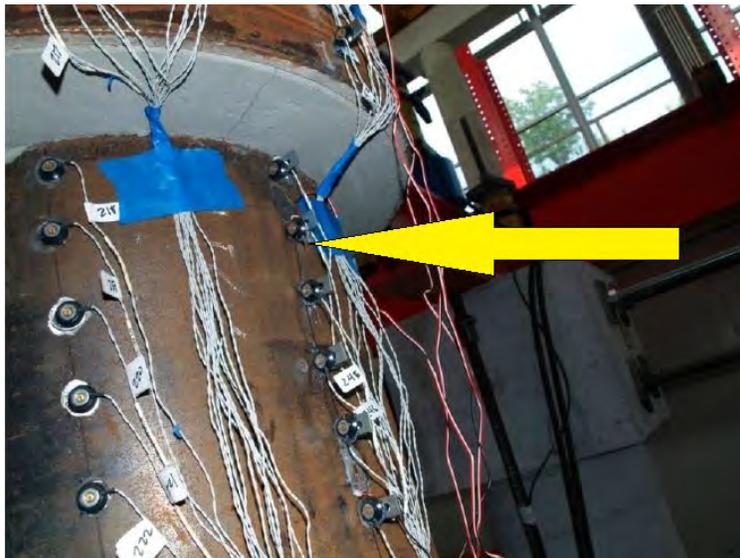
Figure 5.3: Observed local buckling initiation pile wall (Ductility: 2, Cycle: -3, Force: -132 kips, Displacement: -5.62").

Figure 5.4: Observed grout spalling and tear marks on the pile wall (Ductility: 4, Cycle: 3, Force: 85 kips, Displacement: 11.25").

Figure 5.5: Specimen failure mode of pile wall rupture (Ductility: 6, Cycle: -1, Force: -54 kips, Displacement: -16.88").

Figure 5.6: Drift of 12% was observed at termination of Test 0 [18] (Ductility: 6, Cycle: 1, Force: 75 kips, Displacement: 16.88")

This test along with three other similar tests performed by Fulmer et al. [18], conclusively showed that the GSS connection can successfully relocate the plastic hinge, thus protecting the weld connecting the stub pipe to the cap-beam.

5.3 Large Scale Experiments on Two-Column Bridge Bents - II

5.3.1 Introduction

While planning the large scale tests for this project, 96 shears studs per GSS connection were deemed to be overly conservative. The full axial yield force of the column section in a two-column bent is seldom developed. Bending of the columns results in plastic hinging at the peak lateral load. Further cycles will result in reduced loads because of the pinching of the section. Therefore, the critical maximum axial load demand developed in the connection will be the tensile axial load corresponding to the peak lateral load in the system. This demand requires many fewer shear studs.

Table 5.1: Test matrix used to determine the force transfer mechanism of the GSS connection.

Test No.	Test ID	Shear Studs	Stud Area	Socket Depth	Performance
0	SG-96	96	42.4 in^2	24"	**Adequate**
1	SG-32	32	25.1 in^2	24"	**Adequate**
2	DG-32	32	25.1 in^2	24"	**Adequate**
3	DG-16	16	12.6 in^2	24"	**Adequate**
4	DG-16-SS	16	12.6 in^2	16"	**Inadequate**

In tests 1 and 2, discussed in the previous chapter, only 32 shear studs per connection were used. Table 5.1 shows the large scale test matrix used to determine the force transfer mechanism of the GSS connection. The naming scheme for "Test ID" follows "SG", or "DG" for standard grout or deteriorated grout, respectively. The number that follows represents the total number of shear studs per connection. The abbreviation "SS" for Test 4 stands for the shorter stub length. The parameters that were varied in the tests were the number of shear studs per connection and the socket depth of the connection. The number of shear studs was varied in tests 0 through 3, while the socket depth was changed for test 4. It was determined that the socket depth is much more important than the number of shear studs to successfully achieve plastic hinge relocation.

Tests 0, 1, and 2 have already been discussed in detail elsewhere in this report. The next section discusses tests 3 and 4. Following that, this chapter is concluded with results and discussion.

5.3.2 Large Scale Test 3

Introduction

Tests 0, 1, and 2 showed similar results despite the number of shear studs per connection was reduced from 96 to 32. This result suggested that the number of shear studs may not be as important in force transfer as previously thought. However, the plastic bending moment developed at the column-to-connection interface was somehow resisted successfully in all the

three tests. An alternate load path develops to explain this behavior. To be fully certain of the impact of shear studs, the number of shear studs to was reduced further to 16, 8 on the column and 8 on the stub pipe, for the third large scale test.

Experimental Setup

The test specimen was a large scale two-column steel bent similar to the one used in Tests 1, and 2. Important aspects of the test setup are reproduced here. Test 3 followed the same displacement history as that of Test 1. The entire test was performed in displacement control mode. After elastic cycles, three cycles at each ductility level were applied until test termination. The instrumentation scheme consisted of electrical resistance strain gages, string potentiometers, and OPTOTRAK sensors, the same as in Test 1.

Fabrication of the cap-beam pipe-stub assembly was performed in the shop by a certified welder. The shear stud welding on the columns and stubs was also performed by the same welder. Because each stud was welded manually, one sample was subjected to a bend test to ensure the integrity of the welding. The weld did not fracture after the shear stud attained a large plastic deformation, as shown in Figure 5.7. The number of shear studs per connection was reduced to 16 in this test. As a consequence, a choice regarding the locations for each row of shear studs was required. Figure 5.8 shows a schematic of how the rows of shear studs were arranged with relative to each other among the three tests. In test 3, the second and fourth rows of shear studs from the top, were cut off to obtain the desired number of 16 shear studs. The clear grout cover in the connections of the test 3 specimen was 8".

The next step of the construction process was erecting the two pile columns on pin supports. This was achieved by tying the erected piles to the floor using ratchet straps and D-rings. The cap-beam stub assemble was then brought in and lowered onto the two columns. The columns were inserted into the sockets created by the pipe stubs until the cap-beam rested on top of the columns. No additional welding was performed to connect the columns to the cap-beam.

Figure 5.7: Result of the bend test on a sample 1" diameter shear stud.
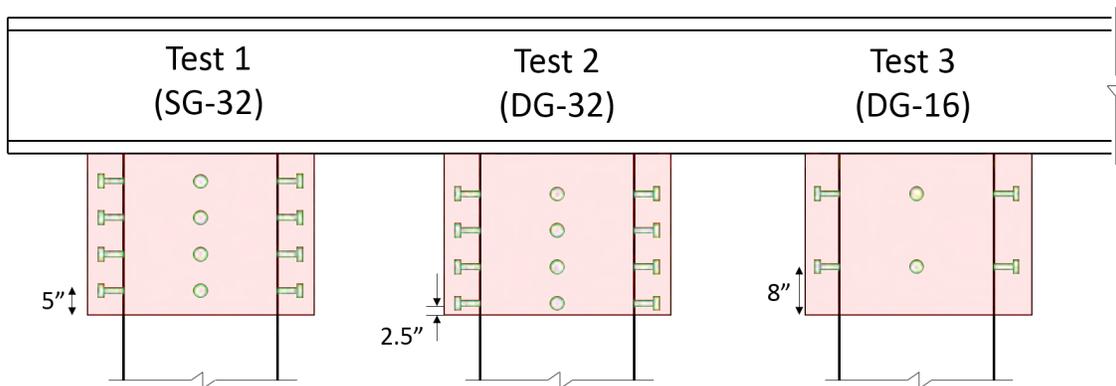
Figure 5.8: Comparison of the locations of shear studs in each of the first three large scale tests (Not to scale).

Figure 5.9: Cracks observed at the neutral axis of the GSS connection (Ductility: 1, Cycle: 1, Force: 111 kips, Displacement: 2.79")

Once the cap-beam was in place, the annular regions surrounding the column tops were filled with grout to complete the GSS connections. The grout was pumped with a pump through an opening on the bottom beam flange at the top of the connection. EPS beads were added to the grout mixture to simulate deterioration. To prevent segregation and migration of EPS beads, the connections were cast in layers as discussed in Chapter 4.

Experimental Summary

The structural test was performed 7 days after casting the grout in the GSS connections. Cyclic quasi-static loading was applied to the two-column steel bent in the displacement control mode. The initial load rate was 1.5 in/min which was later changed to 4 in/min in the inelastic cycles. Two cycles at each force level ($0.25F_y$, $0.50F_y$, $0.75F_y$, and F_y) were applied first. Visible separation of the grout ring from the pile wall was observed around $0.75F_y$. Radial cracks near the neutral axis of the connection started to develop in both connections, as shown in Figure 5.9. The cracks multiplied during the first cycle of ductility 1.

After three cycles at ductility 1, the gap between the grout ring and the pile column

Figure 5.10: The gap between the column wall and the grout ring. (Ductility: 4, Cycle: 1, Force: 119.1 kips, Displacement: 11.19")

opened to about 0.1". This gap increased with each successive ductility level until it reached its widest at ductility 4, around 1.5", as shown in Figure 5.10. Unlike the previous tests, no grout spalling was observed at the bottom of the grout ring on the extreme fibers during bending. Figure 5.11 shows the state of the grout at ductility 3 during this test. By ductility 3, tests 1 and 2 had already started to show signs of grout spalling.

Pile wall local buckling was observed on the south side of the north column on the first push cycle of ductility 3 (Figure 5.12). On the subsequent pull cycle, the north side of the south column also experienced pile wall local buckling. On every subsequent cycle, the load in the system dropped. During the first push of ductility 4, significant local buckling was observed in both columns, as shown in Figure 5.13. All three cycles at ductility 4 were then completed without any sign of tearing or rupture. After the first push cycle of ductility 5, some tear marks developed in the north column. Pile wall rupture was observed during the third cycle of ductility 5, as shown in Figure 5.14. During ductility 5 cycles, two popping sounds were heard similar to that in Test 2. This could have been the shear studs rubbing against the wall of the stub pipe. At the end of Test 3, the load had dropped by 60% and the specimen had attained a drift of 11% as shown in Figure 5.15.

Figure 5.11: GSS connection at ductility 3; No grout spalling was observed in Test 3. (Ductility: 3, Cycle: 1, Force: 145.1 kips, Displacement: 8.39")
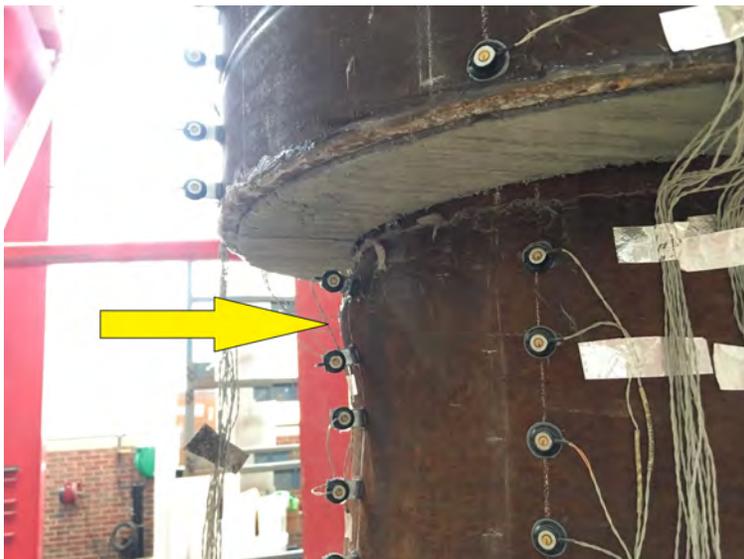
Figure 5.12: Minor buckling observed on the north column. (Ductility: 3, Cycle: 1, Force: 145.1 kips, Displacement: 8.39")

Figure 5.13: Minor buckling observed on the north column. (Ductility: 4, Cycle: 1, Force: 119.1 kips, Displacement: 11.19")

Figure 5.14: Minor buckling observed on the north column. (Ductility: 5, Cycle: 3, Force: -77.5, Displacement: -14.18")

Figure 5.15: Minor buckling observed on the north column. (Ductility: 5, Cycle: 2, Force: 80.3, Displacement: 13.92")

Results and Discussion

A comparison of the force-displacement responses of tests 1 and 2 is shown in Figure 5.16. Overall, the global behavior of both the tests is almost identical. Similarly, the force-displacement response of tests 0 and 1 is compared in Figure 5.17. In both of these comparisons, the only parameter that changed is the number of shear studs per GSS connection. The similarity in their global responses, despite the reduction in the number of shear studs per connection, suggests that the contribution of the shear studs to resisting the bending moment demand on the connection, is likely minor.

A closer look at the individual loops of tests 0, 1, 2, and 3 does show some effect of the number of shear studs in a connection. For example, in Figures 5.18 through 5.21, all four aforementioned tests are compared at each ductility level. In each figure, a zoomed in version of the plot on the left, near the zero force region, is shown on the right. In this region, one can observe a "slip" in the force displacement response of tests 1, 2, and 3, that have 32, 32, and 16 shear studs, respectively. This behavior is not present in the response of test 0, that has 96 shear studs per connection. The magnitude of the slip in displacement is higher for each successive ductility level. It is also clear that the slip increases as the number of
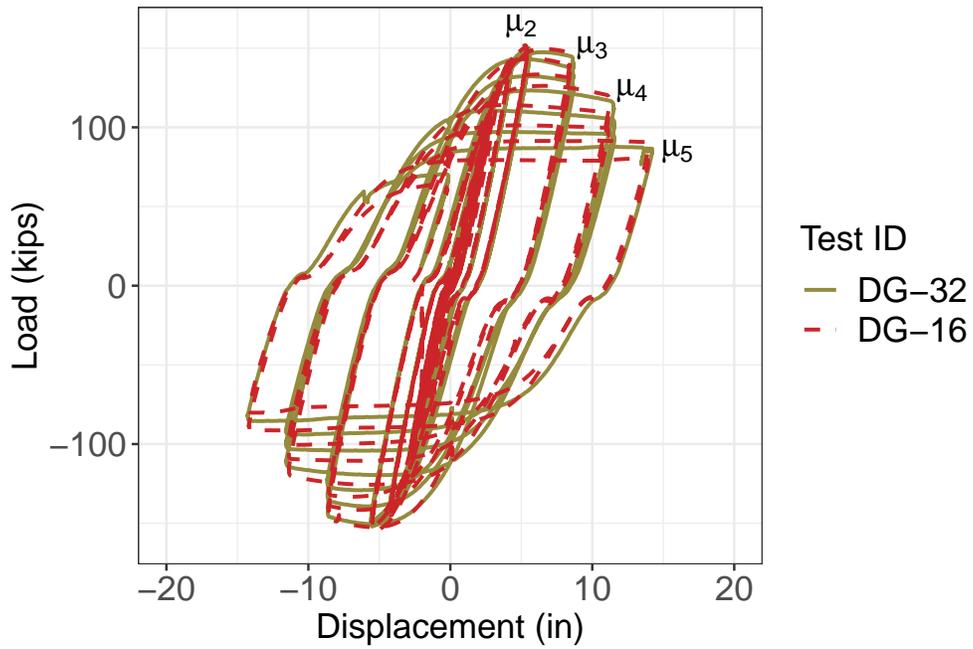
Figure 5.16: A comparison of the force-displacement hysteretic responses: Test 2 (DG-32) and Test 3 (DG-16)
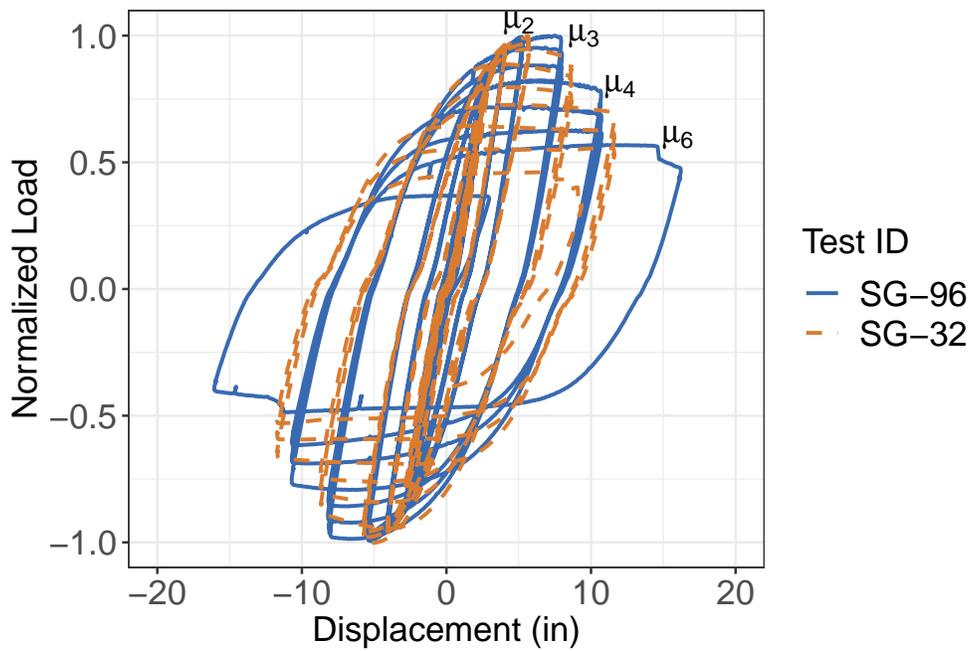
Figure 5.17: A comparison of the force-displacement hysteretic responses: Test 0 (SG-96) and Test 1 (SG-32)

Figure 5.18: Comparison of the slip in the force-displacement response in ductility 1 cycle.

Figure 5.19: Comparison of the slip in the force-displacement response in ductility 2 cycle.

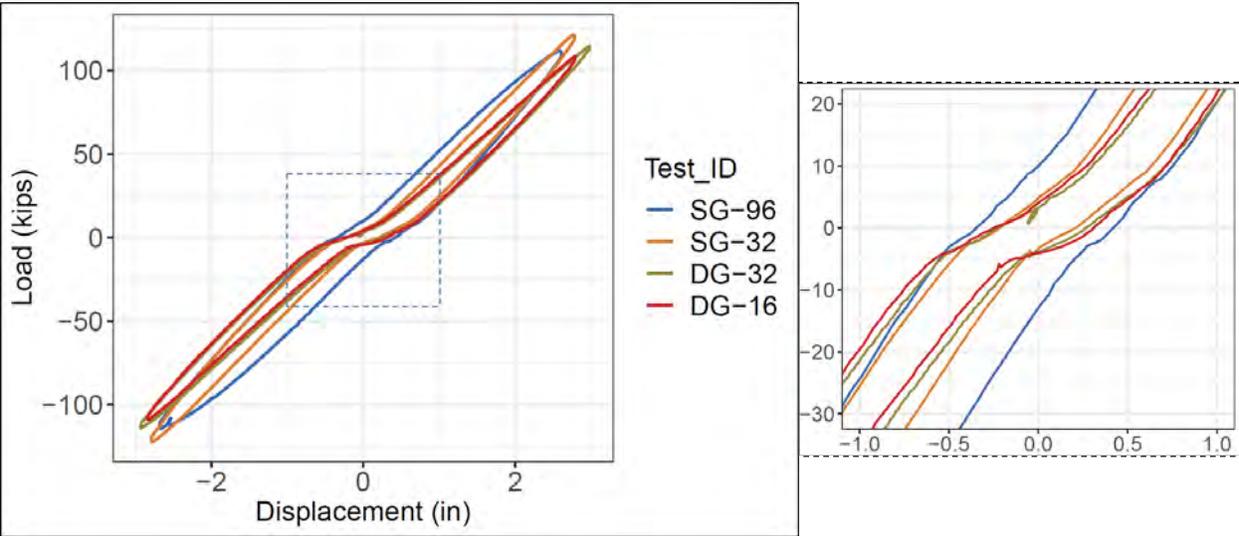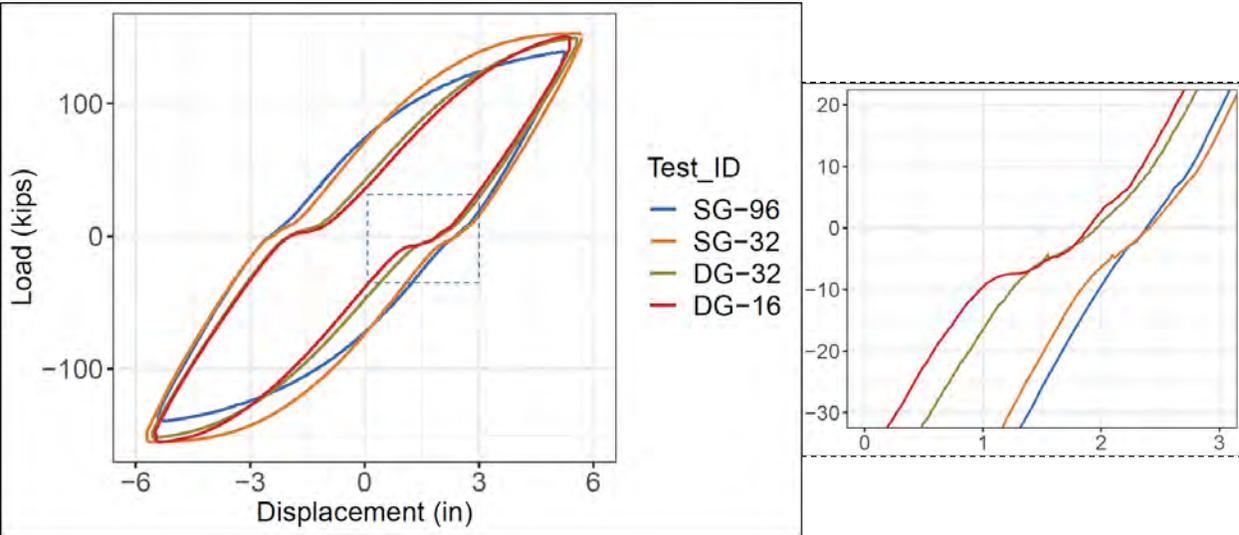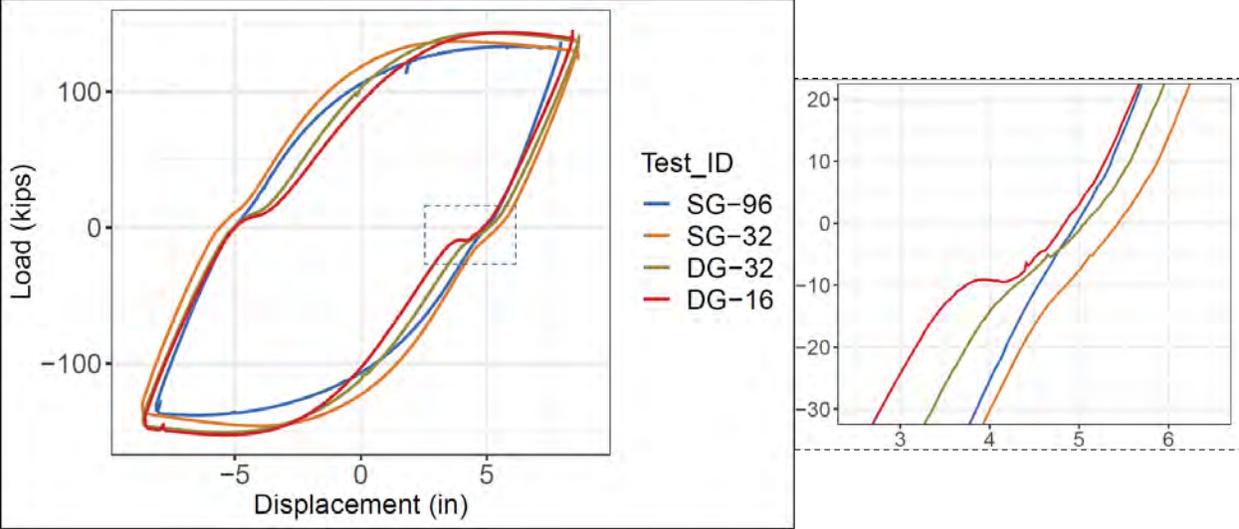Figure 5.20: Comparison of the slip in the force-displacement response in ductility 3 cycle.
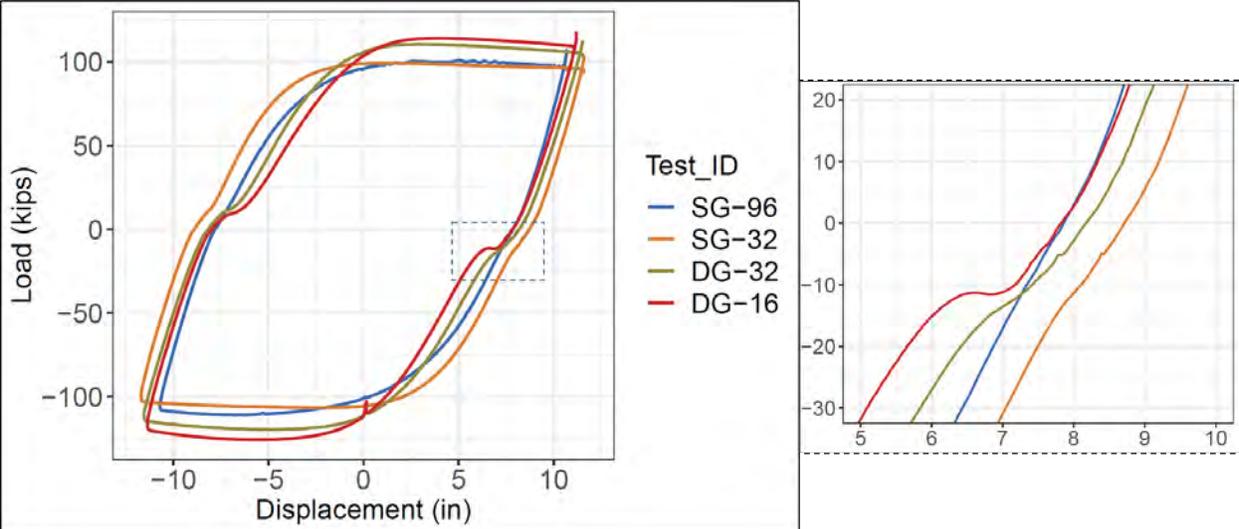
Figure 5.21: Comparison of the slip in the force-displacement response in ductility 4 cycle.

shear studs per connection decreases. Although grout deterioration also contributes to this phenomenon, the contribution of shear studs is also as significant, if not more so.

One hypothesis to explain this behavior is the contribution of the shear studs to the size of the gap that opens between the column wall and the inside of the grout ring. The shear studs close to the bottom of the connection are engaged in tension providing resistance to the opening of the gap. Since test 0 had the highest number of shear studs close to the bottom, the gap size may have been significantly reduced. As the number of shear studs reduced in subsequent tests, the resistance to gap opening reduced, resulting in larger gaps. These gaps allow the columns to rock within the connection. When the gap shifts from one side to the other as the tension and compression sides reverse, the size of the gap dictates the amount of displacement observed with little additional force input, which is reflected as the slip in the hysteretic response. This phenomenon, however, is but a minor observation from the perspective of successful structural performance under lateral loading. The difference in energy dissipation characteristics, as well as the failure limit state achievement is negligible among the four tests. Hence, it is concluded that the number of shear studs may have a relatively minor impact on the structural performance of the GSS connection. A discussion of the role of shear studs is provided in last section of this chapter.

5.3.3   Large Scale Test 4

Introduction

Test 3 results suggested the possibility of alternate load paths to resist the bending moment demand on the GSS connection. A plausible load path that was considered next was a pair of normal forces at the top and bottom of the connection producing a force couple that resists the bending moment.

Figure 5.22 shows a schematic of the dominant force transfer mechanism within the GSS connection. The maximum bending moment demand (M_p) is equal to the plastic moment of the column section. The tensile axial load demand (T_a) is equal to the axial load developed in
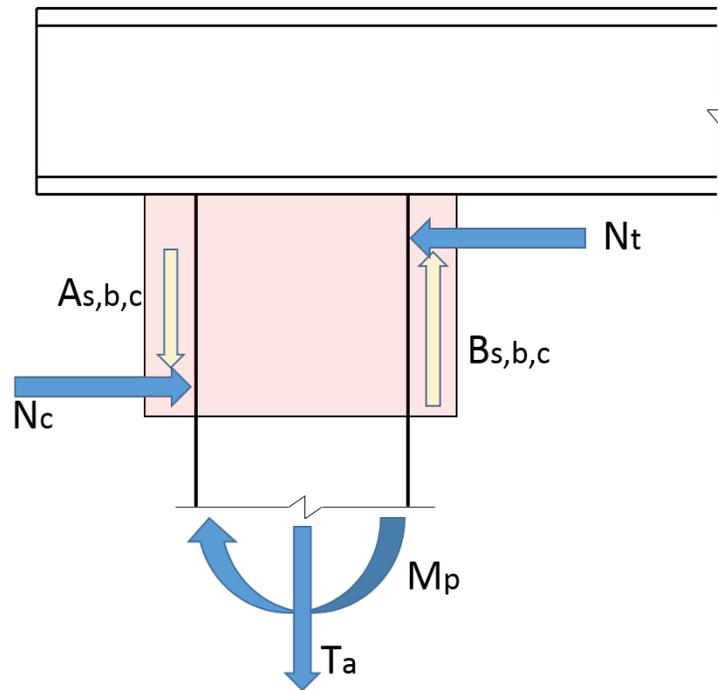
Figure 5.22: Hypothesized force transfer mechanism within the GSS connection.

the tension column of the two-column bent under lateral loading. To equilibrate the bending moment, a pair of normal forces, N_c and N_t, are developed due to the column bearing on the bottom and top of the GSS connection, respectively, under lateral loading. In addition, surface forces are developed parallel to the longitudinal axis of the column. These forces are named $A_{s,b,c}$ and $B_{s,b,c}$. The subscripts represent the potential contribution from multiple mechanisms such as shear strength of the studs (s), bond or friction between the steel and grout (b), and compression struts formed between the shear studs (c). These surface forces are opposite to each other but are not equal. These act in the same direction as the axial force demand in the connection and develop so as to resist pullout of the column.

To evaluate this model, the test 4 specimen was designed so that the GSS connections would have a reduced socket depth. This reduction in turn reduces the lever arm between the two normal forces thereby increasing the magnitude of forces to equilibrate the bending moment. In all of the previous tests, the ratio of the socket depth to the column diameter was 1.5, which meant a 24" deep socket. For test 4, this ratio was reduced to 1, which meant

a 16" deep socket. Figure 5.23 shows a visual comparison of the test specimens with 24" and 16" deep sockets.

Experimental Setup

Test 4 followed the same experimental setup as the previous three large scale tests. However, the socket depth of each connection was reduced to 16". This increased the shear span or clear height of the columns. Due to this increase, a choice regarding the loading protocol for this test was required. The increased clear height meant additional flexibility of the two-column bent system. If the loading protocol was based on system ductility, one would observe higher displacements in test 4 at the same ductility level, than in the previous tests. To be able to compare the force-displacement responses of all tests at equal displacements, it was decided to base the loading protocol on displacement rather than ductility. As a result, the same displacement corresponds to a smaller force in test 4 compared to the other three tests. It is important to note however, that in the following discussion, the term "ductility", is still used to refer to different levels of displacements. This reference to ductility is used for convenience in discussion, and is not the true ductility of the system.

Experimental Summary

During the test, grout cracking and spalling initiated early in the initial cycles at ductility 1, as shown in 5.24. The force in the system was also observed to drop in each successive cycle at ductility 1. A peak load of 108 kips was observed during the first cycle of ductility 2. Grout spalling continued to excessive levels throughout the cycles at ductilities 1.5, and 2. During the first cycle of ductility 2, the gap between the column and the grout ring became visible, as shown in Figure 5.25. The grout above the first row of shear studs started pushing the stud down resulting in permanent bending of the stud on the north side of the north column (Figure 5.26).

The grout material did not mobilize the strength required to resist the bending moment.

Figure 5.23: Specimens for large scale tests: (a) Test 3 (b) Test 4.

(a)
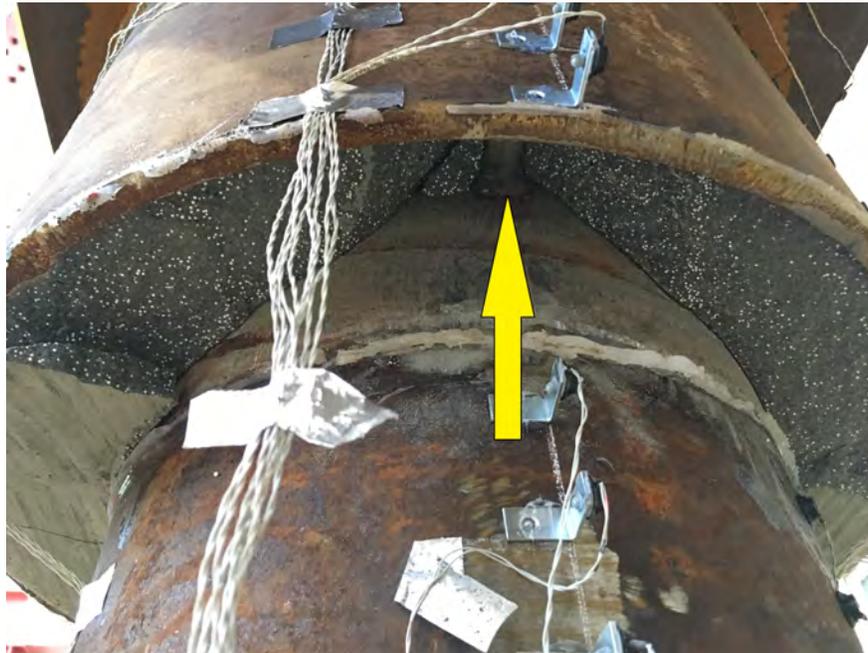
(b)

Figure 5.24: (a) Grout spalling initiated (Ductility: 1, Cycle: 1, Force: 80.4 kips, Displacement: 2.87") (b) The first row of shear studs visible (Ductility: 1, Cycle: 3, Force: 74.4 kips, Displacement: 2.88").

Figure 5.25: Gap opening up between the pile and grout ring (Ductility: 2, Cycle: 1, Force: 107.9 kips, Displacement: 5.46").

Figure 5.26: Bent shear stud (Ductility: 2, Cycle: 3, Force: 85.5 kips, Displacement: 5.49").

Figure 5.27: Column remaining straight under lateral loading (Ductility: 3, Cycle: 1, Force: 96.1 kips, Displacement: 8.48").

Once excessive grout spalling was observed, the column remained straight and rocked inside the connection under lateral load, as shown in Figure 5.27. It was clear at this point that the system did not possess enough capacity to form a plastic hinge in the columns. Hence, the test was terminated after the first cycle at ductility 3.

Results and Discussion

Figure 5.28 shows the comparison of force-displacement response of tests 3 and 4. Both of these tests had the same grout strength and number of shear studs per connection. The only variable was the socket depth. Figure 5.28 shows a striking difference between their responses. A shorter socked depth completely changed the behavior of the lateral load resisting system. The columns did not dissipate energy and were at or below yield. The grout was unable to mobilize enough compressive strength to form the normal force pair.

The results indicate that the mechanism hypothesized earlier in this section may be correct. A deep enough socket depth or a long lever arm is necessary for the GSS connection
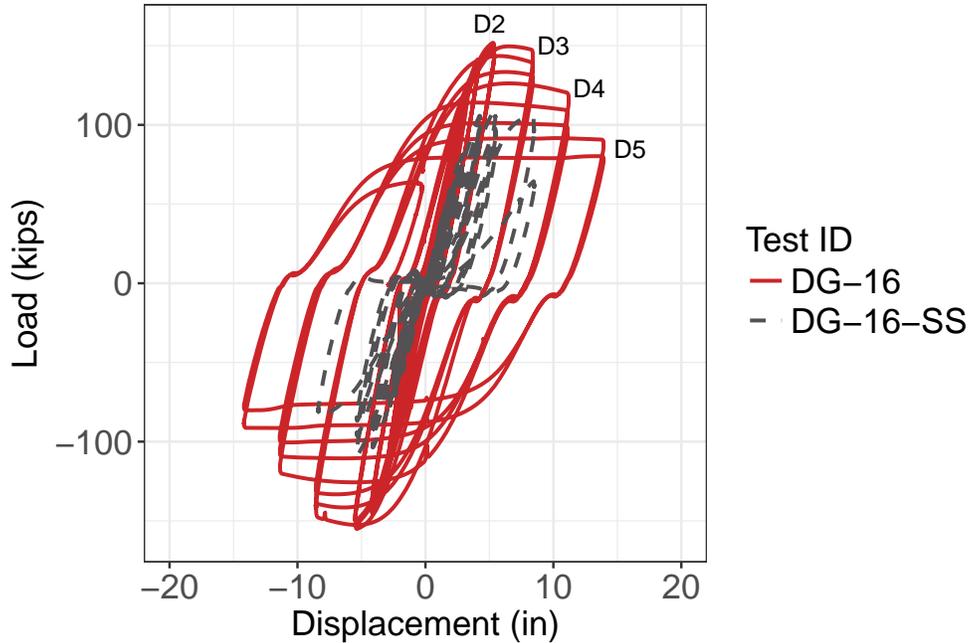
Figure 5.28: A comparison of the force-displacement hysteretic responses: Test 3 (DG-16) v Test 4 (DG-16-SS)

to be able to relocate the plastic hinge to the column without premature failure.

5.4 Limit States from Experimental Observations

Through observations during the large scale tests, we were able to identify five different limit states in the behavior of the GSS connection in a lateral load resisting system. These are discussed in this section. Note that these limit states occurred only for the GSS connections that were able to successfully relocate the plastic hinge to the columns. Experimental photographs from tests 1, 2, and 3 are compiled to discuss how each limit state was attained in each of the three tests.

5.4.1 Cracking at the Neutral Axis

At or above ductility 1, the grout rings in all three tests cracked radially at the neutral axis of the connection. The cracks were aligned transverse to the direction of loading, as shown

in Figure 5.29. This cracking likely develops due to the following. Under lateral loading, the columns bear against the grout rings on the compression side, as shown in Figure 5.30. The bearing pressure on the inside of the grout ring on the compression side induces tensile hoop stresses. When this tensile stress exceeds the tensile strength of the grout material, cracking ensues. Note that this is a simplification, and the hoop stress profile along the grout ring circumference is likely more complicated as the internal pressure is not uniform. Subsequently, the reaction of the grout ring on the column section results ovalization of the section. While the extreme ends are pushed inwards, the section is pushed outwards at the neutral axis. This causes compressive stresses to develop around the neutral axis region of the grout ring which has already cracked. Previous cracking in this region allows the grout to spall.

In test 1, this cracking was observed later (ductility 1.5) than in both tests 2, and 3 (ductility 1). One explanation could be that since the grout material in test 1 was much stronger than in tests 2 and 3, the grout ring could sustain higher stresses before cracking.

5.4.2   Socket Detachment

As the tests progressed past ductility 1, a gap between the outside surface of the column and the inside surface of the grout ring opened. This is termed socket detachment. Due to the ovalization of the column section under lateral loading, the extreme ends get pushed inwards. This causes the tension side of the section to detach from the grout ring resulting in a gap.

The gap became visible at ductility 1.5 in all the three tests, as shown in Figure 5.31. A larger gap was observed in test 3 compared to tests 1 and 2. Test 1 had the smallest gap. Figure 5.32 shows the state of this gap at ductility 3. The gaps at ductility 3 were wider than the corresponding ones at ductility 1. Similar to ductility 1, a comparatively smaller gap was observed for test 1, still larger in Test 2, and the largest in test 3. In short, fewer studs led to larger gaps.
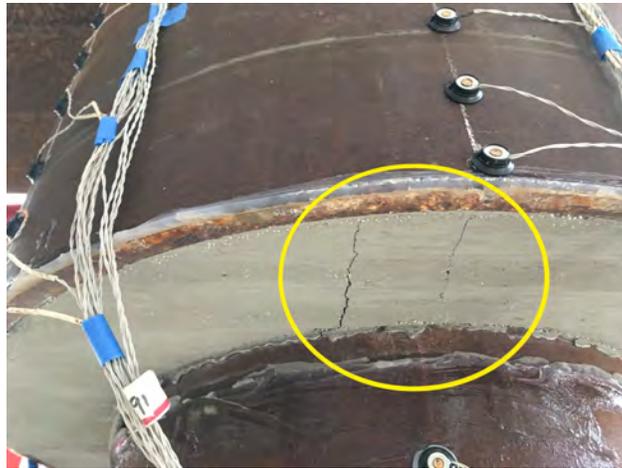
Figure 5.29: Grout cracking observed in the GSS connection transverse to the direction of loading in (a) Test 1 at $\mu_{1.5}$, (b) Test 2 at μ_1, and (c) Test 3 at μ_1
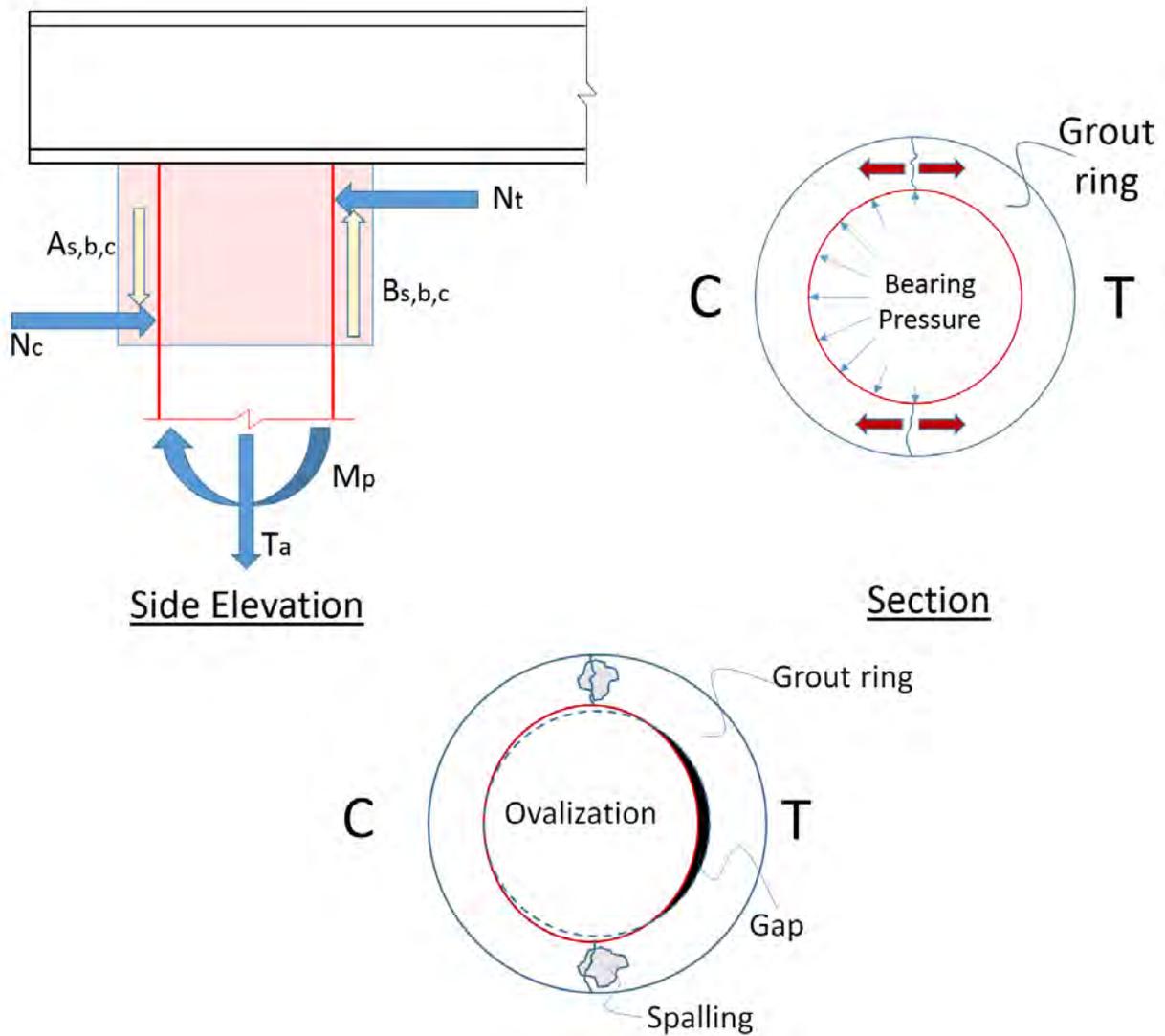
Figure 5.30: A schematic to explain cracking observed at the neutral axis, and the socket detachment limit state of the GSS connection.

(a)

(b)

(c)

Figure 5.31: Socket detachment observed in the GSS connection on the tension side of the column under bending (a) Test 1 at $\mu_{1.5}$, (b) Test 2 at $\mu_{1.5}$, and (c) Test 3 at $\mu_{1.5}$.

Figure 5.32: Socket detachment observed in the GSS connection on the tension side of the column under bending (a) Test 1 at μ_3, (b) Test 2 at μ_3, and (c) Test 3 at μ_3.

The difference in the size of the gap for each test may be attributed to both the strength of the grout and the amount of clear cover in the GSS connections. The compressive strength of the grout and the presence of shear studs close to the bottom of the connection prevent socket detachment by acting in compression and tension, respectively. Test 1 had the strongest grout. The first row of shear studs in test 1 was 5" from the bottom of the connection. Test 3 meanwhile, had a deteriorated grout as well as a large cover of 8". Test 2 also had deteriorated grout; however, the small cover of 2.5" reduced the size of the gap compared to that in Test 3.

5.4.3   Grout Spalling

The grout on the extreme ends (regions farthest from the neutral axis under bending) of the GSS connection spalled off after ductility 2 cycles. However, in test 3, no spalling was observed even past ductility 4. This may be attributed to the absence of a row shear studs close to the bottom of the connection. Figure 5.33 shows the occurrence of this limit state in the first two tests. As has been discussed earlier, the presence of shear studs closer to the bottom of the connection help resisting the widening of the gap between the column and the grout ring. The shear studs are engaged in tension to achieve this resistance. As the shear studs are loaded axially in tension, the grout immediately around them is also subjected to tensile stresses. When this stress exceeds the tensile capacity of the surrounding grout, the grout cracks and spalls out of the connection.

In test 3, there was a large enough grout cover of 8" from the bottom, that the gap at the level of first row of shear studs was smaller compared to the other two tests. This increased cover resulted in a reduced tensile stress demand on the grout surrounding these shear studs. This may explain the observation of no spalling in test 3.

(a)

(b)

(c)

Figure 5.33: Grout spalling observed in a GSS connection in (a) Test 1 at μ_2, and (b) Test 2 at μ_3 (c) No spalling was observed in Test 3.

5.4.4 Pile Wall Buckling

Under cyclic loading, the column section reverses its compression and tension sides. Beyond a certain critical inelastic tensile strain, the pile wall has a propensity to buckle on the subsequent compression cycle. Pile wall buckling followed by plastic hinge formation just beneath the GSS connection is the desirable mode of failure for the bridge bent systems discussed in this report.

Figure 5.34 shows the first instance of visible pile wall buckling in tests 1, 2, and 3. Buckling initiated earlier in test 1 compared to the other two tests. This level of buckling typically straightens itself during the subsequent opposite cycle. Figure 5.35 shows buckling which was permanent. Similar to buckling initiation, this level of buckling also occurs earlier in test 1. And finally, Figure 5.36 shows excessive levels of buckling in the columns before rupture. Once again, test 1 attained the same level of buckling earlier at ductility 4 compared to the other two tests, that attained this at ductility 5.

The grout in test 1 had almost 150% more compressive strength and 40% more elastic modulus than that in tests 2 and 3. These differences resulted in 1) lower penetration of inelastic strains into the GSS connection, and 2) smaller socket detachment and in turn a smaller effective column height, and hence a higher strain demand for the same system displacement. Both of these factors contributed to the critical column section in test 1 attaining a higher curvature demand at every ductility level. This increased curvature demand may have led to the specimen in test 1 to initiate and propagate pile wall buckling sooner than that in tests 2 and 3.

5.4.5 Pile Wall Rupture

The ultimate limit state in the columns in a bridge bent incorporating the GSS connection is pile wall rupture. Figure 5.37 shows pile wall rupture in tests 1 and 3. Although not ruptured, the pile wall in test 2 showed tear marks. Tear marks were also observed in tests 1 and 3 before rupture during subsequent cycles. This limit state occurs after a large number
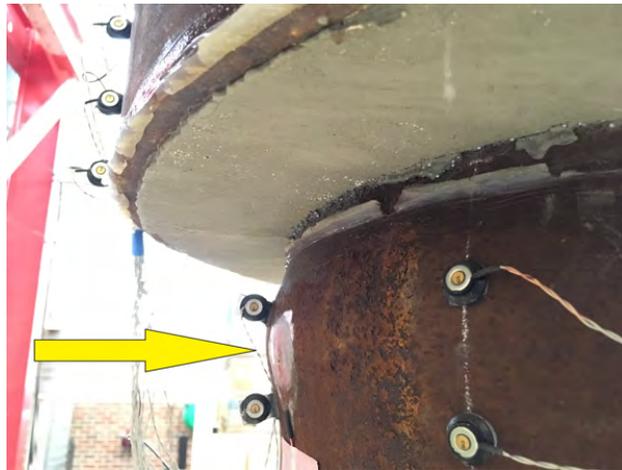
Figure 5.34: Visible pile wall buckling in (a) Test 1 at μ_2, and (b) Test 2 at μ_3 (c) Test 3 at μ_3.

Figure 5.35: Permanent pile wall buckling in (a) Test 1 at μ_3, and (b) Test 2 at μ_4 (c) Test 3 at μ_4.

(a)

(b)

(c)

Figure 5.36: Excessive pile wall buckling in (a) Test 1 at μ_4, and (b) Test 2 at μ_5 (c) Test 3 at μ_5.

of inelastic cycles. In test 1, the pile ruptured during the first push to ductility 5. In tests 2 and 3, this occurred during the final cycle at ductility 5.

5.5   Chapter Summary and Conclusions

The need to better understand the force transfer mechanism within the GSS connection was described, and the background of large scal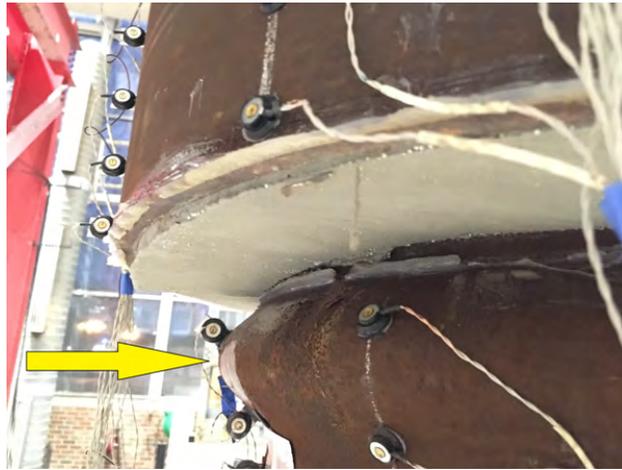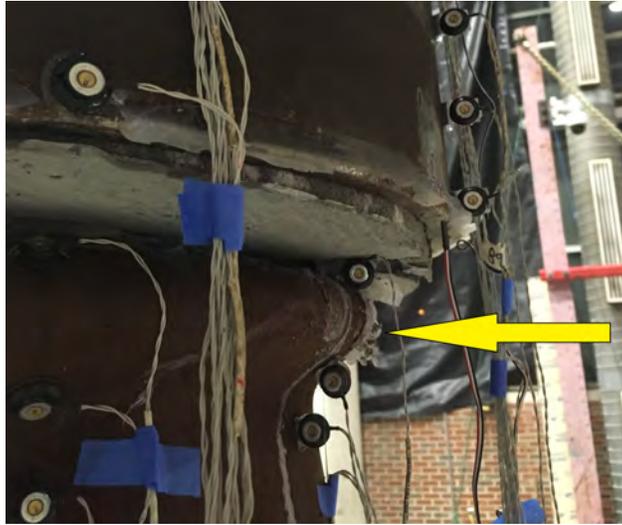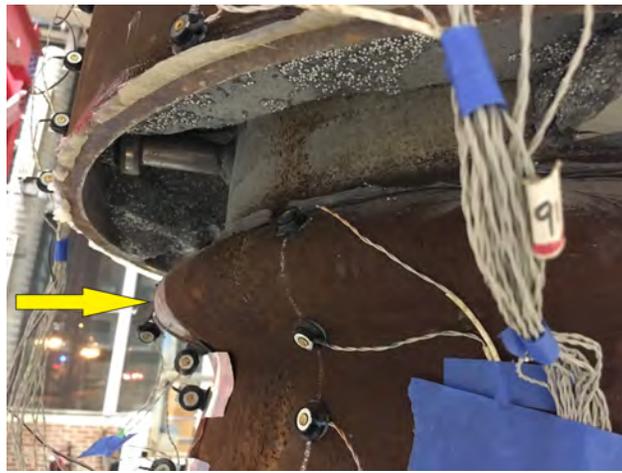e tests performed on steel bridge bents incorporating the GSS connection was discussed. One of the large scale tests from Fulmer et al. [18], referred to as test 0, was then discussed in detail.

The design procedure used by Fulmer et al. [16] to determine the number of required shear studs in a GSS connection was judged to be overly conservative. Two large scale tests (test 3 and test 4), one with GSS connections having a significantly reduced number of shear studs and the other with a reduced socket depth, were performed to investigate the force transfer mechanism.

Test 3 results suggest that the number of shear studs does not have much impact on the global structural performance of the steel bent, provided there is a deep enough socket. Test 4 results suggest that sufficient depth of socket is the most important requirement to successfully transmit the demands in the column to the cap-beam. A qualitative mechanics based model was proposed showing a pair of normal forces which develops to maintain equilibrium of the connection. When the connection fails to mobilize a moment through the normal force pair large enough to resist the bending moment demand, premature failure of the connection ensues, i.e., the column remains straight and rocks within the grout annulus.

Five different limit states were identified for the GSS connection when it successfully relocates the plastic hinge into the column. Because of hoop stress induced by bearing of the column on the inside the of the grout ring, cracking initiates at the neutral axis. Subsequently, ovalization of the column section causes the detachment of the grout ring from the column on the tension side. Further loading causes the grout material on the

(a)
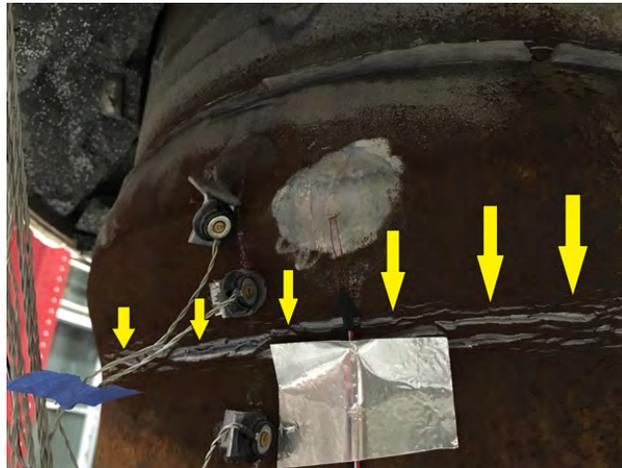
(b)
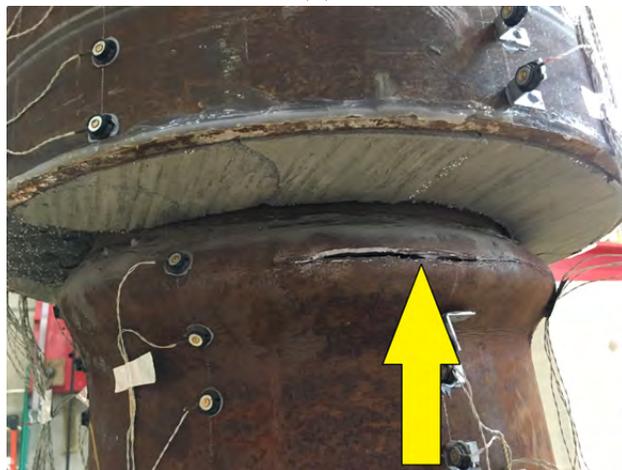
(c)

Figure 5.37: Excessive pile wall buckling in (a) Test 1 at μ_4, and (b) Test 2 at μ_5 (c) Test 3 at μ_5.

extreme ends of the connection to spall. After progressing well into the inelastic range, the pile wall undergoes buckling below the connection. This local buckling is followed by plastic hinge formation and subsequent rupture of the pile wall.

Chapter 6

Conclusions and Recommendations

6.1 Research Problem

The grouted shear stud (GSS) connection was developed as a ductile alternative to conventional directly welded connections in steel bridge substructures. It is a socket type connection in which the socket is formed by a pipe stub which is shop welded to the cap-beam. The steel columns can then be inserted into the socket, and the annular region thus formed can be filled with high-strength cementitious grout to complete the connection. In addition to superior ductility capacity, the GSS connection provides other advantages such as potential use in accelerated bridge construction (ABC), and as a retrofitting option for seismically deficient bridges. See Chapter 1 for a detailed discussion of the advantages of the GSS connection.

Although the GSS connection has been shown to exhibit exceptional structural performance under laboratory conditions, other issues required consideration before widespread deployment of the connection in practice. Since the Alaska Dept. of Transportation and Public Facilities (AKDOT) is interested in using this connection in their bridges, there was a need to investigate its long term durability in extreme cold climates. This project began with the motivation of investigating the durability of the GSS connection in cold climates.

Unlike other steel connection details, the GSS connection introduces a new variable, i.e., the cementitious grout. Cementitious materials are porous and have the propensity to crack under multiple cycles of freeze and thaw. Since studies on the freeze and thaw resistance of commercial cementitious grouts are few, such a study was undertaken.

6.2   Research Approach

The durability of the GSS connection can be viewed from two different perspectives. It can be concluded that the GSS connection is durable in a cold climate if either one of the following statements can be shown to be true.

Statement 1: Commercial cementitious grouts are durable in cold climates.

Statement 2: Grout durability does not have a significant impact on the structural performance of the GSS connection.

Our approach was to attempt to determine whether each of these statements was true or false.

6.3   Durability of Cementitious Grouts

Investigating the durability of all commercial cementitious grouts was as expensive as it was fruitless. First, there are a myriad of competing manufacturers that produce similar products. To procure each one of them was expensive. Second, the chemical composition of every grout is proprietary, and the grouts are constantly being modified by the manufacturers. Results obtained now may not reflect their characteristics after a few years. Third, standard durability tests on cementitious materials specific to cold climate exposure take an extremely long time to perform. Testing one batch of specimens according to ASTM C666 may take up to 75 to 80 days to complete. With due consideration of all of the aforementioned issues, four commercial grouts meeting AKDOT specifications were chosen to be investigated to obtain some information on the suitability of these grouts.

We tested the chosen commercial grouts to determine their vulnerability to freeze and thaw damage, and their propensity to cracking under restrained shrinkage. Although we could not conclusively answer the question of whether cementitious grouts are durable in cold climates, we made some important observations. Some grouts are indeed vulnerable to freeze and thaw degradation while others showed exceptional performance. However, material inconsistency was pervasive even among the grouts that performed well. The potential for restrained shrinkage cracking depends not only on the grout material, but also on the degree of restraint provided to it. The degree of restraint is specific to the practical application of the grout. In the case of the GSS connection, this restraint was found to be high enough to crack all of the grout materials that were tested. However, we also found that the presence of shear studs within the GSS connection helps spread the cracking by providing some reinforcement, and in turn reducing crack widths.

6.4   Structural Consequences of Grout Deterioration

Since the material level inquiry did not conclusively prove that all cementitious grouts are durable in cold climates, we moved on to investigate the consequences of material durability on the structural performance of the GSS connection. Four Large scale steel bridge bent specimens (tests 1 through 4) incorporating the GSS connection were structurally tested. To determine the structural consequences of grout deterioration, the performance of specimens with deteriorated GSS connections (test 2 and test 3) was compared to the performance of a control specimen (test 1). The control specimen had standard high strength grout in its GSS connections, while the remainder of the specimens had grout mixed with expanded polystyrene (EPS) aggregates. The addition of EPS aggregates reduced the structural properties of the grout, such as its compressive strength and elastic modulus, simulating a GSS connection exposed to multiple years of service in cold climates.

Direct comparison between the global structural behavior of the bents with deteriorated

connections and the control specimen suggested that grout deterioration may not have a significant impact on the capability of the GSS connection to successfully relocate the plastic hinge. Therefore, according to the logic our approach was based upon, it can be concluded that the GSS connection is durable in cold climates.

6.5   Force Transfer Mechanism in the GSS Connection

The result that the GSS connection is not affected significantly by grout deterioration became evident after the first two large scale tests. Therefore, AKDOT wanted to use the remaining two large scale tests to answer a different question. To be able to optimally design the GSS connection for satisfactory performance, the need arose to better understand the force transfer mechanism within the GSS connection. Two large scale tests (tests 3 and 4), each varying a single parameter, were performed to obtain some information regarding the force transfer mechanism.

The GSS connections in test 3 used only 16 shear studs per connection, which was a significant reduction from some of the earliest tests on GSS connections that contained 96 shear studs per connection. The objective of test 3 was to determine if the number of shear studs has a significant role in transferring the forces from the column to the cap-beam. We observed that the test 3 specimen performed similarly to all of the previous tests performed on steel bridge bents with the GSS connection. This led us to conclude that the number of shear studs may have less of an impact on the successful performance of the GSS connection than previously thought.

The GSS connections in test 4 used a reduced socket depth. In all of the previous cases, the GSS connections used a socket depth equal to one and a half times the column diameter, i.e., 24" In test 4, the depth was reduced to one times the column diameter, i.e., 16" Results from test 4 showed that for a D/t ratio of 32 (all test columns had a D/t ratio of 32), a socket depth equal to one times the diameter was insufficient in successfully forming the plastic

hinge in the column. This test resulted in poor performance with significantly lower energy dissipation and a reduced maximum load. This led us to conclude that the socket depth is an important parameter in the successful performance of the GSS connection. This conclusion also meant that the dominant moment resisting mechanism in the GSS connection is a pair of equal and opposite normal forces producing a couple opposing the bending moment demand in the connection.

6.6   Recommendations

The recommendations provided in this section address two issues. The first is the issue of achieving the best cold climate durability of cementitious grouts and the GSS connection by association. The second is the optimum design of the GSS connection. It must be noted that the design recommendations provided here are based on structural tests performed on bridge bent specimens with 16" column diameter and a D/t ratio of 32. Recommendations for determining the number of studs and socket depth may be considered as minimum requirements. A computational study to investigate the impact of larger/smaller column diameters and/or D/t ratios has been planned.

6.6.1   GSS Durability Recommendations

1. When choosing a cementitious grout for application in the GSS connection or any other application in cold climates, we recommend using the manufacturer specified Durability Factor (DF) determined in accordance with ASTM C666 Procedure A as an adequate indicator of its durability.

2. Excess water impairs the freeze and thaw resistance of cementitious grouts. Therefore, we recommend that the amount of water mixed per bag of grout be kept to the bag labelled minimum for "flowable" consistency.

3. In the case of the GSS connection, a minimum 28-day grout compressive strength of 7500 psi for "flowable" consistency is sufficient for satisfactory structural performance.

4. Contrary to provisions in some commercial grouts, it is recommended to not extend any grout with pea-gravel aggregates. Extending grout with pea-gravel aggregates results in reduced workability of the wet mixture. Further addition of water to improve workability also results in segregation of the aggregates. Reduced workability and segregation are, of course, undesirable.

6.6.2 Design Recommendations

1. The predominant role of shear studs in the GSS connection is to resist pullout of the column from the socket under axial tensile demand (P_t), induced by the lateral loads on multi-column bridge bents. We recommend that the number of shear studs required to resist this demand be calculated according to Equation 6.1. In Equation 6.1, n is the required number of shear studs on both the column and inside the stub, P_t is the maximum axial tension induced in any of the columns due to the maximum lateral load on the bridge bent, A_s is the cross-section area of a single shear connector, and F_u is the ultimate tensile strength of the shear connector. C is a conservative constant that is based on engineering judgment. We recommend that the value of C not be less than 2.

$$n = C \frac{P_t}{0.6 A_s F_u} \tag{6.1}$$

$$C \geq 2 \tag{6.2}$$

2. We recommend providing the column and the stub with at least 4 vertical lines of

shear connectors at 90° angles to the adjacent lines. This arrangement will result in a total of 8 vertical lines of shear connectors in the GSS connection (4 on column and 4 on stub) at 45° angles to the adjacent lines. Provide at least 2 shear connectors per vertical line.

3. The socket depth (D_s) is the most important parameter of the GSS connection to successfully achieve plastic hinge relocation. We recommend providing a socket depth of at least 1.5 times the diameter of the connecting column (D_c), as shown in Equation 6.3.

$$D_s \geq 1.5D_c \qquad (6.3)$$

After construction, it is recommended that the GSS connections be inspected regularly for loss of grout. In addition, cracks wider than 0.30 mm (0.012 in) are recommended to be repaired with epoxy injection.

References

[1] Standard Test Method for Compressive Strength of Hydraulic Cement Mortars (Using 2-in. or [50-mm] Cube Specimens). Standard, ASTM International, West Conshohocken, PA, 2016.

[2] Standard Test Method for Determining Age at Cracking and Induced Tensile Stress Characteristics of Mortar and Concrete under Restrained Shrinkage. Standard, ASTM International, West Conshohocken, PA, 2018.

[3] Standard Test Method for Fundamental Transverse, Longitudinal, and Torsional Resonant Frequencies of Concrete Specimens. Standard, ASTM International, West Conshohocken, PA, 2014.

[4] Standard Test Method for Compressive Strength of Cylindrical Concrete Specimens. Standard, ASTM International, West Conshohocken, PA, 2018.

[5] Standard Test Method for Resistance of Concrete to Rapid Freezing and Thawing. Standard, ASTM International, West Conshohocken, PA, 2015.

[6] Standard Test Method for Soundness of Aggregates by Use of Sodium Sulfate or Magnesium Sulfate. Standard, ASTM International, West Conshohocken, PA, 2018.

[7] R. Auberg. Application of cif-test in practise for reliable evaluation of frost resistance of concrete. In *International RILEM Workshop on Frost Resistance of Concrete*, pages 255–267. RILEM Publications SARL, 2002.

[8] D. S. Babu, K. G. Babu, and W. Tiong-Huan. Effect of polystyrene aggregate size on strength and moisture migration characteristics of lightweight concrete. *Cement and Concrete Composites*, 28(6):520–527, 2006.

[9] D. S. Babu, K. G. Babu, and T. Wee. Properties of lightweight expanded polystyrene aggregate concretes containing fly ash. *Cement and Concrete Research*, 35(6):1218–1223, 2005.

[10] D. Bager. Qualitative description of the micro-ice body freeze-thaw damage mechanism in concrete. freeze-thaw testing of concrete–input to revision of cen test methods. In *Workshop proceeding From a Nordic Mini-seminar*, pages 4–5, 2010.

[11] C. Bagon and S. Frondistou-Yannas. Marine floating concrete made with polystyrene expanded beads. *Magazine of Concrete Research*, 28(97):225–229, 1976.

[12] R. Bjorhovde. Realistic performance requirements for steel in structures. *Advances in Structural Engineering*, 8(3):203–215, 2005.

[13] B. E. Bucher. Shrinkage and shrinkage cracking behavior of cement systems containing ground limestone, fly ash, and lightweight synthetic particles. 2009.

[14] G. Fagerlund. The critical degree of saturation method of assessing the freeze/thaw resistance of concrete. *Matériaux et Construction*, 10(4):217–229, 1977.

[15] G. Fagerlund. The international cooperative test of the critical degree of saturation method of assessing the freeze/thaw resistance of concrete. *Matériaux et Construction*, 10(4):231–253, 1977.

[16] S. Fulmer, M. Kowalsky, and J. Nau. Grouted shear stud connection for steel bridge substructures. *Journal of Constructional Steel Research*, 109:72–86, 2015.

[17] S. Fulmer, M. Kowalsky, J. Nau, and T. Hassan. Ductility of welded steel pile to steel cap beam connections. In *Structures Congress 2010*, pages 216–227, 2010.

[18] S. J. Fulmer, M. J. Kowalsky, J. M. Nau, and T. Hassan. Ductility of welded steel column to steel cap beam connections. Technical report, 2010.

[19] A. B. Hossain and J. Weiss. Assessing residual stress development and stress relaxation in restrained concrete ring specimens. *Cement and Concrete Composites*, 26(5):531–540, 2004.

[20] A. B. Hossain and J. Weiss. The role of specimen geometry and boundary conditions on stress development and cracking in the restrained ring test. *Cement and Concrete Research*, 36(1):189–199, 2006.

[21] D. Janssen. Requirements for a test of frost resistance of concrete. In *International RILEM Workshop on Frost Resistance of Concrete*, pages 277–286. RILEM Publications SARL, 2002.

[22] K. Khayat, A. Yahia, and P. Duffy. High-performance cement grout for post-tensioning applications. *Materials Journal*, 96(4):471–477, 1999.

[23] M. L. Leming, J. M. Nau, and J. Fukuda. Non-destructive determination of the dynamic modulus of concrete disks. *Materials Journal*, 95(1):50–57, 1998.

[24] W. Li, M. Pour-Ghaz, J. Castro, and J. Weiss. Water absorption and critical degree of saturation relating to freeze-thaw damage in concrete pavement joints. *Journal of Materials in Civil Engineering*, 24(3):299–307, 2011.

[25] G. Litvan. Freeze-thaw durability of porous building materials. In *Durability of building materials and components*. ASTM International, 1980.

[26] G. G. Litvan. *The mechanism of frost action in concrete: Theory and practical implications*. National Research Council Canada, Institute for Research in Construction, 1988.

[27] P. K. Mehta and P. J. Monteiro. Concrete microstructure, properties and materials, 2017.

[28] J.-H. Moon, F. Rajabipour, B. Pease, and J. Weiss. Quantifying the influence of specimen geometry on the results of the restrained ring test. *Journal of ASTM international*, 3(8):1–14, 2006.

[29] J. H. Moon and J. Weiss. Estimating residual stress in the restrained ring test under circumferential drying. *Cement and Concrete Composites*, 28(5):486–496, 2006.

[30] S. Perry, P. Bischoff, and K. Yamura. Mix details and material behaviour of polystyrene aggregate concrete. *Magazine of Concrete Research*, 43(154):71–76, 1991.

[31] T. C. Powers. Physical properties of cement paste. Technical report, 1960.

[32] T. C. Powers and T. L. Brownyard. Studies of the physical properties of hardened portland cement paste. In *Journal Proceedings*, volume 43, pages 101–132, 1946.

[33] R. S. Ravindrarajah and A. Tuck. Properties of hardened concrete containing treated expanded polystyrene beads. *Cement and Concrete Composites*, 16(4):273–277, 1994.

[34] M. Setzer. Micro ice lens formation and frost damage. In *Proceedings of the International RILEM Workshop on Frost damage in concrete, Minneapolis, 28–30 June 1999*, pages 1–15, 1999.

[35] M. Setzer, P. Heine, S. Kasparek, S. Palecki, R. Auberg, V. Feldrappe, and E. Siebel. Test methods of frost resistance of concrete: Cif-test: Capillary suction, internal damage and freeze thaw test - reference method and alternative methods a and b. *Materials and Structures*, 37(10):743–753, 2004.

[36] M. J. Shannag. High-performance cementitious grouts for structural repair. *Cement and Concrete Research*, 32(5):803–808, 2002.

[37] E.-E. Toumbakari, D. Van Gemert, T. Tassios, and N. Tenoutasse. Effect of mixing procedure on injectability of cementitious grouts. *Cement and Concrete Research*, 29(6):867–872, 1999.